DEVELOPMENT OF FLUORESCENT SENSORS FOR THE DETECTION OF LIPIDS INVOLVED IN INTERCELLULAR SIGNALING

A Dissertation

presented to

the Faculty of the Graduate School

at the University of Missouri-Columbia

In Partial Fulfillment

of the Requirements for the Degree

Doctor of Philosophy

---

by

CHAD M. COOLEY

Dr. Timothy E. Glass, Dissertation Supervisor

MAY 2014

The undersigned, appointed by the dean of the Graduate School, have examined the dissertation entitled

DEVELOPMENT OF FLUORESCENT SENSORS FOR THE DETECTION OF LIPIDS INVOLVED IN INTERCELLULAR SIGNALING

presented by Chad M. Cooley, a candidate for the degree of Doctor of Philosophy, and hereby certify that, in their opinion, it is worthy of acceptance.

_____

Professor Timothy E. Glass

_____

Professor Michael Harmata

_____

Professor Silvia S. Jurisson

_____

Professor Michael R. Lewis

Dedication

This dissertation is dedicated to Caitlin Marie Ervin, who I love more than anyone else in the world, and Martin Eugene Cooley, who I miss more than anyone else in the world.

I would like to thank the people who have supported me throughout my years in graduate school. Thanks to Bev Keeler for being the best mom ever (if it's in an official science dissertation it has to be true). John Allen, thank you for being the best friend a nerd can have. Debbie Allen, thank you for being my "Missouri mom." Bill Allen, thank you for opening your home to me. Emily Strubinger, thank you for everything.

ACKNOWLEDGEMENTS

I would like to thank my advisor, Dr. Timothy Glass, for his patience, guidance and encouragement throughout my graduate education. I could not have done this without him as an advisor. I would also like to thank my committee, Dr. Michael Harmata, Dr. Silvia Jurisson, and Dr. Michael Lewis, for their time and attention. I owe a debt of gratitude to Chun Ren, Shaohui Zhang, and Kenneth Hettie for mentoring me as a new graduate student. I am grateful for the help and advice given to me by former and current Glass Group members Jae Lee, Xiaole Shao, Jessica Klockow, Patrick Cavins, Nicholas Cooley, C. W. Littlefield, and Tam Tran.

TABLE OF CONTENTS

LIST OF FIGURES

LIST OF SCHEMES

LIST OF EQUATIONS

LIST OF TABLES

ABSTRACT

A set of fluorescent sensors was synthesized to detect two different types of lipids. A coumarin aldehyde that reversibly forms imines with primary amines in water was developed to selectively detect the lipid head group phosphoserine. A zinc (II) dipicolylamine was appended to the coumarin fluorophore by either a methylphenyl or propyl linker. Titration data showed significantly better binding for the propyl-linked sensor, likely due to conformational restrictions of the phenyl group. The propyl-linked sensor was determined to have a binding constant of 310 M^{-1} for phosphoserine at physiological pH, with a 30-fold fluorescence enhancement. In addition, sensors were synthesized for detection of oxidized phospholipids based on recognition of aldehydes produced from oxidative cleavage of unsaturated lipids. Molecular tubes have previously been reported with selectivity for saturated fatty acids. Based on this work, two "open" molecular tubes were synthesized that shared some of the original molecular tubes' affinity for hydrophobic guests, but that also had either a hydrazone or hydrazide capable of forming hydrazones with aldehydes. The hydrazone version gave a binding constant of 51 M^{-1} towards hexanal, while the hydrazide was not photostable in the presence of aldehyde.

Chapter 1: Molecular Recognition

1.1 Overview

Molecular recognition is the association of two or more molecules through reversible non-covalent interactions.[1] These interactions include ion-ion, dipole-dipole, metal-ligand, hydrogen bonding, π- π stacking, van der Waals, or hydrophobic interactions.[2] Molecular recognition is the basis for DNA base pairing, protein-substrate interactions, and self-assembly of micelles in water. While molecular recognition has historically relied exclusively on non-covalent forces, increasing attention has been paid to functional groups that rapidly and reversibly form covalent bonds. Boronic acids, which form boronate esters with catechols and saccharides, and coumarin aldehydes, which react with amines to form imines, are of particular interest.

In discussing molecular recognition between two different molecules or ions, the species involved are often categorized as either a host or a guest. As an example, in biochemistry an enzyme would be considered a host, and the substrate for the enzyme active site would be a guest. For synthetic systems, host molecules are designed to complement the structure of the intended guest.

1.2 Recognition of Ionic Species

The simplest and most well-studied molecular recognition systems are metal ion receptors. One of the earliest metal ion hosts to be studied was ethylenediaminetetracetic

acid (EDTA) (Scheme 1). Because it is capable of binding to metals through six atoms simultaneously, EDTA shows very strong binding affinity for many metal ions. This has led to its wide-spread use for removing unwanted metals in a number of industrial settings, and more commonly encountered in daily life, as an additive to soap and shampoo to counteract the effects of the ions that cause "hard water."

Scheme 1 EDTA-metal ion binding

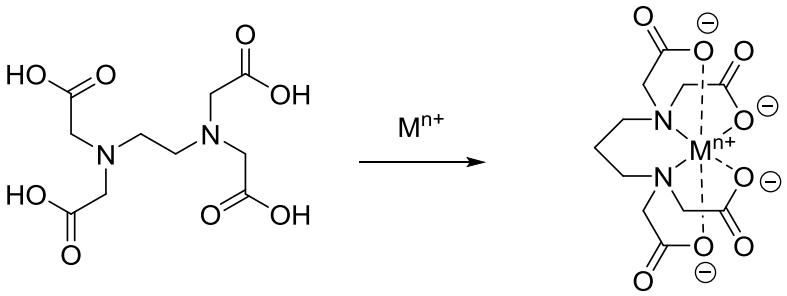

In 1967, Pedersen reported the synthesis of a number of cyclic oligomers of ethylene oxide.[3] The simplest of these crown ethers show selectivity for different metal ions based on size, with 12-crown-4 being selective for the tiny lithium cation, 15-crown-5 for sodium, and 18-crown-6 for the significantly larger potassium ion (Figure 1). When

Figure 1 Crown ethers with alkali metal cations.

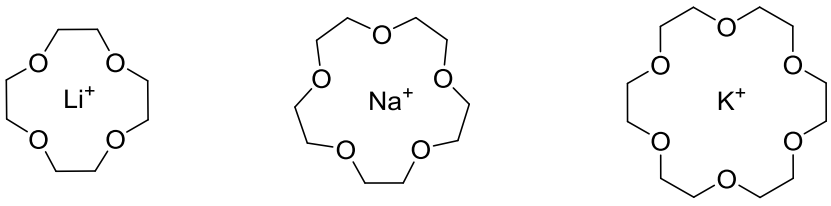

complexing a metal ion, the oxygen atoms are all oriented towards the center of the ring, leaving only the hydrophobic ethylene units exposed to solvent. This allows the crown ether to transfer otherwise insoluble ions into organic solvents. A number of derivatives have since been made that substitute some of the oxygen atoms in these rings with nitrogen or sulfur. These aza- and thio-crown ethers have altered selectivity, allowing for the selective recognition of alkaline earth metals, various transition metals, mercury, lead, etc.

1.3 Hydrogen-Bonding Receptors

In general, hydrogen-bonding receptors are quite effective in organic media, particularly in less polar sytems where the polar host and guest would preferentially interact with one another instead of the non-polar solvent. In polar solvents, especially water, the guest and host are both well solvated, and host-guest binding requires displacement of enthalpically favorable solvent shells, significantly shifting the equilibrium away from the host-guest complex.

Because of the importance of hydrogen bonding to biological systems, significant work has been done on the development of rigid hydrogen-bonding systems that mimic the types of arrangements found in DNA base pairs (Figure 2a) and protein β sheets (Figure 2b).

Because of the high degree of symmetry they display, urea, benzamidines and the guanidinium ion have received particular attention.[4-7] A number of receptors for the recognition of guanidinium species, including the amino acid arginine, have been

Figure 2 (a) Hydrogen bonding between thymine and adenine (top) and guanine and cytosine (bottom). (b) Hydrogen bonding in an anti-parallel protein β sheet.

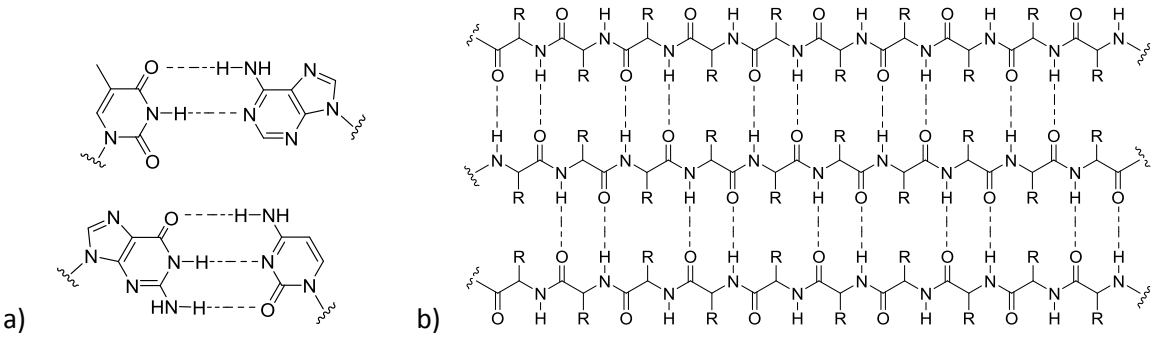

developed (Figure 3).[8] To accommodate the planar guanidinium ion, optimal receptors are generally also planar. The symmetry of guanidinium makes it relatively simple to design receptors with near-optimal hydrogen bond angles and lengths, 180º and approximately 3 Å, respectively.

Figure 3 Hydrogen-bonding receptor for arginine.

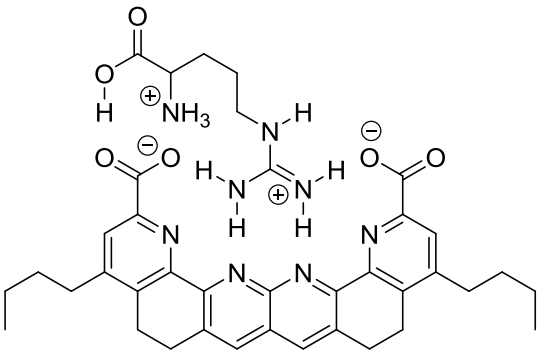

The crown ethers mentioned above have also seen use as receptors for hydrogen-bonding guests, including hydronium, ammonium, and lysine cations (Figure 4).[9-12]

Figure 4 18-Crown-6 hydrogen-bonding complex with lysine.

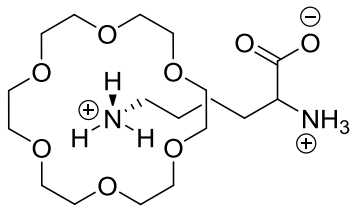

1.4 Hydrophobic Interactions

Water is unique in that each molecule can form four hydrogen bonds to four other solvent molecules simultaneously (Figure 5). This leads to extensive networks of hydrogen bonding in water that must be disrupted in order to make room for any solutes, at a relatively high energetic cost compared to most other solvents.

Figure 5 Hydrogen bonding interactions of water molecules.

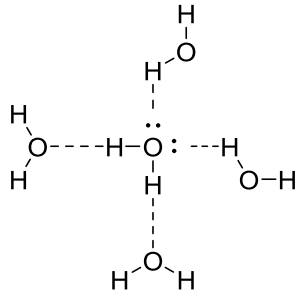

When hydrophobic molecules are dissolved in water they create a hole in the hydrogen bond network, replacing strong hydrogen bonding interactions with significantly weaker dipole-dipole and/or van der Waals interactions. If the hydrophobic solute molecules associate together, excluding water from between them, the water-solute interactions are minimized and the water-water hydrogen bonding interactions are maximized (Scheme 2). This overall energy optimization is what leads to the spontaneous formation of miscelles when lipids are suspended in water.

Scheme 2 Hydrophobic effect for hexane.

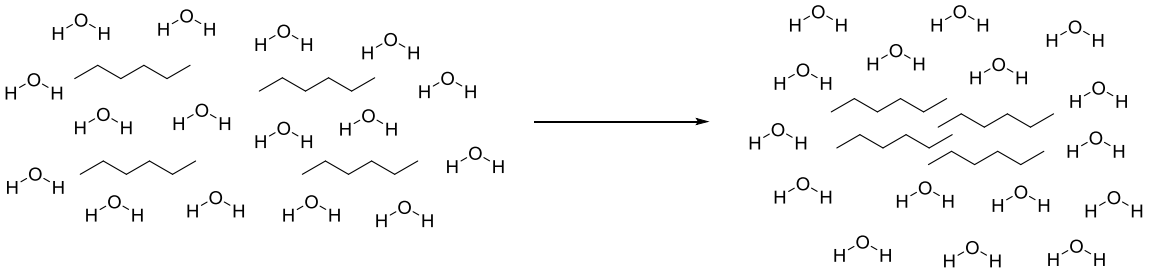

Molecular recognition based on hydrophobic interactions is well-known for a wide variety of systems including cavitands, carcerands, molecular clips and molecular tweezers. Cyclodextrin (Figure 6), a conical oligomer of glucose, was one of the first receptors discovered that uses a hydrophobic cavity for the encapsulation of a guest molecule (Scheme 3).[13]

Figure 6 Structure of β-Cyclodextrin.

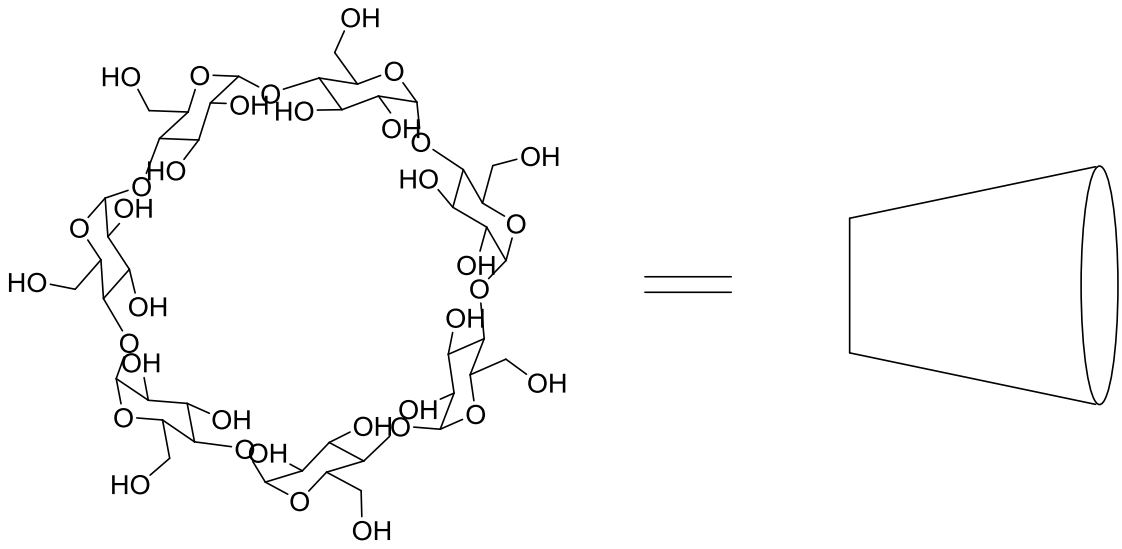

The rigid structure of the macrocycle is enforced, in part, by intramolecular hydrogen bonding on the interior surface of the cone. With these hydrogens and oxygens already involved in strong hydrogen bonding, they are less available for interactions with other molecules inside the cavity. This makes the inside of the cone much less polar than

Scheme 3 Host-guest complex formation between β-cyclodextrin and cholesterol.

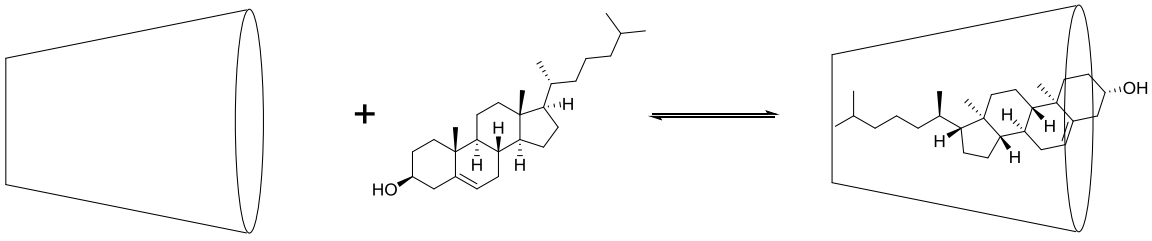

the exterior surface, and very greatly less polar than the bulk solvent. This leads to the inclusion of hydrophobic molecules inside the cone. A number of different cyclodextrin oligomers exist that vary only in the size of the cavity, allowing for some selectivity in which hydrophobic guests are incorporated into the receptor based on complimentary fit of size and shape.

1.5 Reversible Covalent Binding

While the term "molecular recognition" is typically reserved for non-covalent interactions, discrimination can be achieved between a receptor and its substrate by interactions that are covalent in nature but exist in equilibrium. The most well-studied examples to date are the boronic acids, which reversibly form esters with diols in aqueous solution (Scheme 4).[14] This reaction leads to their use as receptors for sugars, especially glucose, whose concentration in blood needs to be regularly monitored by the over 25 million people in the United States who suffer from diabetes.[15]

Scheme 4 Formation of boronate ester between phenylboronic acid and glucose.

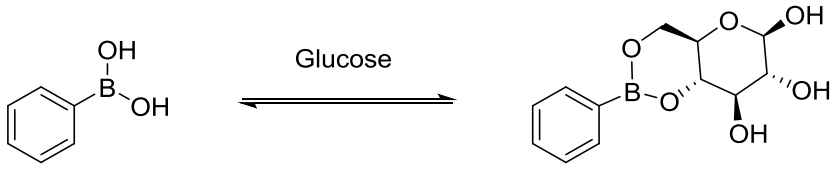

Shinkai developed one of the first boronic acid receptors selective for glucose over other monosacharides.[16] This diboronic acid was shown to selectively recognize glucose over other mono- and disaccharides by circular dichroism (Scheme 5). Glucose

binds to the receptor 190 times more favorably than the next strongest-binding analyte, maltose.

Scheme 5 Binding of glucose to a diboronic acid receptor.

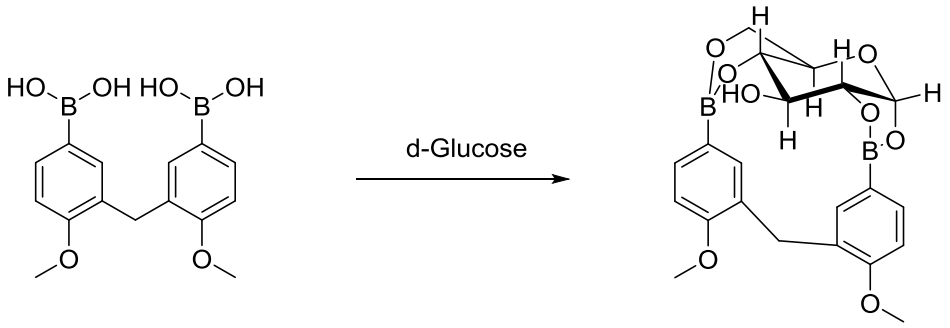

The reversible reaction between aldehydes and primary amines to form imines has also sparked a great deal of interest. The Glass group has used coumarin aldehydes to determine concentrations of a number of biologically active amines under physiological conditions as well as in cells.[17] A recent example of amino acid sensing by imine formation is shown in Scheme 6. Kynurenine, a metabolite of the amino acid tryptophan,

Scheme 6 Coumarin aldeyde sensor for kynurenine.

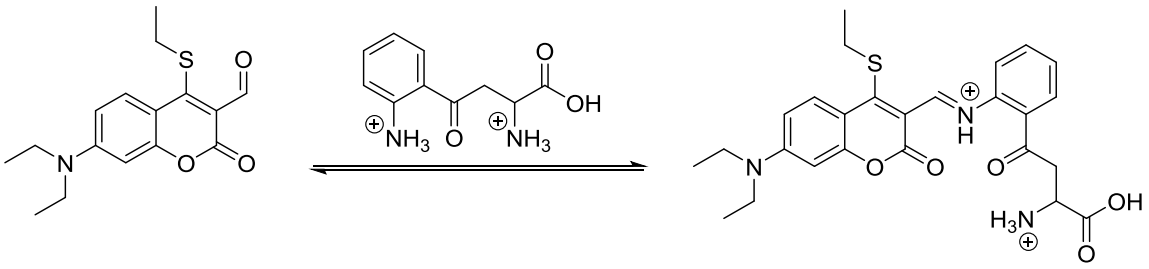

selectively reacts with 7-diethylamino-4-ethylthio-coumarin-3-carbaldehyde over other biological amines at low pH.[18]

1.6 Chelation and Preorganization

The strength of interaction between molecules A and B when they form supramolecular complex AB (Equation 1) is characterized by the association constant, K_a (Equation 2).

$$A + B \rightleftharpoons AB \qquad \textbf{eq. 1}$$

$$K_a = \frac{[AB]}{[A][B]} \qquad \textbf{eq. 2}$$

In molecules that have multiple recognition elements to interact with a single guest, K_a will be increased by the chelation effect. The equilibrium constant is related to the Gibbs free energy (ΔG) of the interaction by Equation 3, where R is the ideal gas

$$\Delta G = -RTln(K_a) \qquad \textbf{eq. 3}$$

constant, T is the temperature. ΔG has a dependence on entropy (ΔS) (Equation 4).

$$\Delta G = \Delta H - T\Delta S \qquad \textbf{eq. 4}$$

For the formation of a 4:1 complex between ammonia and copper (II) ion (Scheme 7), there is a decrease in the total number of particles from five to one, causing a large decrease in the translational entropy of the system. A decrease in entropy makes ΔG more positive, and thus the reaction less favorable.

Scheme 7 Coordination of ammonia to copper (II) ion.

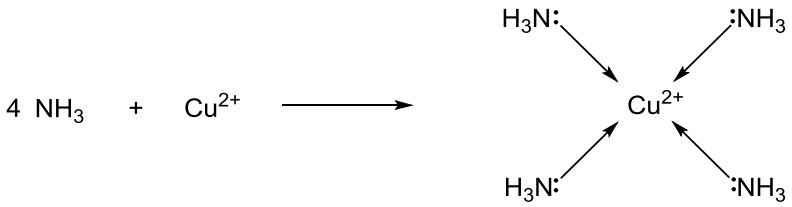

For complexation of ethylenediamine to Cu^{2+} (Scheme 8), the change in enthalpy is approximately the same because the same number of N-Cu dative bonds are made, but the decrease in translational entropy is much smaller since the number of particles only decreases from three to one. The smaller negative value of ΔS makes ΔG more negative

Scheme 8 Coordination of ethylenediamine to copper (II) ion.

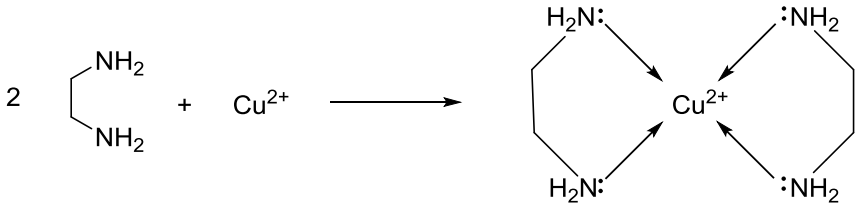

for $[Cu(en)_2]^{2+}$ than for $[Cu(NH_3)_4]^{2+}$ and thus the formation of $[Cu(en)_2]^{2+}$ is more favorable than that of $[Cu(NH_3)_4]^{2+}$. This is the chelation effect.

Just as the chelation effect makes host-guest interactions with multiple binding sites more favorable thermodynamically by reducing the translational entropic cost of binding, when the host molecule also has its binding sites in a closed ring there is an additional "macrocyclic effect" that increases the value of K_a by decreasing the amount of rotational entropy that is lost upon binding. In the open-chain oligo-ether shown in Figure 7, binding to the potassium ion with all six oxygens requires a specific conformation of the host chain, severely restricting its ability to rotate freely about it's C-C and C-O bonds. In the macrocyclic crown ether, the rotational freedom was lost in the synthesis of the receptor, long before the binding event occurred. In this case, there is very little loss of rotational entropy on binding the potassium ion, and so ΔG is significantly more negative for the macrocycle than it is for its open-chain counterpart.

Figure 7 Macrocyclic effect for 18-crown-6.

1.7 Conclusion

Molecular recognition covers a wide variety of reversible interactions for the association of two or more molecular species in solution. The strength of the interaction is dependent on complementarity of size, shape and charge between the receptor and its guest. These parameters allow for optimization of binding strength for a wide variety of chemical species. The extent of host-guest complex formation is quantified by the association constant, K_a, which is also related to the strength of the binding interaction. Molecular recognition has applications for cleaning, catalysis, and chemical sensing, among many others.

Chapter 2: Chemical Sensing

2.1 Overview

Chemical sensing[19,20] occurs when a molecular recognition event corresponds with a measurable change in some property of the system being studied. Useful properties for sensing include electrical potential (potentiometry), current (amperometry), absorbance of light (colorimetry), and emission of fluorescence (fluorimetry).

Colorimetry and fluorimetry use similar instrumentation that is easy to operate and can be portable. They both give results that can often be detected by the human eye for qualitative detection, can often be used on liquid samples without further sample preparation and have fast response times that can allow for real-time monitoring. Both methods are also biocompatable and non-destructive. Fluorimetry has the added bonus of usually having much lower background signal over colorimetry due to the fact that many molecules absorb light but very few fluoresce, leading to a lower limit of detection. These properties lead to fluorescence being an ideal method of detection in complex biological samples and cellular environments.

2.2 Fluorescence

Fluorescent molecules (fluorophores) are organic compounds with extensive conjugated π-systems. Fluorescence occurs due to electron transitions between the highest occupied molecular orbital (HOMO) and the lowest unoccupied molecular orbital

(LUMO). The larger the conjugated π-system, the smaller the HOMO-LUMO energy gap becomes, resulting in photon absorption and emission at longer wavelengths.

Fluorescence begins when the fluorophore absorbs a photon.[21] The energy absorbed promotes an electron from the electronic ground state, S_0, to an electronically excited state, often the lowest-lying excited state, S_1, without changing the spin of the electron. The excitation energy promotes the electron to a vibrationally excited level of S_1, and the molecule subsequently relaxes, lowering the electron to the vibrational ground state of S_1 by transferring energy collisionally to the solvent. From here the electron drops to a vibrationally excited state of S_0 and emits a photon with an energy equal to the difference between these two energy levels. These photophysical processes are represented as a Jablonski diagram (Figure 8). Not every photon that is absorbed leads to

Figure 8 Jablonski diagram.

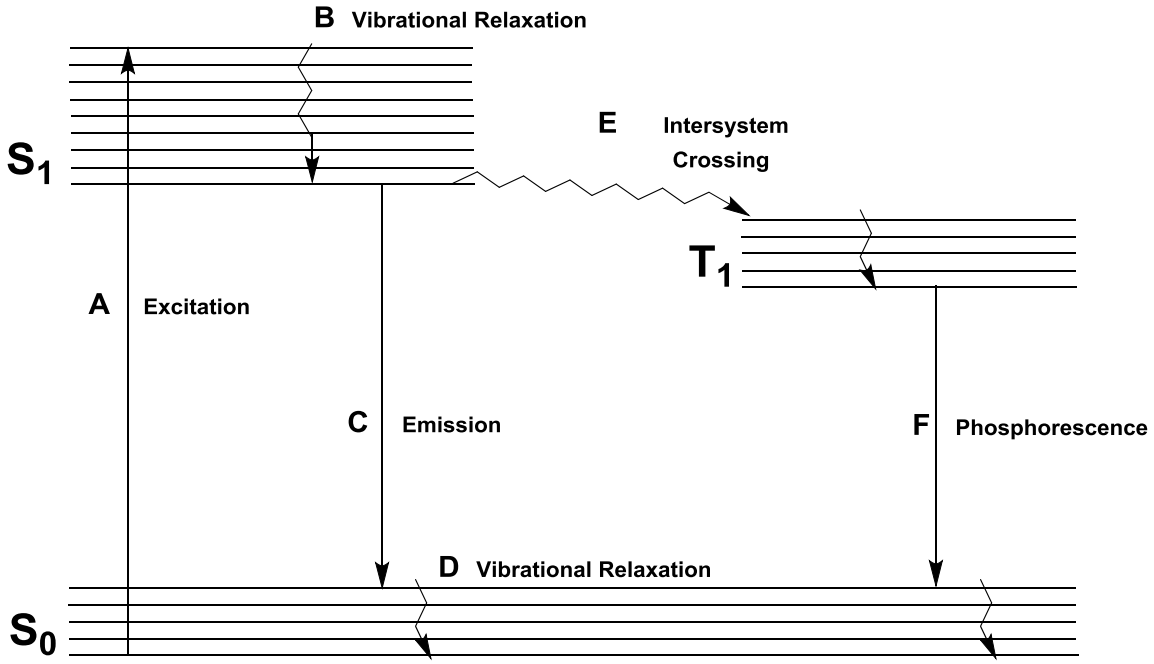

the emission of another photon (*vide infra*).The ratio of photons emitted per photon absorbed is referred to as the quantum yield, Φ.

Arrow A is the excitation event. The electron is most likely to occupy the lowest vibrational energy level of the fluorophore, and so most excitation events occur from the vibrational ground state. In this example, the molecule is excited, promoting an electron to a vibrationally excited state of the second electronic excited state, a process which takes approximately 10^{-15} seconds and can be practically approximated as instantaneous. The molecule relaxes vibrationally until the electron reaches the vibrational ground state of S_1 (arrow B). This vibrational relaxation occurs in approximately 10^{-12} seconds. In the next 10^{-8} seconds, the electron drops from S_1 to a vibrationally excited level of S_0, emitting a photon in the process (arrow C), before finally relaxing to the vibrational ground state of S_0 (arrow D).

The majority of molecules that absorb light do not fluoresce. There are a number of reasons for this, with the most important ones being internal conversion (*vide supra*) from S_1 to S_0, energy transfer to solvent, and intersystem crossing. Collisions with solvent molecules lead to a transfer of energy from the fluorophore to the solvent, dropping the excited electron to the electronic ground state. Intersystem crossing, represented in Figure 1 as arrow E, occurs when the excited electron changes its multiplicity, going from the singlet S_1 state to the triplet T_1. This is a forbidden transition by quantum mechanical selection rules, and so the probability of occurrence is typically small. In molecules that do exhibit intersystem crossing, the relaxation from T_1 to S_0 is also a forbidden transition, as is reversing from T_1 back to S_1. As a result, the lifetime of the excited state is extended significantly. This results in a decrease in fluorescence

through allowing more time for non-radiative decay pathways such as collisional quenching by other molecules, as well as reducing the number of radiative decay pathways that can occur at once so that some luminescence does occur, but the intensity is too low to be detected easily. Radiative decay from the triplet state is called phosphorescence (arrow F), and can occur over a range of time from microseconds to hours.

From this qualitative diagram, it can be seen that arrow A must be longer than arrow E, and so the emitted photon has less energy than the absorbed photon. The excitation occurs at a shorter wavelength (more blue) and the emission at a longer wavelength (more red). This phenomenon is the Stokes shift[21] of the fluorophore, which is measured as the difference between the wavelength of maximum excitation and wavelength of maximum emission (Figure 9). The magnitude of the Stokes shift depends on the fluorophore, and often on the solvent.

Figure 9 Stokes shift between absorbance maximum and fluorescence maximum.

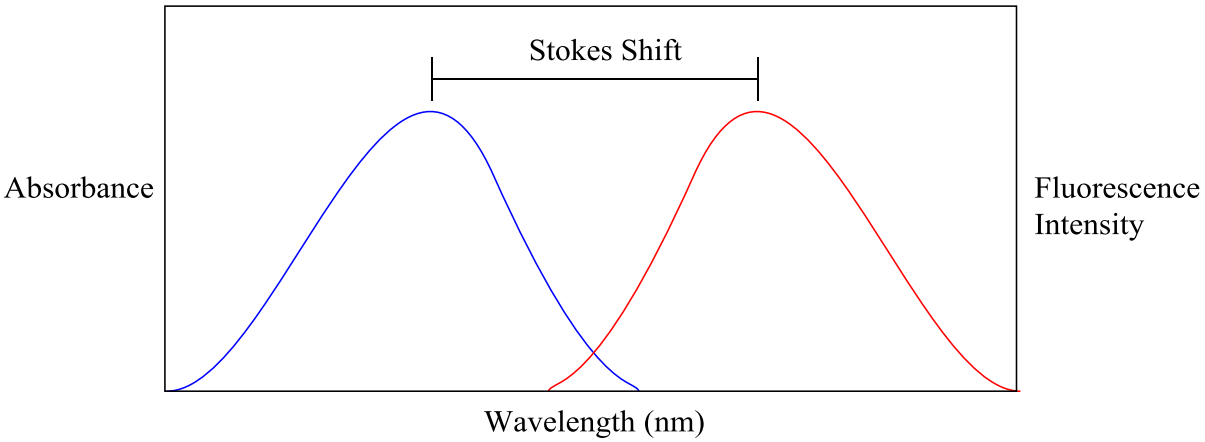

2.3 Intramolecular Charge Transfer and Solvatochromism

Solvent effects on the Stokes shift are referred to as solvatochromism, and it is especially pronounced in molecules that display intramolecular charge transfer (ICT). In these molecules an electron donor is in conjugation with an electron acceptor, giving rise to resonance structures such as those shown for dansyl amide (Figure 10).[22]

Figure 10 Major resonance contributors of dansyl amide.

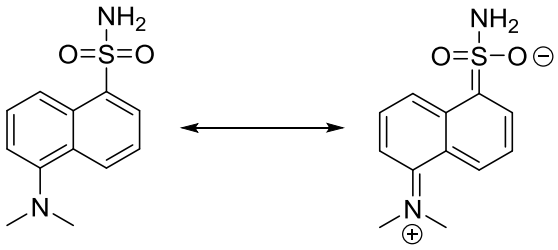

1 **2**

Compound **1** is uncharged, while resonance structure **2** has separated charges. The ground state of the fluorophore most closely resembles **1**, while the first excited state electron distribution is very similar to **2**. This leads to preferential stabilization of the excited state with respect to the ground state in polar solvents, resulting in a decrease in the energy of emitted light without significantly affecting the wavelength of excitation. As Figure 11 demonstrates, placing dansyl amide in a more polar solvent red-shifts the fluorescence, while putting it in a less polar solvent blue-shifts the emission spectrum.

Figure 11 Normalized fluorescence spectra of dansyl amide in cyclohexane (CH), dichloromethane (DCM), ethanol (EtOH), bmimPF_6 (IL), 90 wt% glycerol in water (GW), and water.[22]

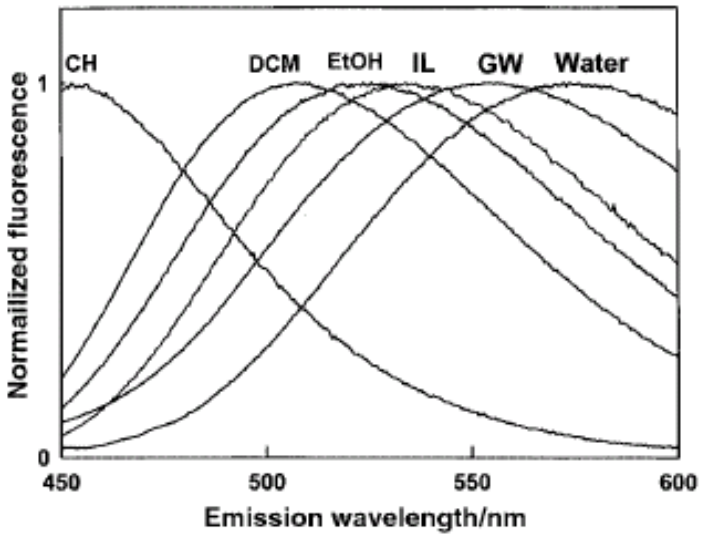

In Figure 11, the relative intensities of dansyl amide have been normalized for each spectrum. Like the wavelength of maximum emission (λ_{max}), the intensity of fluorescence emission (I) for **1** also varies with solvent polarity. Normalization removes the confounding variable of intensity in order to make it easier to determine differences in emission wavelength between the spectra. Normalization sets the amplitude of the maximum emission wavelength for each spectrum to the same arbitrary number, typically one, making it easier to compare not only λ_{max} values but also features such as the shape and breadth of the emission peak(s), which can provide information about molecular structure, ionization state, and intermolecular complex formation, between different spectra of varying intensities.

Solvatochromism allows the measurement of solvent polarity in the environment around a fluorophore. 2,5-(4′-nitrophenylethenyl)-styrylfuran (**3**, Figure 12) shows a dramatic red-shift in fluorescence of almost 250 nm as the molecule is dissolved in more

Figure 12 Structure of 2,5-(4′-nitrophenylethenyl)-styrylfuran.

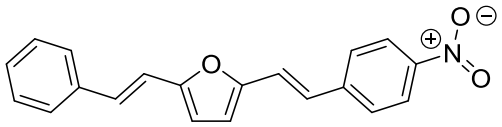

3

polar solvents (Figure 13).[23] This property has been put to use extensively in the probing of cellular environments for determining the relative fluidity of membranes.[24-27]

Figure 13 Emission spectra of 2,5-(4'-nitrophenylethenyl)-styrylfuran in (left to right) isopentane, hexane, cyclohexane, carbon tetrachloride, toluene, ethyl acetate, bromonaphthalene, acetone, and acetonitrile.[23]

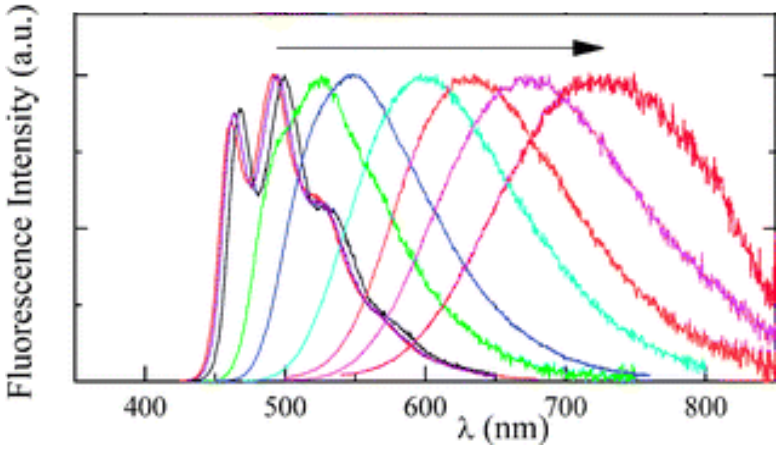

Solvatochromism is only one way of changing fluorescence output. Modification of the π-system, quenching, photoinduced electron transfer, Förster resonance energy transfer (FRET), and excimer formation have all been used to indicate changes in environment and the presence of chemical species.[28-30]

2.4 π-System Modification

Binding events that extend or reduce the degree of π-system conjugation lead to shifts in the wavelength of light absorbed or emitted. Michael acceptors are a particularly common sensing motif for reversible soft nucleophiles, as conjugate addition results in the loss of a π-bond. Sensor **4** was developed for detection of sulfite anion (Scheme 9).[31] Malonitrile is conjugated to the coumarin fluorophore, leading to long wavelengths of absorption (492 nm) and emission (578 nm) due to the extended conjugation. On addition of sodium sulfite, a rapid change in color is observed due to the 1,4-addition of sulfite, resulting in new, lower wavelengths of absorption and emission (413 and 480 nm, respectively).

Scheme 9 Coumarin sensor for sulfite anion.

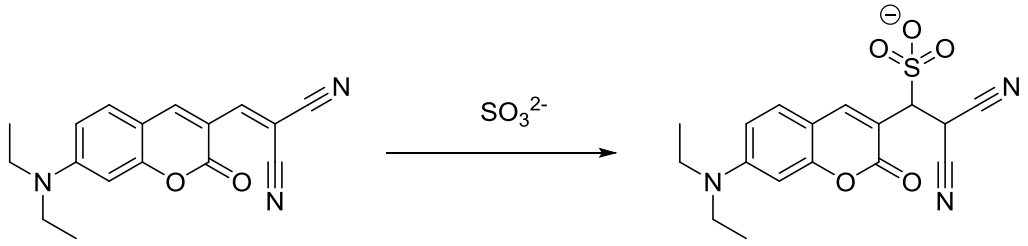

4

A different mode of π-system modification can be seen in Scheme 10.[32] Compound **5** is a pyridine-containing analog to the green fluorescent protein (GFP) fluorophore. In solution the double bond connecting the two ring systems undergoes E,Z isomerization upon excitation instead of fluorescing, effectively quenching emission. Upon chelating a zinc ion, the two rings are brought into a rigid, near-planar structure, enforcing the conjugation between the two ring systems and turning on the fluorescence.

Scheme 10 Fluorescent zinc sensor.

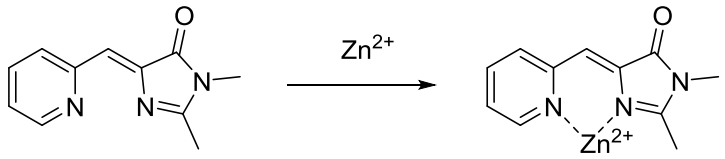

5

2.5 Fluorescence Quenching

Quenching is a decrease in fluorescence intensity. Collisional quenching occurs when two molecules come in contact transiently in solution. Oxygen and halide ions are well-studied collisional quenchers that act through a process called spin-orbit coupling, which increases the rate of intersystem crossing, preventing radiative decay from S_1 to S_0. In oxygen, this occurs due to the triplet nature of the molecule's ground state, while in chloride, bromide, iodide, and several metal species the phenomenon is referred to as the heavy atom effect.[21] Sensors for halides have been developed based on this fact,

Figure 14 Acridinium fluorescent sensor for iodide.

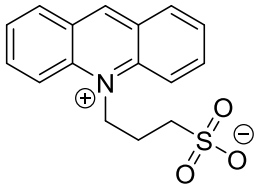

6

including **6** (Figure 14).[33] The positive charge on the fluorophore attracts the negative iodide, and iodide's proximity leads to quenching of the fluorophore by spin-orbit coupling.

The decrease in fluorescence intensity makes **6** a turn-off sensor. Turn-off is a valid sensing option, but its reliability is limited by the fact that there are many different ways that fluorescence can be reduced, including quenching by species other than the desired analyte, particularly molecular oxygen, decomposition of the fluorophore, and photobleaching.

2.6 Photoinduced Electron Transfer (PET)

During excitation, the fluorophore has two half-filled orbitals with a significant energy gap between them. If another molecule, or a part of the same molecule that is not conjugated with the fluorophore, has a HOMO or LUMO within this energy gap, photoinduced electron transfer (PET) can occur in one of two ways (Figures 15 and 16).

If the HOMO of the other molecule is higher than the HOMO of the fluorophore it can transfer an electron into the lower energy, half-empty fluorophore orbital. This process is referred to as acceptor-PET (a-PET) since the fluorophore is acting as an electron acceptor (Figure 15).

Figure 15 HOMO-LUMO energy diagrams for electron transfer between excited fluorophore and nearby electron donor.

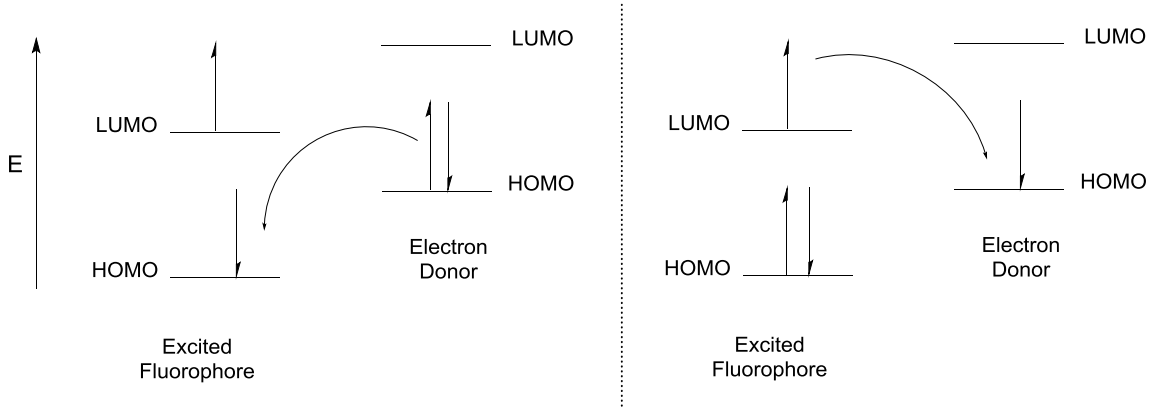

If the LUMO of the other molecule is higher than the HOMO of the fluorophore the excited electron can transfer from the fluorophore LUMO to the LUMO of the second molecule, instead of dropping to the fluorophore HOMO and directly fluorescing (Figure 16). This mechanism is refered to as donor-PET (d-PET), with the fluorophore acting as an electron donor.

Figure 16 HOMO-LUMO energy diagrams for electron transfer between excited fluorophore and nearby electron acceptor.

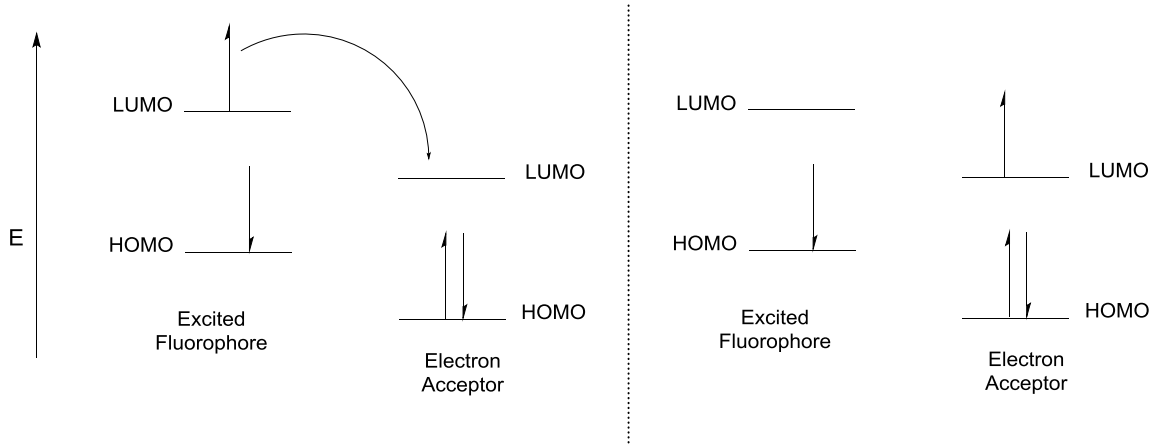

In Scheme 11, **7** is composed of a BODIPY fluorophore with a diaminobenzene moiety attached at the meso position.[34] The diaminobenzene unit is not conjugated with the fluorophore due to steric interactions between the ortho hydrogens and the two methyl groups forcing the ring to twist out of the plane of the BODIPY. In **7**, the fluorophore is PET quenched by the HOMO electrons of the electron-rich diaminobenzene, making this an example of a-PET. In the presence of methylglyoxal, the aniline nitrogens are converted to imines. This transformation changes the arene pi-system from being quite electron-rich to relatively electron-poor, lowering its HOMO energy level below that of the fluorophore, and thus preventing PET quenching and increasing fluorescence intensity. This is an example of a turn-on sensor.

Scheme 11 BODIPY a-PET sensor for methylglyoxal.

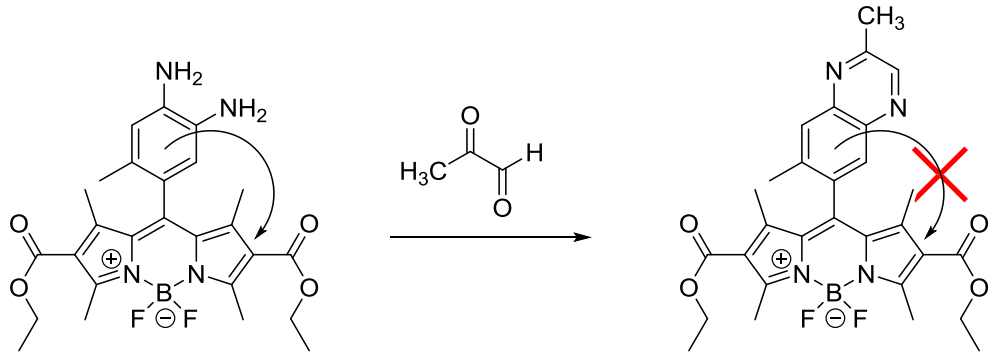

7

2.7 Conclusion

Chemical sensing uses molecular recognition to quantify the concentration of a particular analyte in a system. Fluorescence is a particularly useful output for sensors since it is non-destructive, non-invasive, and fast. There are a variety of ways to modulate fluorescence output, either by turning the emission on or off or changing the wavelength of the emission on interacting with the analyte.

Chapter 3: Lipids

3.1 Overview

Lipids (Figure 17) are a large class of biomolecules that are either hydrophobic or amphipathic, and so have limited solubility in water. Their most important role is as the primary components of cellular membranes, which protect the cell and allow compartmentalization of cellular processes. In eukaryotes the most common lipid classes are fatty acids (**8**), triglycerides (**9**), phospholipids (**10**), sphingolipids (**11**), and terpene derivatives (**12**).[35]

Figure 17 Common categories of lipids.

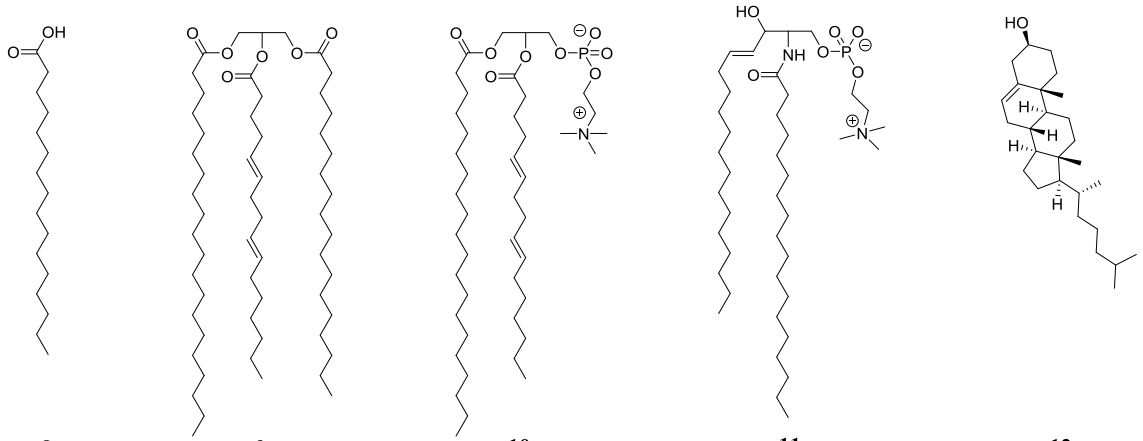

A fatty acid (**8)** is a long-chain carboxylic acid, most often containing between 12 and 20 carbon atoms.[36] Fatty acids chains can be saturated, unsaturated or polyunsaturated. In addition to comprising an important and structurally diverse category of lipids in their own right, fatty acids are also a major component in other lipids classes, since triglycerides, phospholipids and sphingolipids all have one or more fatty acid esters in their structures. They are most commonly found as components of more complex lipids. Triglycerides, or triacylglycerols, are triesters of fatty acids and glycerol (**9**). They are primarily involved in energy storage in animals and are stored in adipose tissue.[37]

Phospholipids (**10**) are the main component of cellular membranes, and are responsible for a number of cell to cell signaling pathways including clotting and apoptosis. Most phospholipids are diacylphosphoglycerides, with the phosphate on the 3-position of the glycerol (Figure 18). The most common groups attached to the phosphate are choline (**13**), which accounts for 35-45% of all phospholipids in cell membranes, ethanolamine (**14**, 22-29%) and serine (**15**, 12-19%).[38] For all phospholipids,

Figure 18 Common phospholipid head groups.

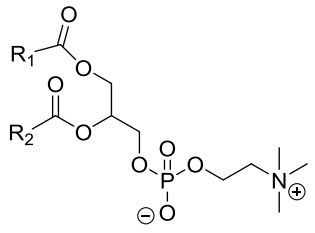

13

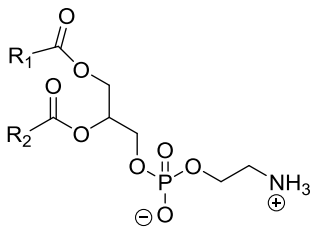

14

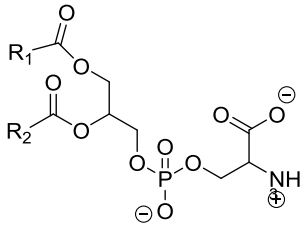

15

the two fatty acid chains are anchored in the membrane, while the phosphate group is exposed to the water outside the membrane.

Sphingolipids (**11**, Figure 19) are also a major component of cellular membranes, but they differ from phospholipids in that they contain a sphingosine (**16**) backbone with one fatty acid residue attached at the 2-amino position of sphingosine. The terminal hydroxy group can be substituted with a phosphate ester, as with phospholipids, which results in a sphingomyelin molecule (**17**), or to a sugar acetal, producing a cerebroside (**18**).[39]

Figure 19 Sphingosine (**16**) and common sphingolipids.

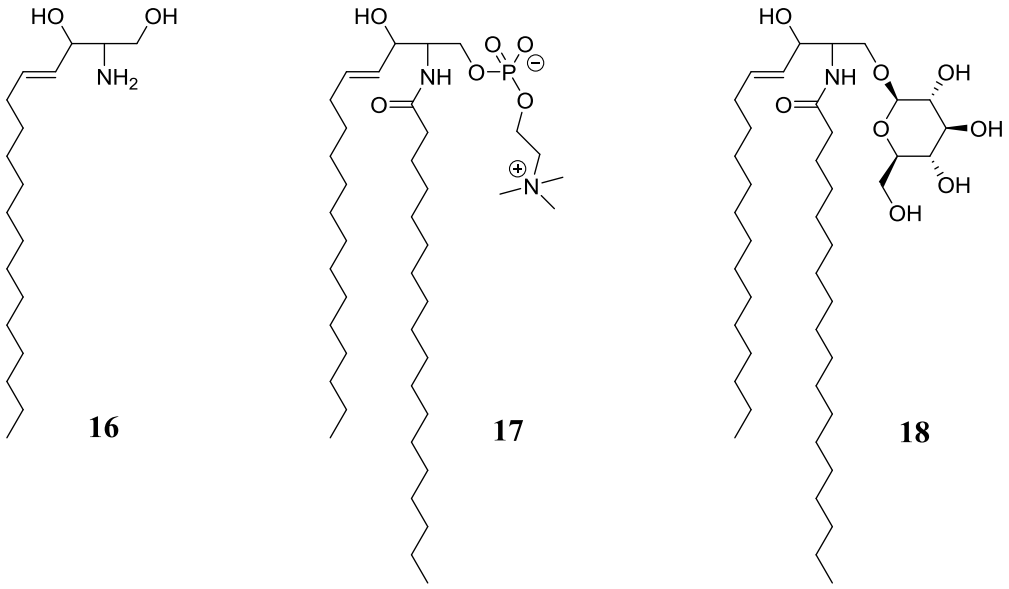

Terpene derivatives (**12**) are formally oligimers of isoprene, 2-methyl-1,3-butadiene. In cell membranes, cholesterol (**19**) is the predominant terpene derivative present. Cholesterol is a member of the steroid class of terpenoids, which also includes

testosterone, estradiol, and bile acids.[40] Other important terpenoids include retinal (**20**), which is the active form of vitamin A necessary for retina function, carotenoids such as β-carotene and lycopene, xanthophylls which give rise to autumn leaves' colors, and natural rubber, a polymer of isoprene.[35]

Figure 20 Structures of cholesterol (**19**) and retinal (**20**).

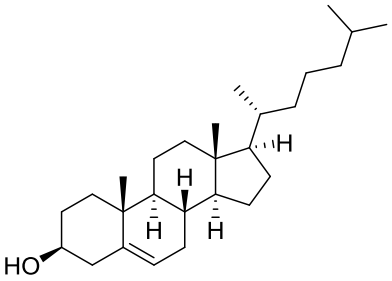

19

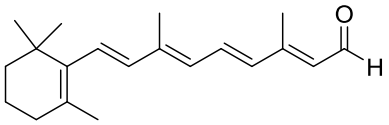

20

3.2 Low-Density Lipoprotein

A significant amount of lipid synthesis occurs in the liver. These lipids need to be transported from the liver to other sites in the body where they are needed for energy production, as components of new cell membranes during cell growth or division, or to be stored in adipose tissue for future energy needs. Individual lipid molecules are insoluble in water, and so for transport they are packaged into lipoprotein particles. The lipoprotein is a micelle with an outer surface of phospholipids and cholesterol and a single protein, called an apoprotein. The interior of the particle is an aggregate of triglycerides and esterified cholesterol, which are completely insoluble in water.

The two primary categories of lipoprotein are low-density lipoprotein (LDL) and high-density lipoprotein (HDL).[40,41] LDL packages lipids in the liver for transport out to the rest of the body. The apoprotein binds to cellular receptors, which triggers endocytosis. Excess lipids are transported back to the liver for degradation by HDL. High levels of LDL and low levels of HDL correlate with increased risk of heart disease, particularly atherosclerosis.[42,43]

3.3 Oxidized Phospholipids and Atherosclerosis

Atherosclerosis is the thickening and hardening of arterial walls due to the formation of plaques. Rupturing of these plaques leads to blood clots in arteries, blocking blood flow and eventually leading to heart attacks and strokes. Oxidation of unsaturated phospholipids on the surface of LDL particles is a triggering event in the formation of arterial plaques.[44-46]

LDL particles can penetrate the outer tissue layer of the arterial wall, where they become oxidized. Unsaturated phospholipids undergo oxidation at the carbon-carbon double bond due to the action of radicals, including nitric oxide and other reactive oxygen species, as well as by certain enzymes such as lipoxygenase.[47] Oxidation leads to a number of epoxide, hydroxide and oxo products. Oxidative cleavage of the double bond in phospholipids containing an unsaturated fatty acid results in formation of an aldehyde at the cleavage site (Scheme 12).[48]

Aldehydes on LDL particles are recognized by receptors on macrophages which then engulf the particle.[49] The macrophages are incapable of completely digesting the LDL particles and continue engulfing particles until they burst. This releases the oxidized

Scheme 12 Oxidative cleavage of unsaturated phospholipid to an aldehyde.

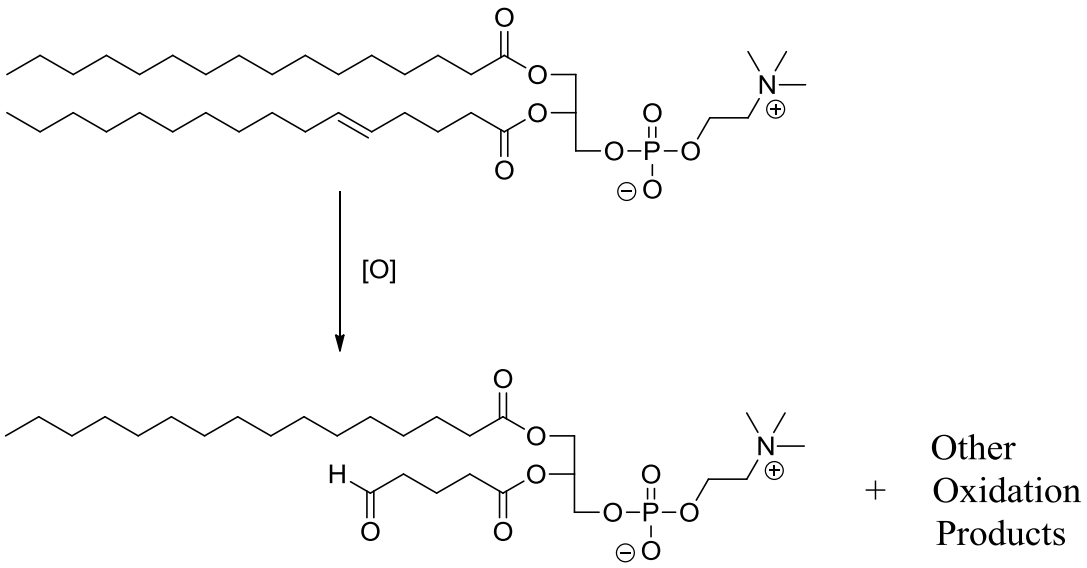

phospholipids where they can then trigger consumption by more macrophages. The burst cells also release inflammatory molecules that trigger further immune responses leading to swelling and further action by macrophage cells, growing the developing plaque into the artery, which restricts blood flow and raises blood pressure. Further growth damages the surrounding tissue until the plaque ruptures, releasing fat deposits, fibrous material and clotting factors that restrict blood flow, resulting in heart attacks and strokes.

3.4 Current Detection Methods

Early detection of oxidized phospholipids is desirable for the prevention of heart attacks and strokes, as well as the early treatment of other symptoms of cardiovascular disease. Currently, atherosclerosis is detected most readily by invasive angiography of arteries, and is only detectable once the plaque is well-developed.

Detection of higher levels of oxidized LDL particles in blood correlates with atherosclerotic plaque growth, and is a minimally invasive technique.[50] At present, the majority of work on the detection of oxidized phospholipids in blood and serum requires mass spectroscopy, which has limitations for clinical applications.[51-57] The samples are complex, requiring separation by electrophoresis or liquid chromatography, and a large number of similar lipids are present that may be modified in many different ways, which makes analysis of the mass spectrum complicated. In addition, the instrumentation is relatively expensive and requires significant training to use, which may be cost-prohibitive for many clinical settings.

Attempts have been made to detect oxidized phospholipids by other means, including x-ray diffraction of cellular membranes,[58,59] absorbance spectroscopy of antibodies that target oxidized lipids,[60] and fluorescence spectroscopy of environment-sensitive membrane probes. Howlett's group[59] has been able to show that the ratio of oxidized phospholipid in LDL particles is proportional to the intensity of fluorescence from thioflavin T (Figure 21, **21**), a common fluorescent stain for protein aggregates, and that oxidation of LDL particles also causes birefringence with the Congo Red dye (**22**) when viewed under polarized light that is similarly proportional to the ratio of oxidized phospholipids in the micellular membrane.

Jungwirth *et* al.[61] demonstrated that cellular membranes become more permeable to water as the oxidized phospholipid content increases, a result of less tight packing in

Figure 21 Structures of fluorescent membrane probes for oxidized phospholipids.

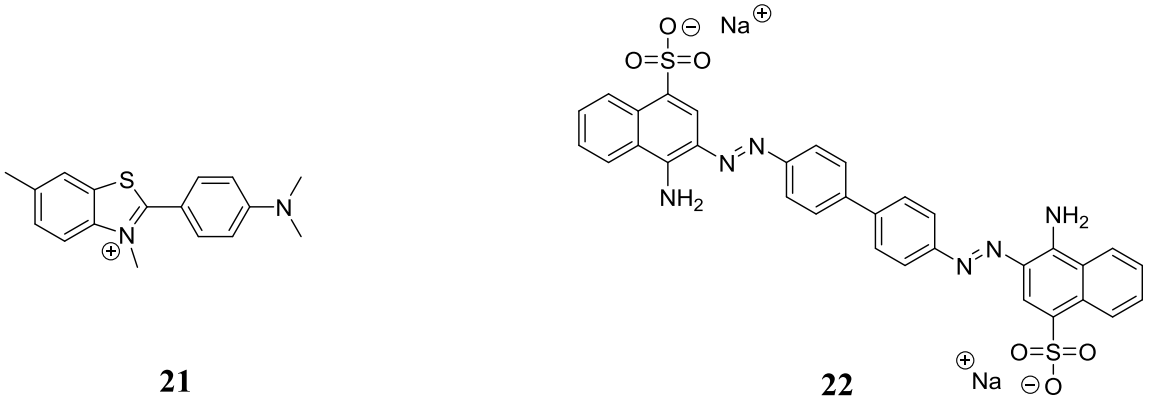

21 **22**

the lipid bilayer, by using the polarity-sensitive fluorophore Laurdan (Figure 22, **23**). They further explored the effect of increased levels of oxidation by monitoring membrane fluidity and mobility with a BODIPY lipid derivative, BODIPY C_{12}-HPC (**24**).

Figure 22 Structures of fluorescent membrane fluidity probes.

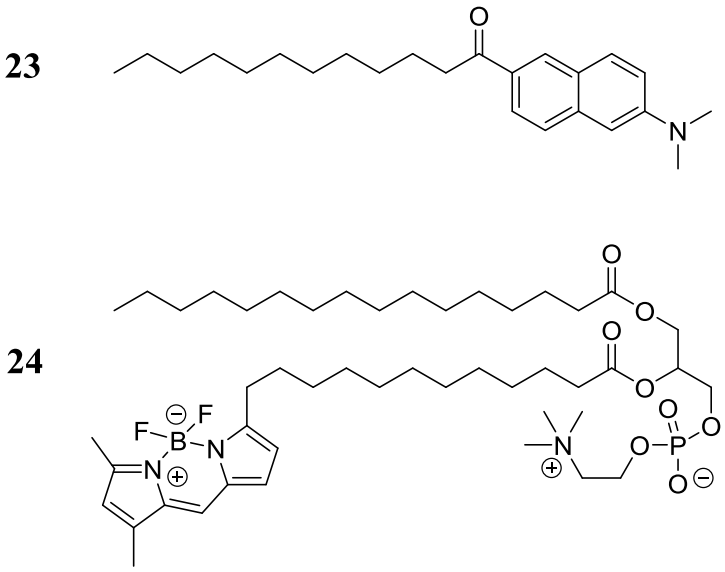

23

24

In the above cases, while the data correlate with changes in oxidized phospholipid content, there was no attempt to quantify the amount of oxidized lipid in a sample based on fluorescence measurements. Fluorescence measurements using selective chemosensors would be preferable to the mass spectrometry techniques currently employed for quantitative analysis in that it could be done on complex samples with little to no sample preparation or purification, with simple instrumentation requiring a minimum of training to operate and low maintenance expense.

3.5 Conclusion

Lipids are important for maintaining cellular structure, storing energy for future metabolic needs, and are involved in a wide variety of intercellular signaling processes. Intercellular signaling by oxidized phospholipids on the surface of LDL particles is implicated in the development of atherosclerosis, one of the leading causes of death in the United States. Early diagnosis of atherosclerosis by the detection of oxidized phospholipids could lead to better preventative treatment and reduce deaths from heart attacks and strokes.

Chapter 4: Calixarenes

4.1 Overview

Calixarenes are macrocycles formed by the condensation of equal amounts of an aldehyde and an electron-rich aromatic ring, typically a phenol. Phenolic calixarenes allow for intramolecular hydrogen bonding, which gives them the cup shape for which they are named (Figure 23). The easiest calixarenes to prepare are the 4-subunit oligomers, calix[4]arenes, although up to calix[8]arenes can be prepared with reasonable efficiency.

Figure 23 General structure of calix[4]arene.

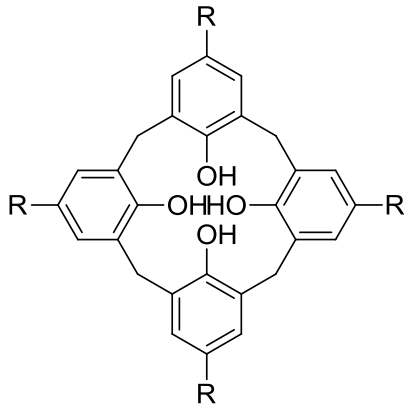

The basic calixarene motif is very versatile. In addition to substituted benzene, calixarenes have been made with pyroles,[62-64] furans,[65] (Figure 24, **25**) and naphthalenes

(**26**).[66,67] They have been used as surfactants[68,69] and phase-transfer catalysts,[70-72] molecular probes,[73] and catalysts.[74]

Figure 24 Heteroaromatic (**25**) and naphthyl (**26**) calix[4]arenes.

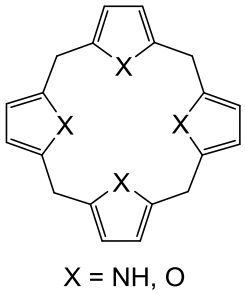

25

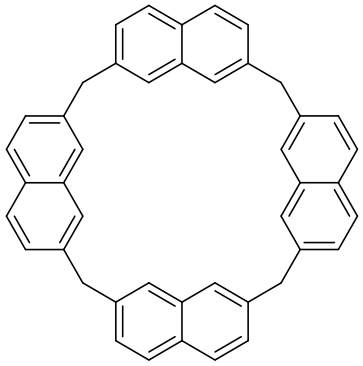

26

Calixarenes have been studied for a wide range of applications, but their pre-organized cavity has led to extensive use as molecular receptors. The cavity can either interact hydrophobically for binding non-polar molecules, including fullerenes[75,76] and hydrocarbons[77] or as an electron-donor for binding cations[78,79] and metal nanoparticles.[80]

4.2 Design of Novel Calixarene

Based on the large-cavity naphthalene-based calixarenes already reported,[66,67] the Glass group decided to extend the library of calixarenes to include the 1,8-naphthyridine compound **27** (Figure 25). Naphthyridines are too electron-poor to perform the typical aldehyde condensation used to form many other calixarenes, and so Buchwald-Hartwig

Figure 25 Structure of naphthyridine-based calix[4]arene.

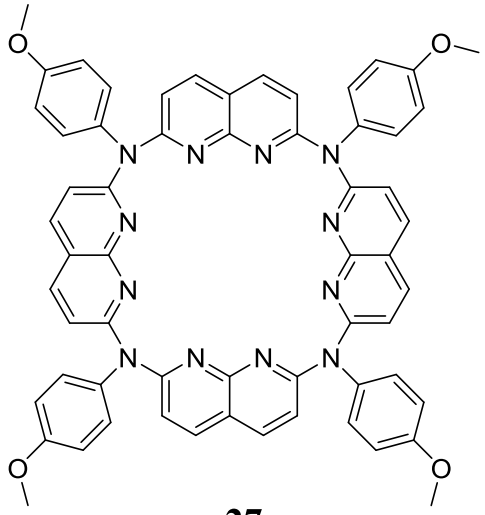

27

palladium cross-coupling was used to place a nitrogen bridge between the naphthyridine units instead of methylene.

While phenolic calixarenes have hydrogen bonds that affect the shape of the cavity, the nitrogen lone pairs of this naphthyridine-based calixarene are expected to allow cation coordination to affect the cavity geometry. Two possible binding modes include metal chelation between two adjacent naphthyridine units (Figure 26, **28**) and hydrogen-bonding by guanidinium or amidinium to both nitrogens of a single naphthyridine unit (**29**). Figures 27 and 28 show computer models of **28** and **29**, respectively, indicating the unique three-dimensional structure each complex is expected to take upon binding. In each of these figures the methoxybenzene units have been removed for clarity.

Figure 26 Metal (**28**) and amidinium (**29**) coordination to calix[4]naphthyridine.

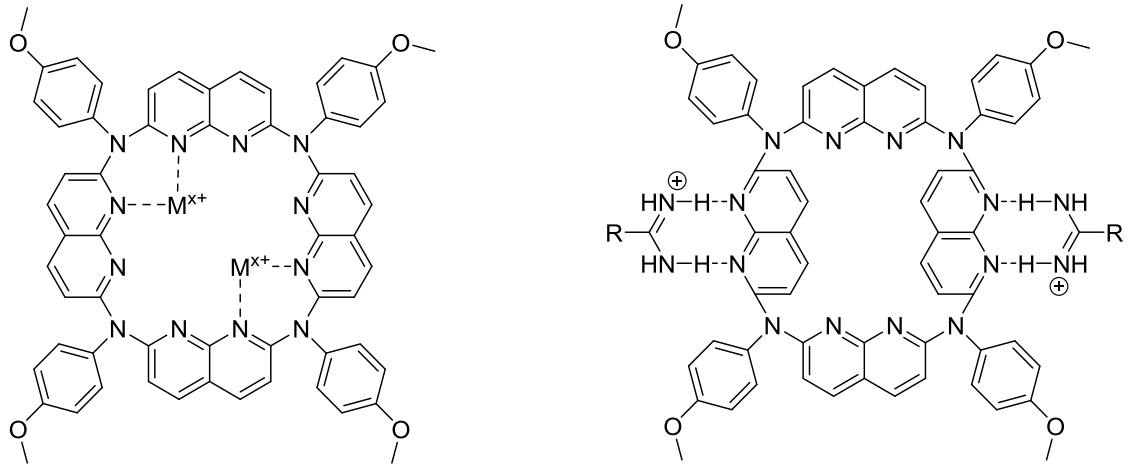

28 **29**

Figure 27 Spartan model of metal-bound calix[4]naphthyridine (**28**).

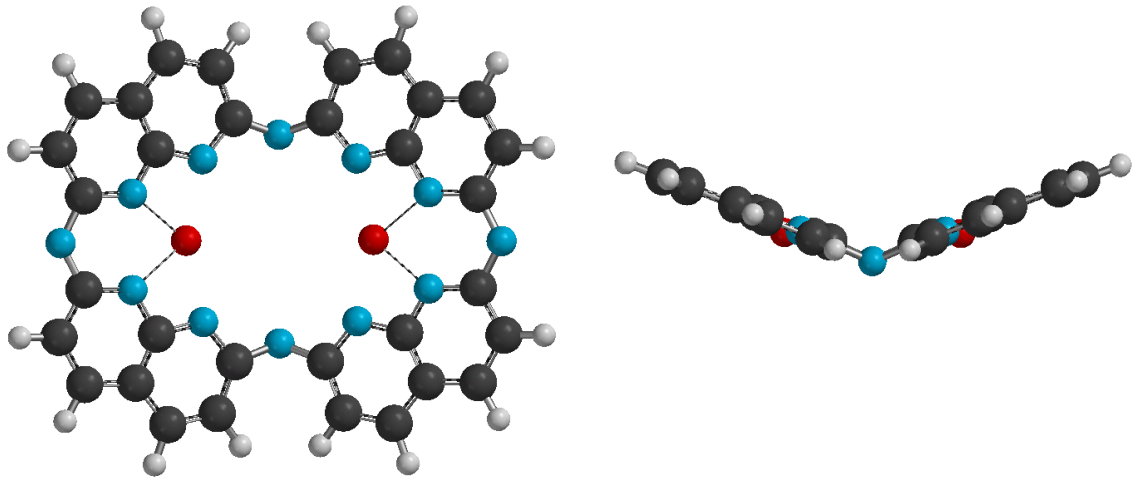

Figure 28 Spartan model of amidinium-bound calix[4]naphthyridine (**29**).

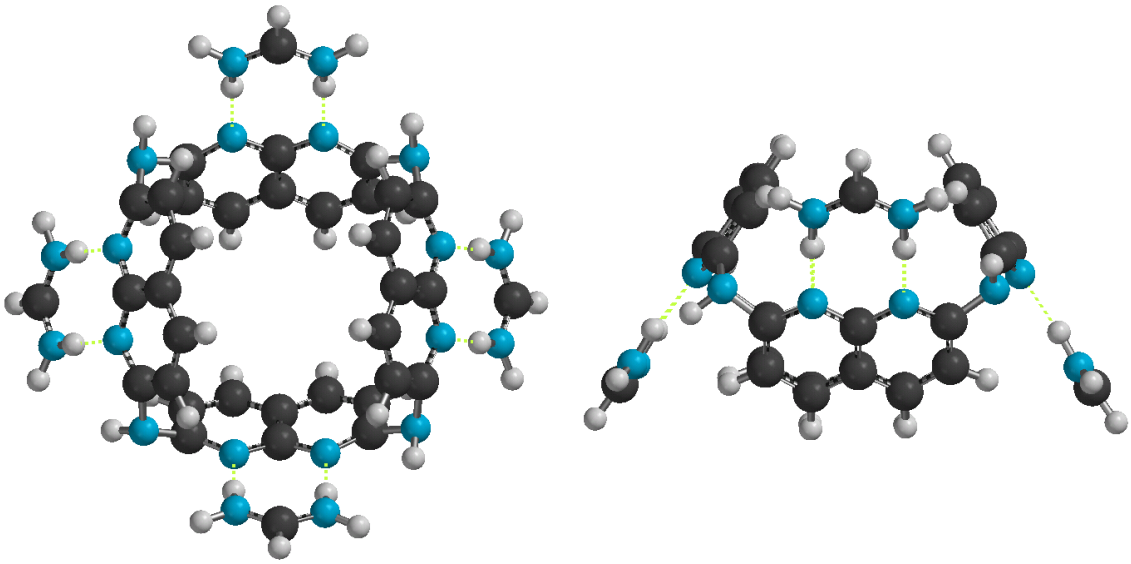

4.3 Synthesis of Naphthyridine-Based Calixarene

2,6-Diaminopyridine was combined with *d,l*-malic acid in concentrated sulfuric acid and heated to 120 °C to produce 1,8-naphthyridine **30** with greater than 90% yield. The amine was converted to a diazonium by reaction with sodium nitrite in concentrated sulfuric acid, and a water work-up afforded the 2,7-diol **31** in 85% yield (Scheme 13).

Scheme 13 Synthesis of 2,7-dihydroxy-1,8-naphthyridine

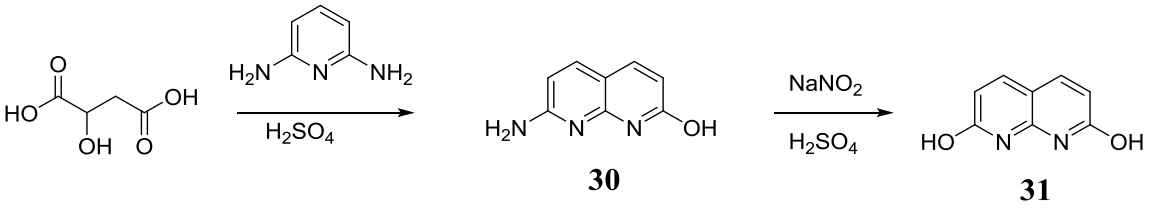

Diol **31** was reacted with phosphorus oxychloride and phosphorus pentachloride at 120 °C to afford the 2,7-dichloro compound **32** with 44% yield. Buchwald-Hartwig amination of dichloride **32** with 4-methoxyaniline, catalyzed by tris(dibenzylideneacetone)dipalladium and bis(diphenylphosphino)propane gave calixarene **27** with a yield of 10% (Scheme 14).

Scheme 14 Synthesis of calix[4]naphthyridine

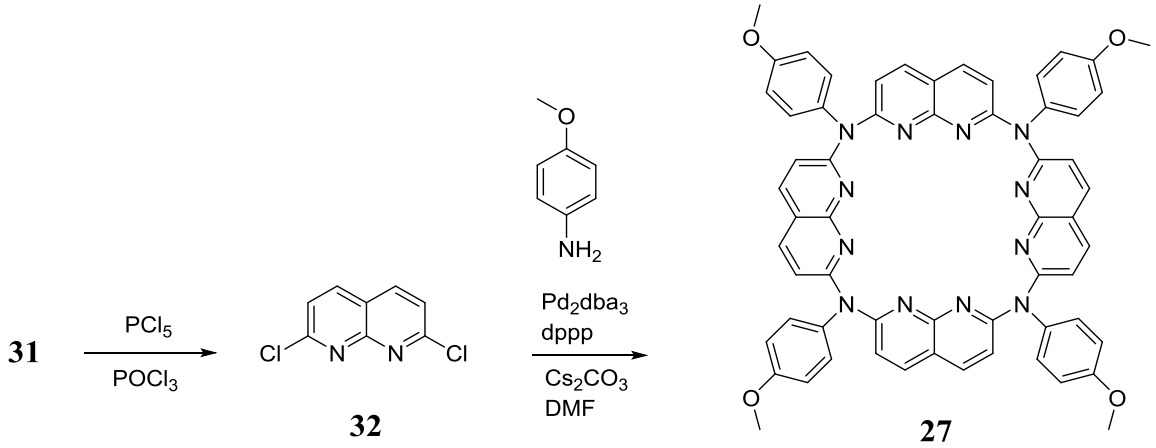

Compound **27** was recrystalized from a toluene/methanol mixture the resulting crystals were used for x-ray crystallography. The resulting structure, shown in Figure 29 with the methoxybenzene groups removed for clarity, confirms the identity of **27**. In the crystal, two of the naphthyridine units directly opposite one another are nearly parallel, while the others are splayed outward, making an approximately 100° angle with the first two naphthyridines.

Figure 29 X-ray crystal structure of calix[4]naphthyridine.

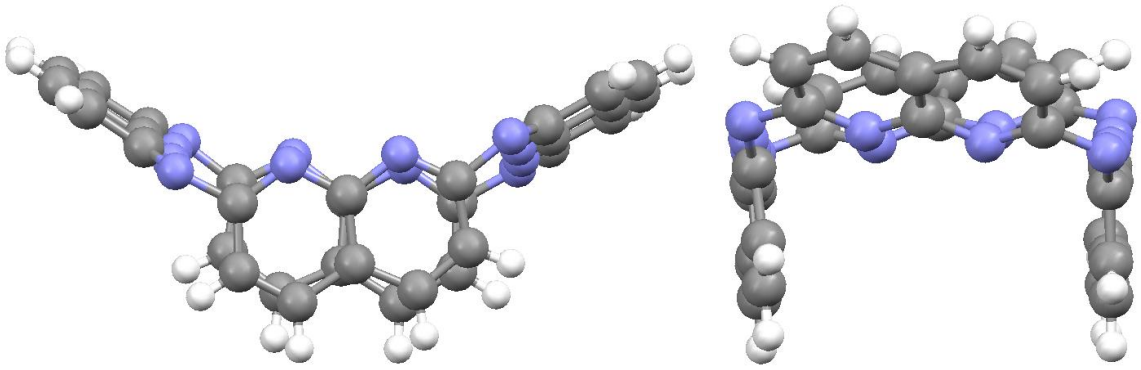

4.4 Conclusions and Future Directions

Future work on this project includes attempts to form crystals of calixarene **27** with metal salts, including copper (II) and silver (I), and hydrogen bond donors, including benzamidine, in order to examine the effects binding has on the calixarene geometry. Attempts will also be made to extend the calixarene motif to other naphthyridine derivatives.

Chapter 5: Coumarin Aldehyde Sensor for Phosphoserine

5.1 Overview

Phospholipids constitute the dominant class of lipids composing the lipid bilayer of cellular membranes and confer structural support, organization of membrane proteins, and intercellular signaling mechanisms.[81-86] Phosphatidylcholine (PC), sphingomyelin (SM), phosphatidylethanolamine (PE), and phosphatidylserine (PS) represent over 97% of the total phospholipid composition and are asymmetrically distributed between the inner and outer leaflets of a cellular membrane.[87] In quiescent cells, PC and SM constitute approximately 87% of the total phospholipid content of the outer leaflet, with PS being exclusively restricted to and comprising approximately 30% of the total phospholipid content of the inner leaflet (Figure 30). Cell death randomizes the asymmetric distribution of phospholipids between the inner and outer leaflets, thereby externalizing PS to the outer cell surface.[88–90] In fact, exposure of PS to the outer leaflet of the cellular membrane is the hallmark molecular biomarker for all types of cell death and serves as a signal for phagocytosis by providing approximately 10^6–10^9 binding sites per cell.[91]

Several methods to tag apoptotic cells and phospho-amino acid residues have appeared in the literature.[92–97] In addition to biological probes (e.g., annexin assays), the vast majority of synthetic approaches have focused on detecting anionic phospholipid

Figure 30 (a) Common cellular membrane phospholipid head groups. PC = phosphatidylcholine, SM = sphingomyelin, PS = phosphatidylserine, PE = phosphatidylethanolamine, PG = phosphatidylglycerol, PGP = Phosphatidylglucopyranose. (b) Asymmetric phospholipid composition (mol%) of the outer and inner leaflets of healthy human cellular membranes.[87]

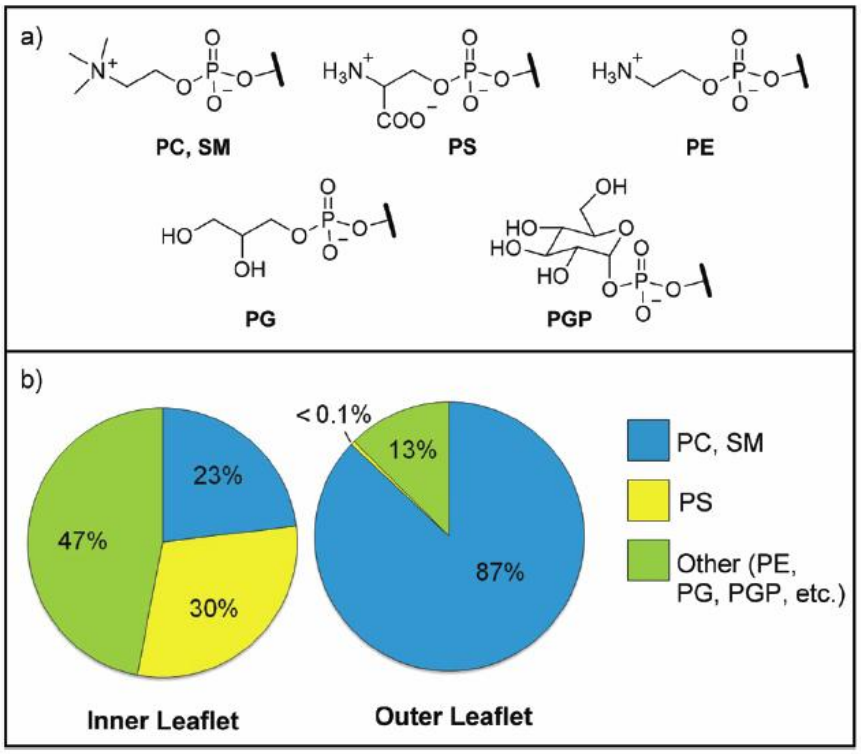

head groups, which includes phosphoserine. In particular, zinc(II)–dipicolylamine (Zn^{2+}–DPA) complexes have proven to be admirable receptors for negatively-charged lipid head groups and have been used to tag apoptotic cells as well as bacterial cells.[91,92,94,95,98,99] These primarily consist of two pre-coordinated Zn^{2+}–DPA units tethered to a synthetic fluorophore that associates with the membrane surface of apoptotic cells through strong multipoint interactions with the anionic phospholipid head groups. These molecular probes are phospholipid tags and do not operate in a turn-on fashion. By contrast, a turn-

on sensor for PS could give quantitative information about the amount of lipid present with low background as well as enable new types of experiments such as the ability to monitor the progression of cell death in a cell population.

Recently, we have been exploring the use of water-soluble shape-selective molecular tubes for hydrophobic sensing of lipids.[100] In order to build selective sensors for PS, we require a head-group binding unit. We chose to use the highly-water soluble head groups as a model system for the analyses to demonstrate sensor efficacy because the head groups are the exposed units at the cell surface and the phospholipids lack water solubility. The head groups lack the hydrophobic lipid, yet remain functionally equivalent to the phospholipids and are reasonable analogues for evaluating head group binding units. In the case of phosphoserine, both the head group and PS possess a primary amine and an anionic phosphoester. Herein, we present a fluorescent turn-on molecular sensor based on the coumarin aldehyde scaffold for the selective recognition and sensing of phosphoserine (Figure 31).[101]

Figure 31 (a) Structure of NeuroSensor 521. (b) Ditopic sensors for phosphoserine.

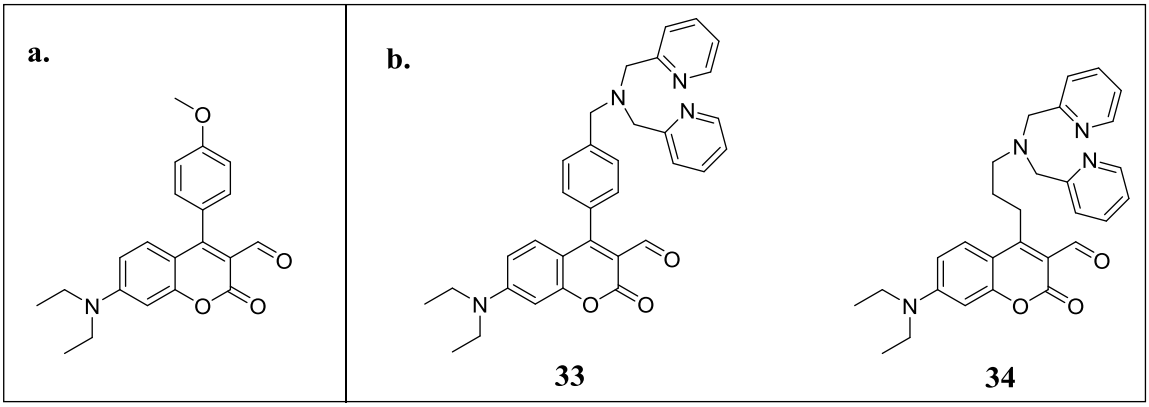

The ditopic sensors **33** and **34** consist of an aldehyde recognition element that is integrated into the coumarin fluorophore and a single Zn^{2+} –DPA recognition element appended to the coumarin scaffold to afford reversible binding to the primary amine and anionic phosphate moieties of phosphoserine, respectively (Scheme 15). The coumarin

Scheme 15 Ditopic binding of 2–Zn2+ to phosphoserine.

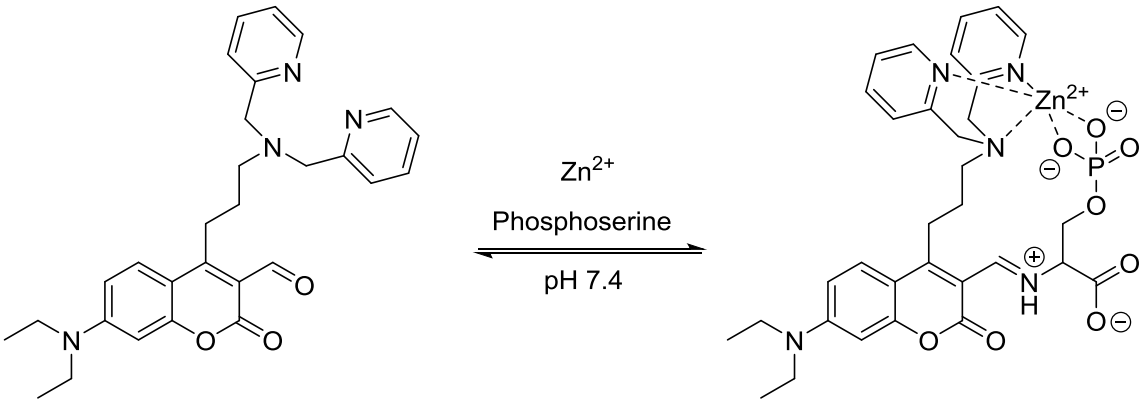

aldehyde has been shown to effectively produce a turn-on response to amine binding. Indeed, NeuroSensor 521 (NS521, Figure 31a) was developed as a monotopic receptor for catecholamines and provides a turn-on response in live cells.[102] In this study, we modified the NS521 scaffold by appending a Zn^{2+}–DPA unit to the C4 position of the coumarin with both a rigid and flexible spacer to afford sensors **33** and **34**, respectively. We hypothesized that a more rigid linker would provide stronger binding to the analyte but developed a flexible linker for comparison. Molecular models indicated that the methyl phenyl and propyl linkers would provide the optimal spacing for phosphoserine (Figure 32).

Figure 32 Spartan models of phosphoserine-bound **33** and **34.**

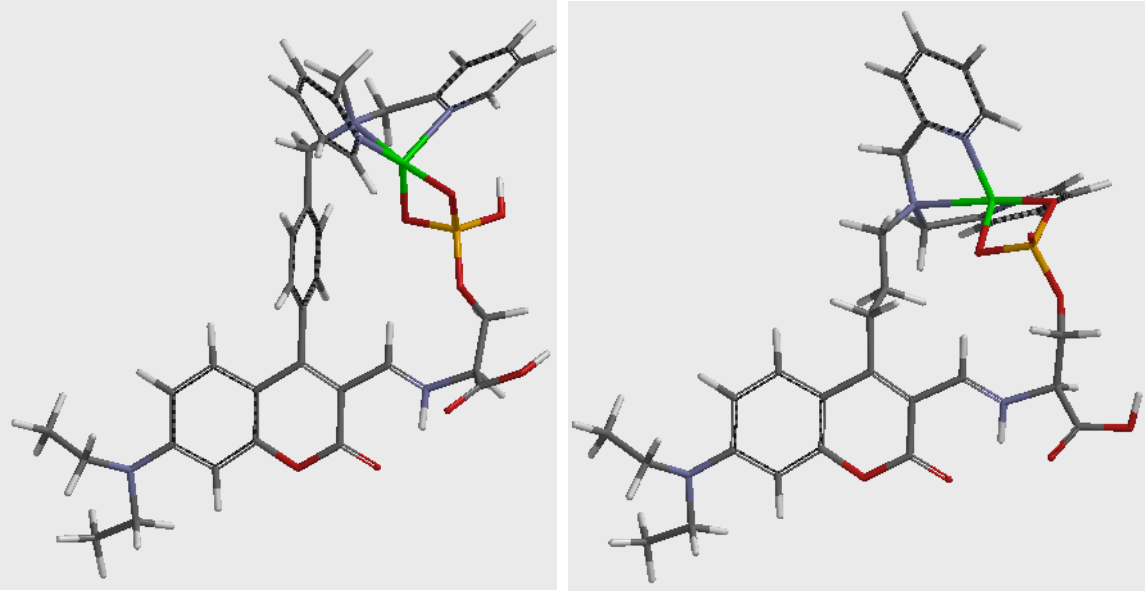

We reasoned that only phospholipid head groups with primary amines should bind to the coumarin aldehyde and form an iminium ion, which causes an approximately 40 nm bathochromic shift in absorption.[102–104] By exciting the fluorophore at this new, more red wavelength, we can visualize a fluorescence increase due only to the bound sensor. The Zn^{2+}–DPA group is likely the best receptor for phosphates in water and was incorporated to achieve selectivity.

5.2 Synthesis of Ditopic Sensors

The syntheses of sensors **33** and **34** are shown in Scheme 16 and 17, respectively. To make sensor **33**, compound **35** was coupled via its tosylate to an aryl boronic acid to produce compound **36**. Chlorination followed by formylation using the Vilsmeier reagent gave compound **38**, which was alkylated with a dipicolylamine unit to yield sensor **33**.

Sensor **34** was prepared from alcohol **39**[104] by conversion to iodide **40** followed by alkylation with dipicolylamine.

Scheme 16 Synthesis of sensor **33.**

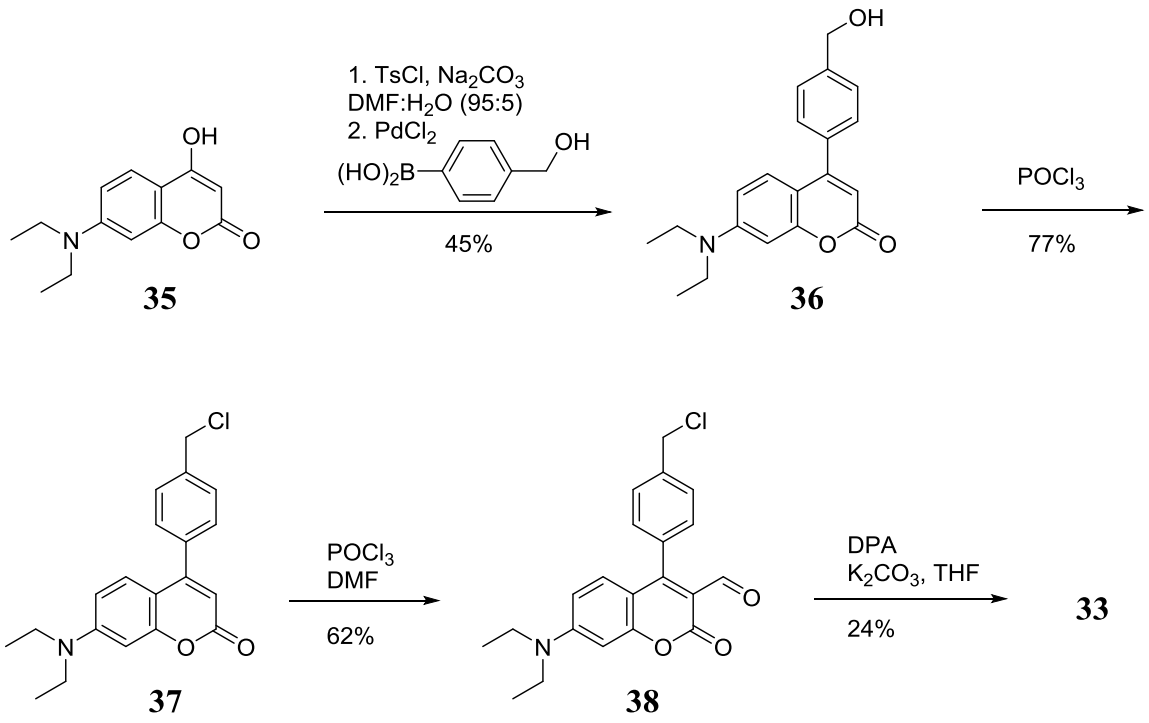

Scheme 17 Synthesis of sensor **34.**

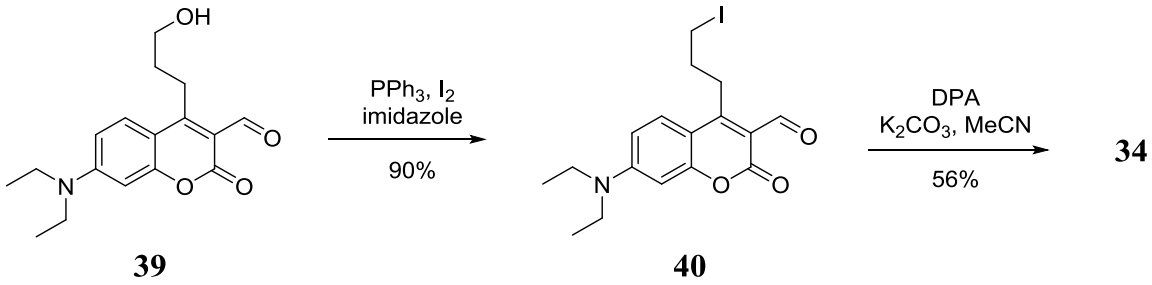

5.3 Spectroscopic Properties.

When unbound, sensor **33** absorbs at 453 nm and emits at 517 nm. The quantum yield (Φ) was measured to be 0.0125 using fluorescein as a standard.[105] Sensor **34** absorbs at 454 nm and emits at 513 nm with a quantum yield of 0.0213.

5.4 Binding Titrations.

In order to calculate association constants for sensors **33** and **34**, the concentration of analyte was plotted against $I / I_o - 1$, where I is the fluorescence intensity, I_o is the initial fluorescence intensity of sensor alone. The plotted data was fit to a one-site binding isotherm using Equation 5, where B_{max} is the theoretical maximum fluorescence

$$\frac{I}{I_o} - 1 = \frac{B_{max}[analyte]}{K_d + [analyte]} \qquad \textbf{eq. 5}$$

intensity when the sensor is saturated with analyte and K_d is the dissociation constant for the sensor-analyte complex. K_d is the inverse of K_a, defined in Equation 2.

Sensors **33** and **34** were titrated with several phospholipid head groups: phosphoserine, phosphoethanolamine, phosphocholine, α-glycerolphosphate, and D-gluco-pyranose-1-phosphate, as well as the primary amines glutamate and glycine under buffered aqueous conditions (50 mM HEPES, 100 mM NaCl, pH 7.4). Glutamate and glycine served as controls for amine binding as they lack phosphate groups. The binding and spectroscopic data are summarized in Table 1. The absorbance of **33**–Zn^{2+} shifted to

Table 1 Binding constants (K_a) and spectroscopic properties of sensors **33** and **34** with various analytes.[a]

	33		**33**-Zn^{2+} [b]		**34**		**34**-Zn^{2+} [b]	
Analyte	K_a (M^{-1})	I_{sat}/I_o [c]	K_a (M^{-1})	I_{sat}/I_o [c]	K_a (M^{-1})	I_{sat}/I_o [c]	K_a (M^{-1})	I_{sat}/I_o [c]
Phosphoserine	3.1	7.2	5.4	6.2	120	5.8	310	30
Phosphoethanolamine	5.7	4.8	5.7	4.9	93	9.1	180	39
Glutamate	4.7	7.0	7.0	4.3	22	13	190	17
Glycine	6.1	6.1	6.2	4.0	5.3	16	6.6	29

[a] Analytes of various concentrations were added to sensor (10 μM) in buffer (50 mM HEPES, 100 mM NaCl, pH 7.4). Sensor **1** was titrated in 97 : 3 buffer–DMSO and sensor **2** was titrated in 100% buffer. [b] Zinc acetate (10 μM) was pre-coordinated with sensor prior to addition of analyte. [c] I_{sat} was taken from the theoretical maximum of the binding isotherm; λ_{ex} = 488 nm; λ_{em}, **1** = 521 nm, λ_{em}, **2** = 513 nm.

488 nm upon the addition of phosphoserine, phosphoethanolamine, glutamate, and glycine. Phosphocholine, α-glycerolphosphate, and D-gluco-pyranose-1-phosphate did not bind to the coumarin aldehyde of **33**–Zn^{2+} and therefore did not alter the spectroscopic properties. All primary amine analytes bound to the coumarin aldehyde with low affinity and relatively low fluorescence enhancements (<7-fold) with emission maxima at 521 nm when excited at 488 nm. The binding results were similar to the control experiments conducted without Zn^{2+} indicating that the Zn^{2+}–DPA had little effect on enhancing analyte binding to the coumarin aldehyde. Indeed, these binding constants are similar to those achieved with simple, unsubstituted coumarin aldehydes.[102–104]

Sensor **34** displayed similar absorption properties compared to sensor **33**. The absorbance of **34**–Zn^{2+} also shifted to the red only upon addition of phosphoserine, phosphoethanolamine, glutamate, and glycine. As seen with sensor **33**, the phospholipid head groups that did not contain primary amines did not bind. The binding for phosphoserine was remarkably higher than for the other analytes tested with Ka = 310 M^{-1} (Figure 33).

For sensor **34**, the spectroscopic properties with Zn^{2+} were much more favorable than the control experiments without Zn^{2+}, though the binding constants of **34** with phosphoserine, phosphoethanolamine, and glutamate were elevated compared to the

Figure 33 (a) UV/Vis and (b) fluorescence spectra of **34**–Zn^{2+} (10 μM) with aliquots of 100 mM phosphoserine in buffer (50 mM HEPES, 100 mM NaCl, pH 7.4). λ_{ex} = 488 nm. λ_{em} = 513 nm. Inset is the fit to a binding isotherm. Titrations with phosphoethanolamine and glutamate also demonstrated reasonable affinity, though not as high as with phosphoserine. The fluorescence increased over 30-fold with the addition of both phosphoserine and phosphoethanolamine, with emission at 513 nm when excited at 488 nm.

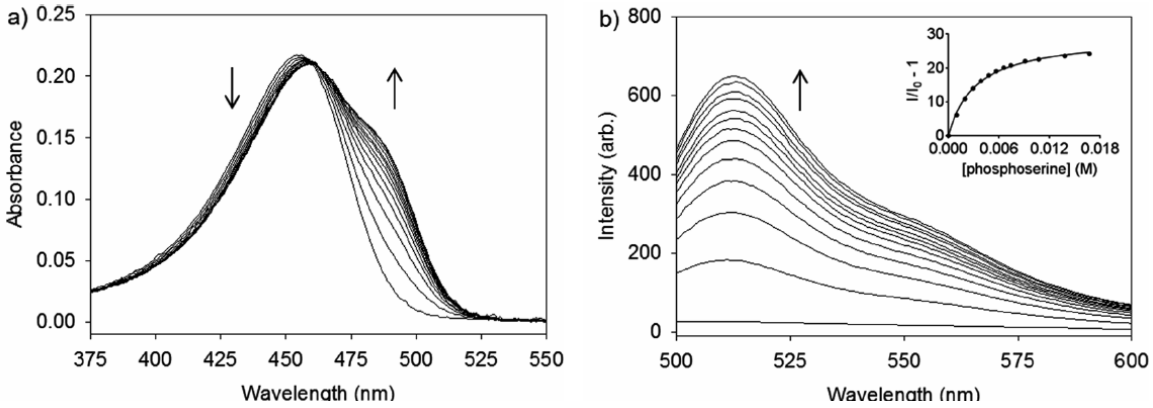

typical low binding constants seen with monotopic coumarin aldehyde sensors.[102–104] Presumably, the protonated form of the DPA can interact favorably with the charged phosphate to enhance binding. The fluorescence response of sensor **34** was lower without Zn^{2+} due to photoinduced electron transfer quenching from the uncoordinated DPA.

It is clear from the spectroscopic studies of both sensors that **34**–Zn^{2+} is the best sensor for phosphoserine both in terms of binding constant and maximum fluorescence response (Figure 34). Because of the flexible linker, **34**–Zn^{2+} demonstrated more than two orders of magnitude better binding than the more rigid sensor **33**. Clearly, the rigid structure for **33**–Zn^{2+} prohibits a two-point binding interaction. Even sensor **34** lacking Zn^{2+} was a better receptor for phosphoserine than sensor **33**.

Figure 34 (a) Binding constants and (b) fluorescence enhancements (I_{sat}/I_0) of sensors **33** and **34** with phosphoserine.

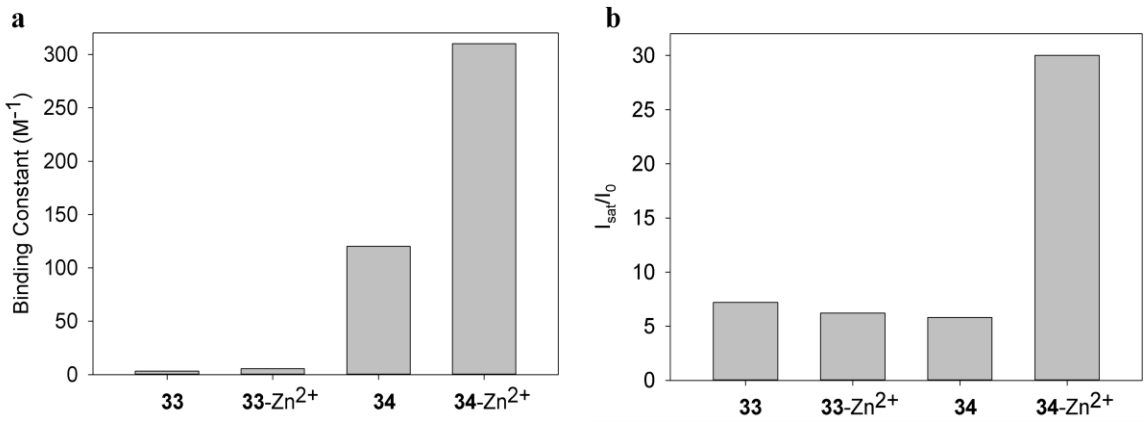

Compared to the phospholipid tagging probes, **34**–Zn^{2+} is unique in that it can coordinate to the analyte phosphate group and primary amine to achieve selective binding

to phosphoserine over other phospholipid head groups. Thus, the head groups phosphocholine, α-glycerolphosphate, and D-gluco-pyranose-1-phosphate give no response, which is extremely important since the majority of membrane phospholipids are choline-based. In addition, **34**–Zn^{2+} is also sensitive to the charge on the head group. Phosphoethanolamine and glutamate bind less effectively, as each bears one less negative charge than phosphoserine. It should be noted that while glutamate and glycine gave enhanced binding and fluorescence output, they are not expressed at high concentrations on a cellular membrane.

5.5 Conclusions and Future Directions

In conclusion, **34**–Zn^{2+} demonstrates a means to selectively sense phosphoserine over other major phospholipid head groups by forming a two-point binding interaction with the phosphate and primary amine functional groups of the analyte under buffered aqueous conditions. Future work in this area will focus on joining this head group binding unit to our lipid receptor to produce sensitive and selective sensors for bioactive lipids.

Chapter 6: Open Molecular Tube Sensor for Oxidized Phospholipids

6.1 Prior Group Work

6.1.1 Overview of Molecular Tubes

The Glass group has previously reported development of fluorescent chemosensors for the detection of saturated lipids.[100,106] These molecules were built on a naphthalene dimer scaffold (Scheme 18). Two molecules of 2,7-dihydroxynaphthalene

Scheme 18 Synthesis and 3D structure of naphthalene dimer scaffold.

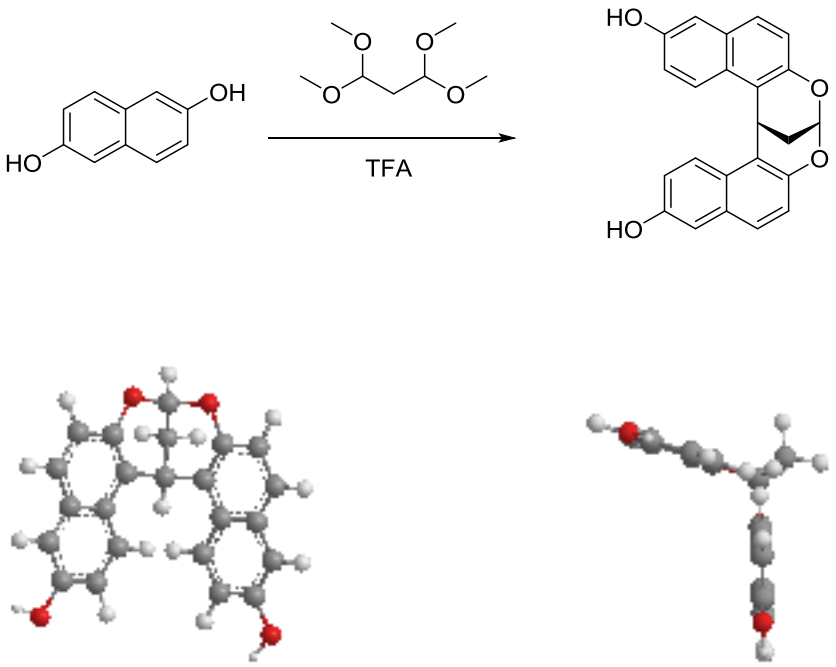

reacted with the tetramethyl acetal of malonaldehyde to form a rigid, hydrophobic pocket. Connecting two of these dimers generated a series of molecules referred to as molecular tubes (Figure 35).

Figure 35 General structure of molecular tube.

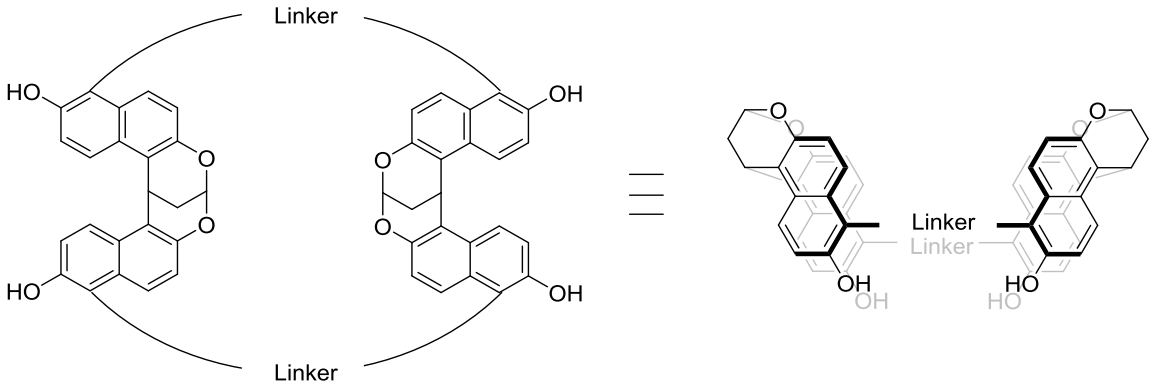

In order to avoid polymerization by reaction of acetals at both hydroxyl groups, the general synthesis of these molecular tubes began with alkylation of one hydroxyl. In order to provide water solubility for the final sensor it would be convenient to have a carboxylic acid at this position, and so alkylation to provide compound **41** was performed with ethyl bromoacetate, the ester providing better solubility during synthesis and being readily saponified in the final step of the reaction sequence (Scheme 19).

Acid-catalyzed condensation with tetramethyl malonaldehyde acetal afforded the naphthalene dimer **42**. From here, electrophilic aromatic substitution resulted in either the

Scheme 19 Synthesis of functionalized naphthalene dimers.

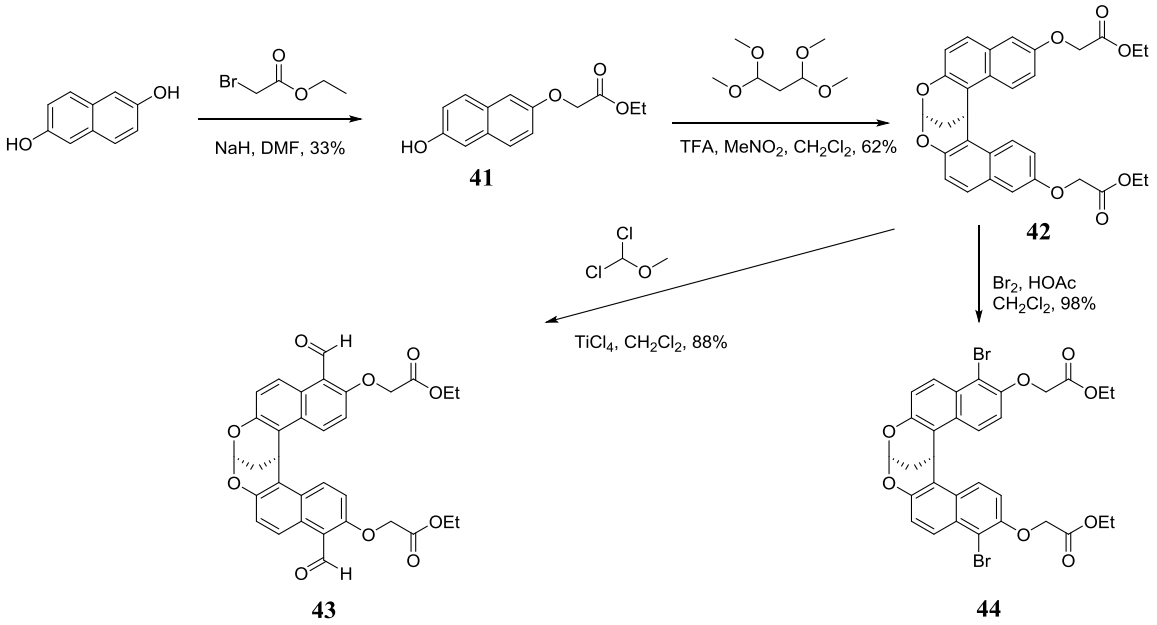

dialdehyde **43** or the dibromide **44**, which would allow for a variety of different connections to be made between the two naphthalene dimer units.

6.1.2 Amide-Linked Tube

Molecular modeling indicated that linking the two naphthalene dimers by a three-atom spacer would provide an inner diameter apporopriate for hosting a saturated alkyl chain. Relatively rigid amide and allyl linkers were chosen to enforce an open cavity for lipid inclusion. The amide-linked tube was made from two equivalents of the formylated naphthalene dimer by oxidation of the aldehyde to a carboxylic acid for one equivalent, and reductive amination to the aminomethyl for the second equivalent. A PyBOP

coupling of these two products followed by saponification resulted in the full amide-linked molecular tube **45**, which was produced as a mixture of syn- and anti-isomers, with respect to the relative orientation of the two naphthalene dimers (Scheme 20). These isomers were separated by HPLC and studied independently.

Scheme 20 Synthesis of amide-linked molecular tube.

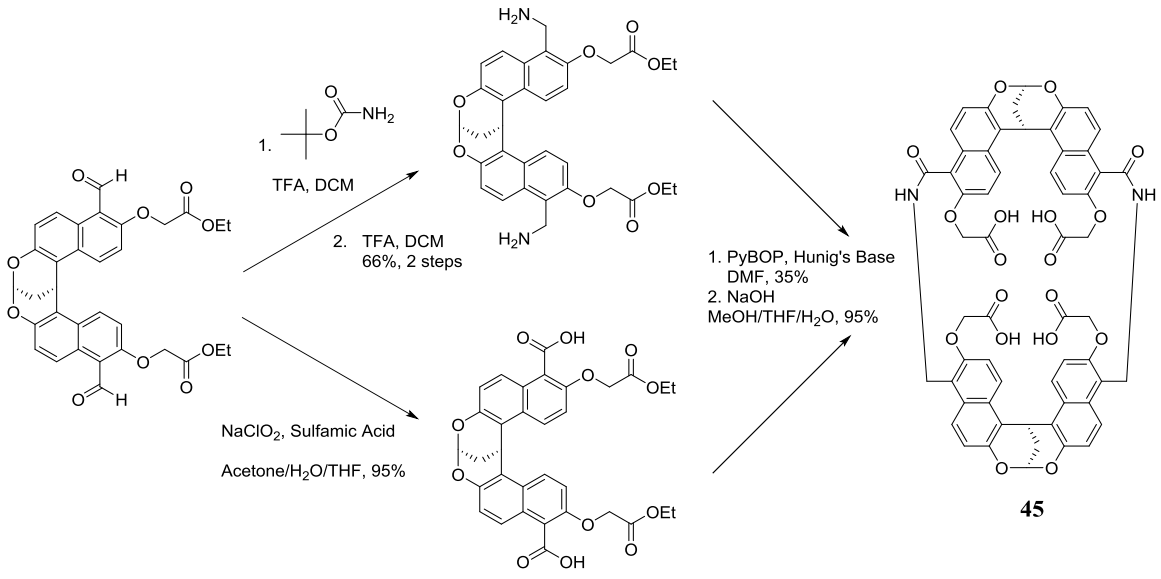

Both syn- and anti-isomers were capable of binding lipids. They showed very little change in their absorbance spectra on lipid binding, but significant changes of fluorescence from the naphthalenes was observed. In general, for both tubes, longer fatty acids showed increased binding constants, presumably due to increased van der Waals interactions over a larger surface. Neutral heptanol had an association constant that was fifty times that of hexanoic acid and a twenty-fold increase over octanoic acid, both of

which have hydrophobic surfaces similar to that of heptanol but suffer from electrostatic repulsion of the negatively charged carboxylates with those on the tube. The importance of electrostatics was further demonstrated by the fact that heptylamine, which is protonated and positively charged under the titration conditions (pH = 8.4) had a binding constant that was approximately eighty times greater than that for octanoic acid. Methyl-substituted alkyl chains and unsaturated fatty acids had lower binding constants than their straight-chain, saturated counterparts due to steric restrictions for entering the cavity of the molecular tube. These results are shown in Table 2 for both the syn- and anti-isomers of **45**.

Table 2 Binding affinities for long-chain hydrophobic analytes with amide-linked molecular tube.

	Syn Tube	Anti Tube
Analyte	**K_a (M^{-1})**	**K_a (M^{-1})**
Butyric Acid	17	18
Hexanoic Acid	100	72
Octanoic Acid	250	190
Decanoic Acid	3,500	3,800
Dodecanoic Acid	18,000	27,000
4-Methyloctanoic Acid	71	200
8-Methylnonanoic Acid	1,600	690
1-Heptanol	4,900	6,700
Heptylamine	16,000	16,000
cis -4-Hepten-1-ol	1,200	5,200
trans -3-Octenoic Acid	92	110

6.1.3 Allyl-Linked Molecular Tubes

While the amide-linked tube was relatively rigid due to the resonance of the amide bond, there was still a possibility for the tube to bow in on itself, excluding water and increasing hydrophobic interactions intramolecularly. If this was the case, the first step in binding a lipid would be to re-open the cavity, which has an enthalpic and entropic cost that would subsequently lower the association constant for the lipid. In order to avoid this problem, a more rigid linker was required.

Synthesis of the allyl-linked tube (Scheme 21) began with the brominated naphthalene dimer. Stille coupling with tributyl allyl tin afforded the allyl-substituted

Scheme 21 Synthesis of allyl-linked molecular tube.

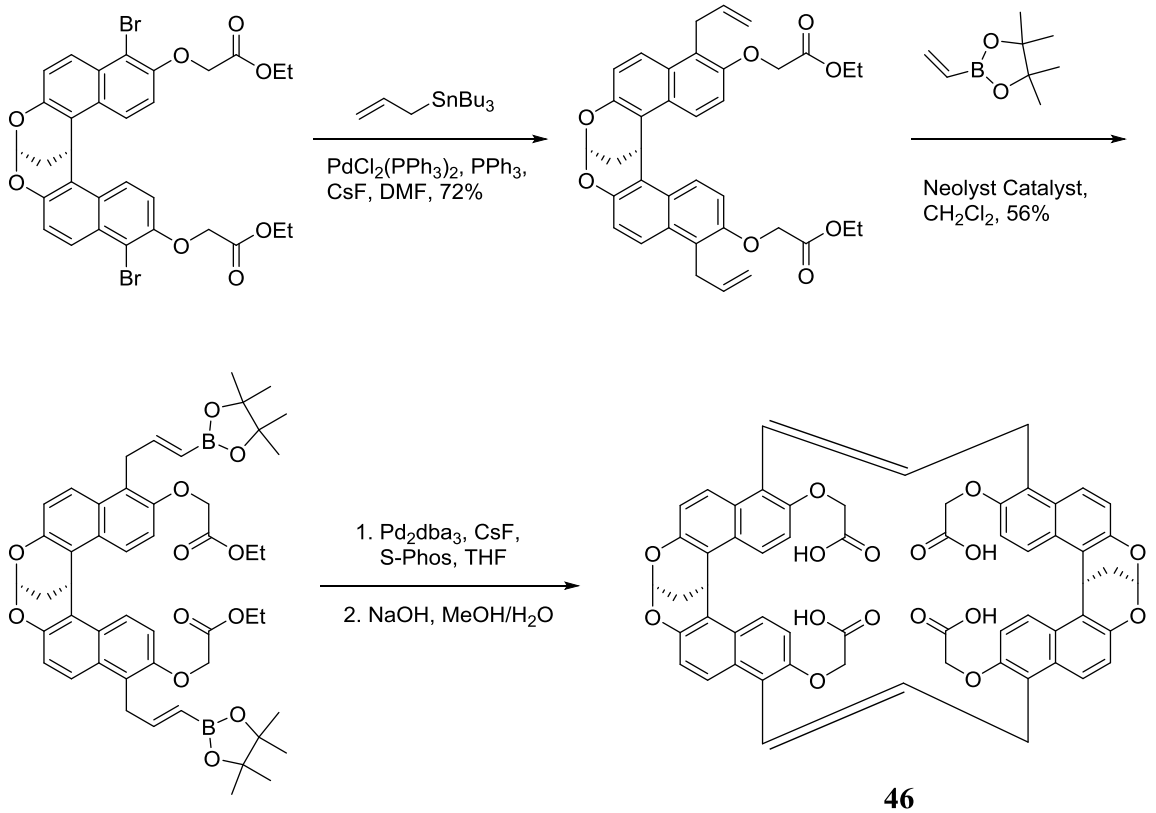

46

naphthalene dimer, which was then functionalized with a pinacol boronic ester via a cross-metathesis reaction. Suzuki coupling with the original brominated naphthalene dimer produced the allyl-linked tube, **46**, as both the syn- and anti-isomers, which were separated by HPLC.

Titration results with **46** supported the hypothesis that a more rigid linker provides a higher binding affinity. The allyl tube showed association constants of up to 5.9 x 10^5 M^{-1} for saturated fatty acids, which means that this sensor should be most sensitive to changes in concentration in the low micromolar range. These results are summarized in Table 3.

Table 3 Binding affinities for long-chain hydrophobic analytes with allyl-linked molecular tube.

	Syn Tube	Anti Tube
Analyte	**K_a (M^{-1})**	**K_a (M^{-1})**
Butyric Acid	-	-
Hexanoic Acid	800	-
Octanoic Acid	17,000	5,400
Decanoic Acid	140,000	120,000
Dodecanoic Acid	590,000	350,000
4-Methyloctanoic Acid	5,200	5,800
8-Methylnonanoic Acid	93,000	12,000
1-Heptanol	420,000	240,000
Heptylamine	2,000,000	8,200,000
cis-4-Hepten-1-ol	39,000	28,000
trans-3-Octenoic Acid	1,300	7,200

6.2 Open Molecular Tube for the Detection of Oxidized Phospholipids

6.2.1 Drawbacks to Full Molecular Tubes

The molecular tubes discussed in the previous sections both showed excellent binding affinity towards aliphatic molecules and selectivity for straight, saturated chains over branched and unsaturated chains. The rigid allyl-linked tube was particularly effective in binding lipids because it was pre-organized in the open conformation, minimizing any entropic penalty for the binding event. Unfortunately, these molecules suffered from several disadvantages, including difficulties in synthesis, poor fluorescence properties, and difficulty in further modification.

The syntheses for the closed tubes involved a macrocyclization near the end of the synthetic route. Macrocyclizations often suffer from low yields due to the loss of entropy required to close the ring and competition with intermolecular reactions that lead to oligomers. A further problem with this particular macrocyclization was the fact that two isomers of the tube were formed, syn and anti, which severely restricted the yield of the more desirable syn-isomer.

The other significant drawbacks to the full tube sensors are due to the naphthalene dimers that formed the core of the tube. The naphthalene fluorophores used in the molecular tubes showed relatively small changes in fluorescence upon binding lipid. This problem was compounded by the fact that the excitation maximum for the fluorophore was in the ultraviolet range and the fluorescence was in the violet region, where a number of endogenous chromophores and fluorophores absorb and emit in biological samples, which would lead to high background signals.

Finally, the naphthalene units were already substituted at four positions, and during synthesis, approach from the face of the dimer that was inside the hydrophobic cleft was crowded by the adjacent naphthalene. Further modification was hindered by these steric interactions, and without such modification it was impossible to develop sensors capable of selectivity for one type of saturated lipid over another. Since we were interested in developing chemosensors for a number of different types of lipids, including phosphatidylserine, cerebrosides, glycolipids, and oxidized phospholipids, it was important to have some way of functionalizing the tube with different recognition elements for these different analytes.

6.2.2 Benefits of Open Tubes

Our approach to overcoming the difficulties with the molecular tubes is shown in Figure 36. By making the tube an open structure, we could avoid several problems and open up opportunities that were not available with the closed tubes.

Figure 36 General structure of open molecular tube.

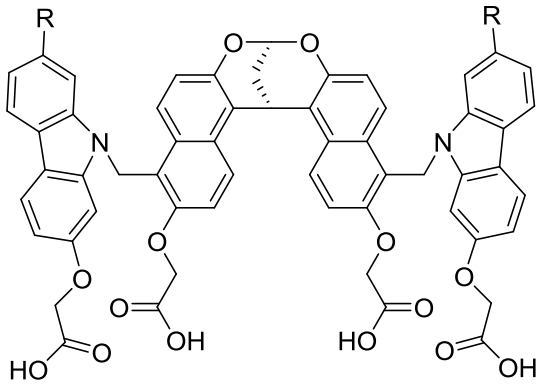

The open structure avoids the macrocyclization problem, which limited yield due to entropic factors, unwanted oligimerization, and syn-/anti-isomer production. This has the possibility to greatly improve yield in the final steps of the synthesis. It also allows for different fluorophores to be attached to the naphthalene dimer, giving improved fluorescence properties over naphthalene itself. These fluorophores can be constructed independently of the dimer core of the tube, allowing for functional groups to be installed that can selectively recognize one type of lipid over another, such as boronic acids for glycolipid head groups.

The main drawback to the open structure is the loss of pre-organization that was present in the rigid full tubes. This would likely lead to lower binding constants for the aliphatic portion of the lipid, but binding to the second recognition element (R in Figure 36) by the headgroup or some other portion of the lipid should overcome some of the lost association affinity.

6.2.3 Design of Oxidized Phospholipid Sensor

The core of the open tubes remained the naphthalene dimer, made in the same way as shown in Scheme 19. Carbazole was chosen as the fluorophore due to having longer wavelengths of absorbance and emission than naphthalene, an easy method to attach it to the core, and the possibility to build a number of carbazoles that are functionalized at different positions.

For the detection of oxidized phospholipids, a recognition element was required that was selective for the aldehyde of the cleaved lipid chain over other, more common

functional groups. For this purpose a hydrazide was chosen. Hydrazides and hydrazines have been used for the identification of aldehydes and ketones in qualitative organic analysis and fluorescent hydrazine derivatives have seen recent use in the detection of ketones and aldehydes in biological samples.[107-110]

The design and expected sensing mechanism of sensor **47** is shown in Scheme 22. While the carbazole hydrazide is unbound, the carbazole's fluorescence would be quenched by photoinduced electron transfer (PET) from the lone pair of the terminal

Scheme 22 Proposed mode of sensing for oxidized phospholipids.

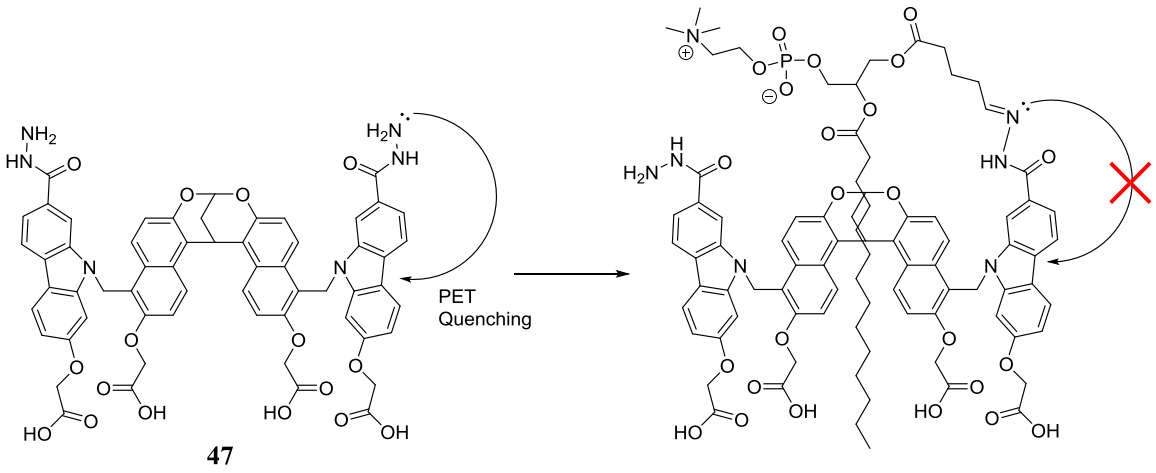

47

nitrogen. On encountering an oxidized phospholipid, a hydrazone would be formed between the aldehyde and terminal nitrogen of the hydrazide. This would change the hybridization of the nitrogen lone pair orbital from sp^3 to sp^2, leading to greater stability

for the electrons and less propensity to participate in PET quenching. Hydrazone formation with an oxidized phospholipid should therefore increase fluorescence intensity of the carbazole, and thus **47** was expected to be a turn-on sensor.

6.2.4 Synthesis Carbazole Hydrazide

The synthesis of the naphthalene dimer core was identical to that shown in Scheme 19, leading to the formylated dimer **43**. The carbazole fluorophore was synthesized beginning with 4-chloro-3-nitrophenol, which was alkylated with ethyl bromoacetate to give **48**. A Suzuki coupling with 4-formylphenylboronic acid gave the biphenyl **49**, which underwent a reductive cyclization with triphenylphosphine to give the carbazole **50** in good overall yield (Scheme 23).

Scheme 23 Synthesis of carbazole aldehyde with ethyl ester.

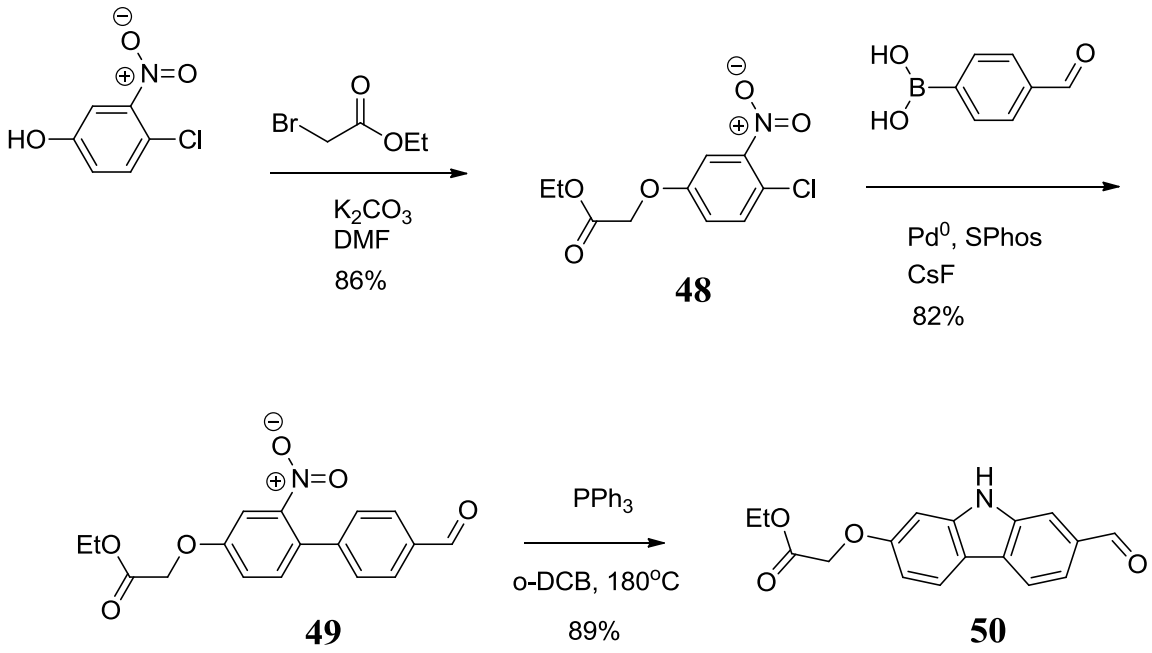

As a proof-of-concept, carbazole hydrazide **53** was synthesized independent of the core to test aldehyde recognition (Scheme 24). The carbazole nitrogen was first alkylated with 1-iodobutane, followed by oxidation of the aldehyde to **52**. A number of oxidation conditions were explored. Sodium chlorate led to chlorination of the carbazole by electrophilic aromatic substitution. Treatment with Oxone resulted in loss of the carbonyl carbon, likely due to Baeyer-Villiger oxidation to the formate ester followed by decomposition. Pyridinium dichromate (PDC) provided up to 25% of the product carboxylic acid and returned 75% starting material. Chromic acid gave complex mixtures. Finally, potassium permanganate in acetone at 0^{o} C afforded product **52** with 78% yield. The carboxylic acid was converted to hydrazide **53** using an EDC coupling.

Scheme 24 Synthesis of carbazole hydrazide.

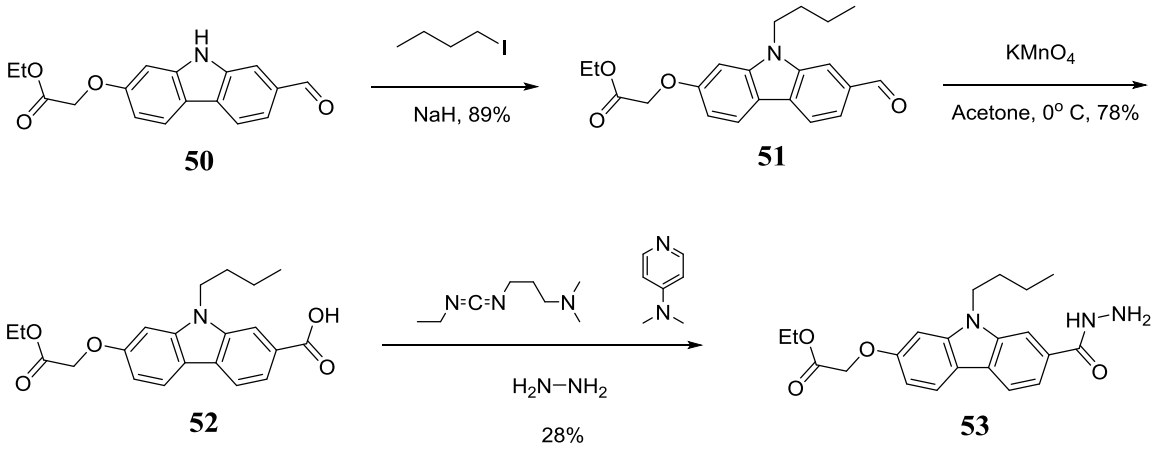

Carbazole **53** was titrated with propanal in HEPES buffer at pH 7.4 with 100 mM NaCl (Figure 37). Increasing concentration of aldehyde increased the fluorescence of the

carbazole, as expected. The binding constant was relatively weak (3.9 M^{-1}), but in the full sensor the main contribution to binding will come from the hydrophobic effect between the saturated alkyl chain of the lipid and the interior of the open tube. Once the lipid chain is bound, the high effective concentration of aldehyde near the sensor will ensure formation of the hydrazone and cause a change in fluorescence.

Figure 37 Fluorescence titration of **53** with propanal in HEPES buffer.

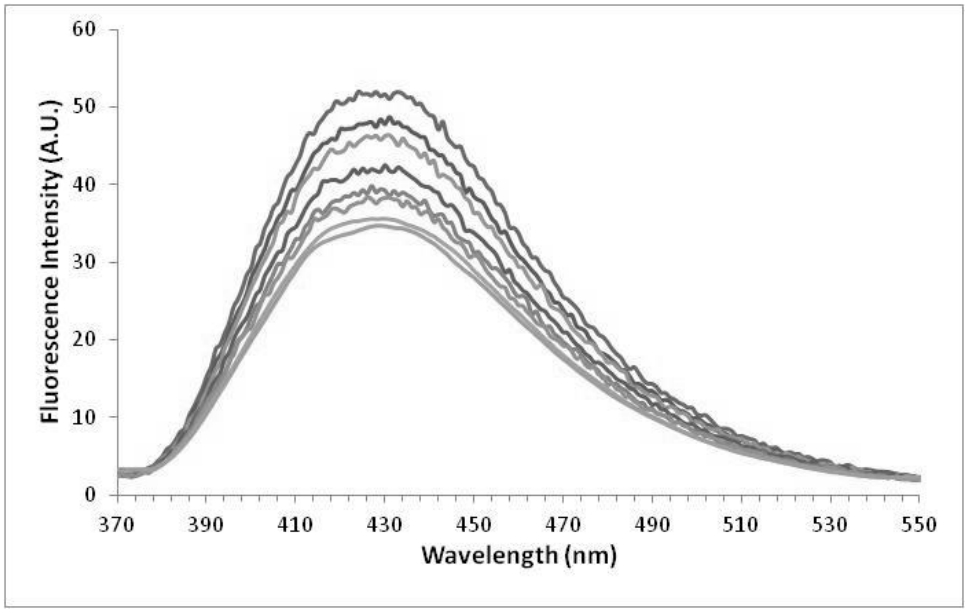

6.2.5 Synthesis of Open Tube

In order to connect the carbazole to the core, the formylated naphthalene dimer was reduced to the alcohol with sodium borohydride, followed by substitution to the benzyl bromide with phosphorus tribromide (Scheme 25). Nucleophilic substitution by

Scheme 25 Synthesis of open molecular tube **56**.

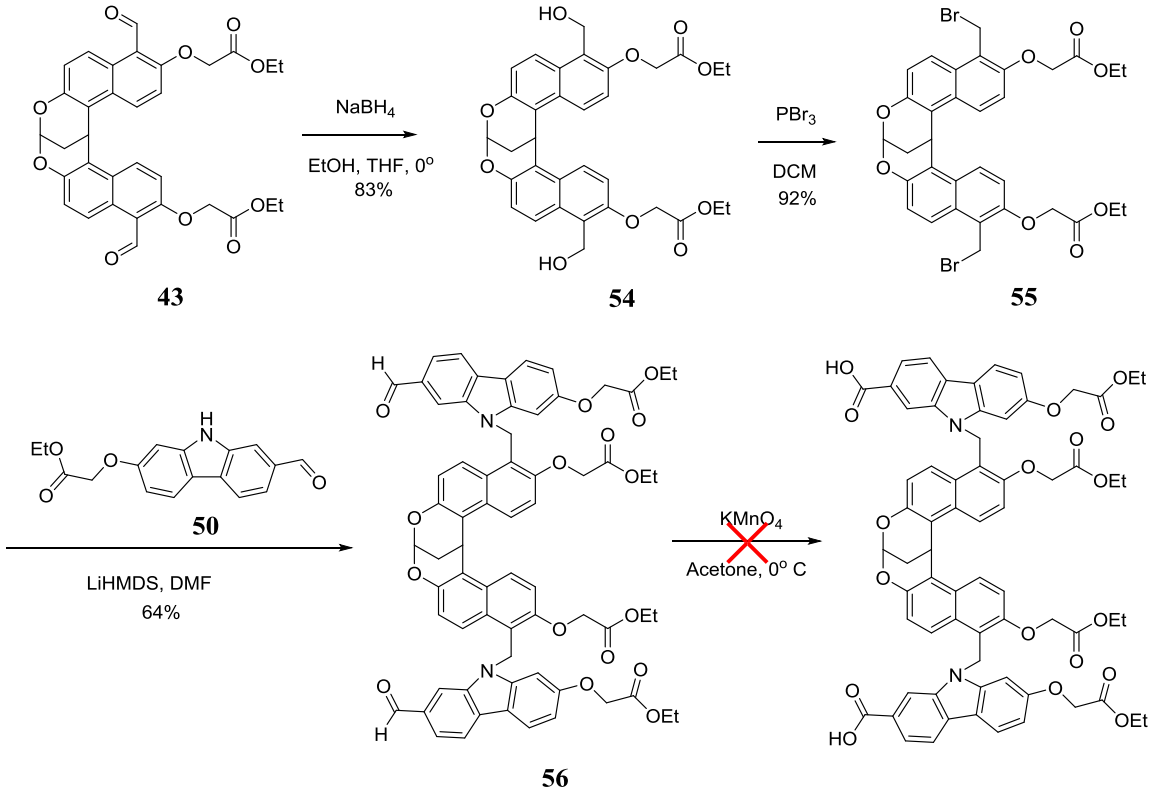

carbazole on the bromomethyl core was done using lithium bis(trimethylsilyl)amide (LiHMDS) to afford the open tube **56**.

Oxidation of the open tube aldehyde was attempted, but only returned starting material due to its poor solubility. The open tube with ethyl esters was not readily dissolved in any solvents explored except DMF and DMSO. Due to the difficulty of working with compounds with low solubility, the synthesis was restarted with hexyl esters instead of ethyl esters on both the naphthalene and the carbazole (Scheme 26 and Scheme 27).

Scheme 26 Synthesis of carbazole aldehyde with hexyl ester.

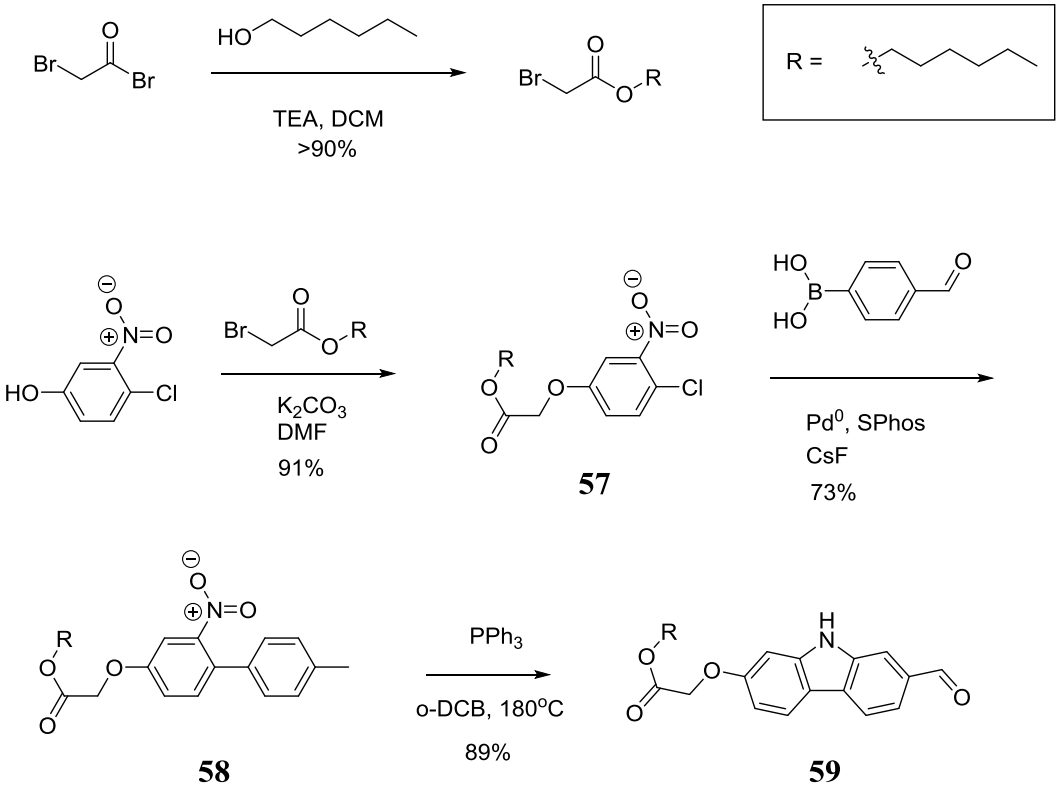

The hexyl ester compounds showed increased solubility in organic solvents at every stage of the synthesis. Unfortunately, once the carbazole was attached to the naphthalene core to form **65**, the solubility of the resulting open tube was still poor in most solvents. Reaction with potassium permanganate in acetone at 0^{o} C still resulted in only returned starting material due to poor solubility of the open tube. Attempting the reaction at room temperature, where the solubility of the open tube was still very low, resulted in a complex mixture of oxidation products.

Scheme 27 Synthesis of open molecular tube **65**.

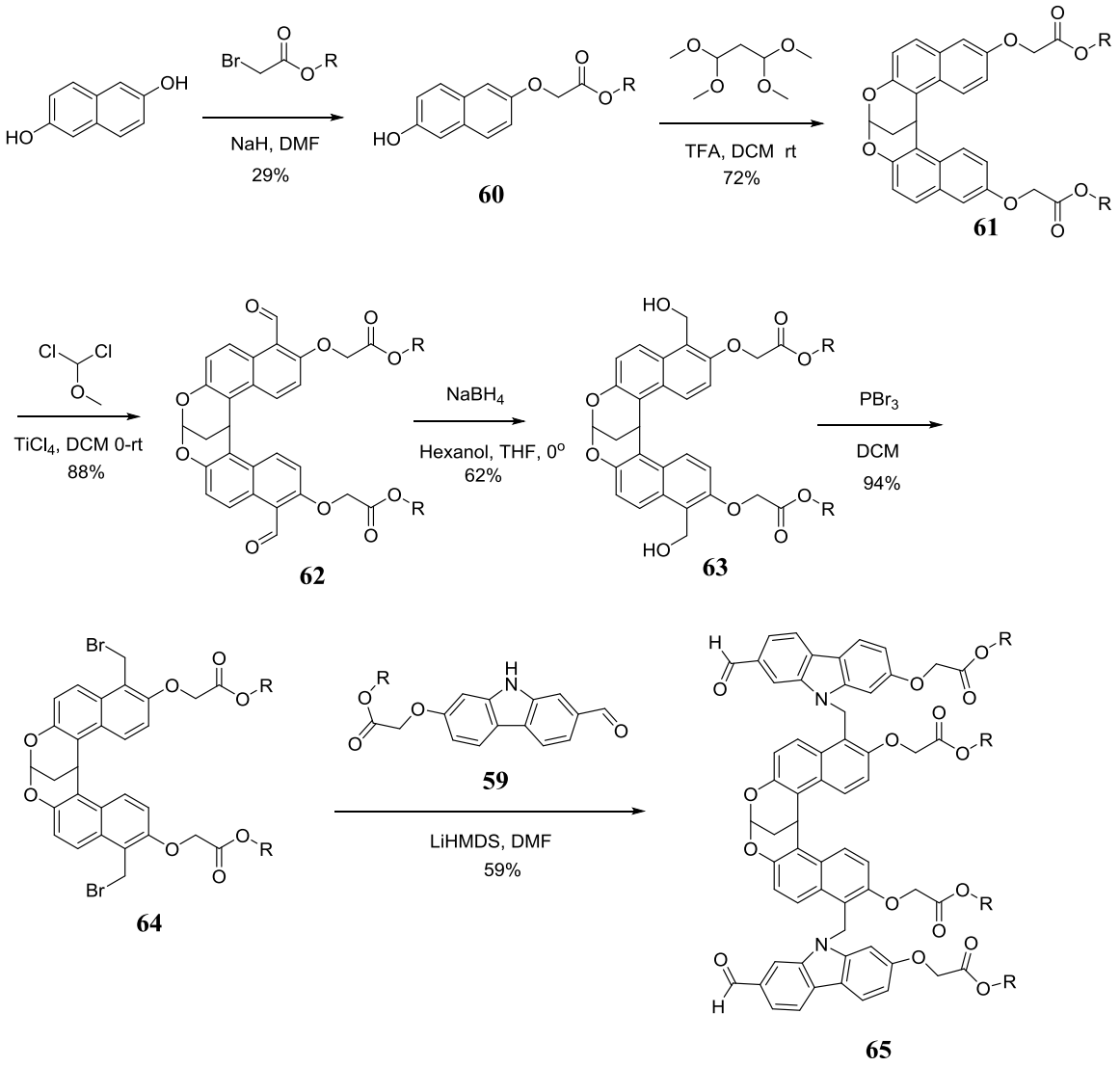

Due to the difficulty in oxidizing the open tube aldehyde **65**, we attempted to make the hydrazone instead of the hydrazide to determine if it could perform as a sensor for oxidized phospholipids by generating the dihydrazone. To this end, the esters of **65**

were converted to the carboxylic acids by saponification, and the resulting tetracarboxylic acid was treated with a large excess of hydrazine hydrate to produce the final sensor, **67** (Scheme 28).

Scheme 28 Synthesis of hydrazone-functionalized open molecular tube.

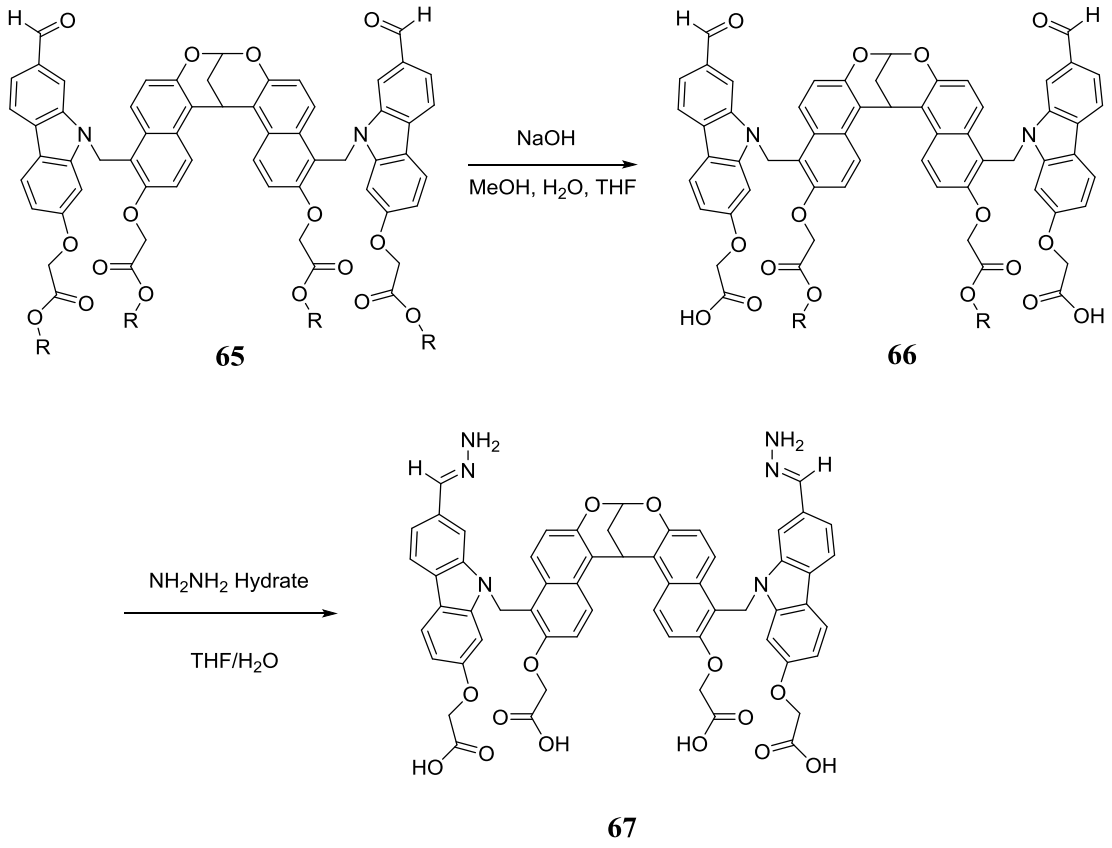

65 **66** **67**

Titrations of **67** were performed with hexanal in citrate buffer. The results of our titrations can be seen in Figure 38. The fluorescence band at 393 nm decreased and a new band appeared at 450 nm as the concentration of hexanal was increased. The titrations

Figure 38 Fluorescence titration of **67** with hexanal in citrate buffer.

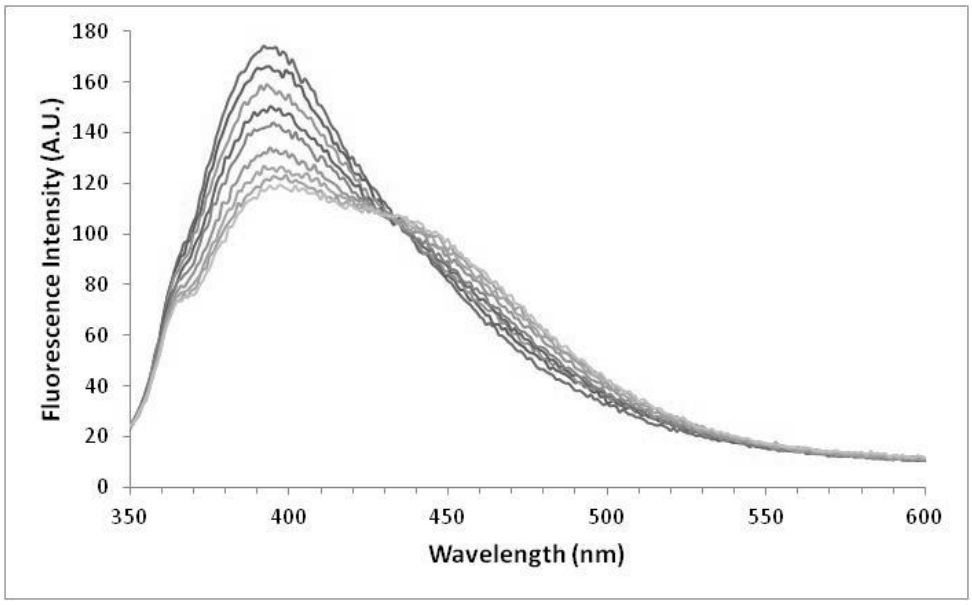

were performed at the relatively low pH of 5.5 due to the fact that hydrazone formation is significantly more favorable at this pH. Others have reported virtually no hydrazone formation at neutral pH when attempting to conjugate fluorophores onto biomolecules.[108,110]

The results fit a binding isotherm with an equilibrium constant of 51 M^{-1}. By comparison, the full, rigid allyl-linked tube had a binding constant for hexanoic acid of 800 M^{-1}, and the less rigid amide-linked tube had a binding constant of 100 M^{-1}. Our result was in line with this data, as the lipid binding would be expected to be weaker in the open tube due to the reduced degree of pre-organization/greater degree of freedom in the open carbazole arms. Further experiments on **67** were performed with decanal, but

due to its very low solubility in water no reliable data could be gathered. Titrations were also performed in 10% DMSO/citrate buffer at pH 5.5 (Figure 39), which demonstrated a significantly lower association constant of 11 M^{-1}, indicating the importance of the hydrophobic interaction to the binding affinity of the open tube for aliphatic aldehydes.

Figure 39 Fluorescence titration of **67** with hexanal in 10% DMSO/citrate buffer.

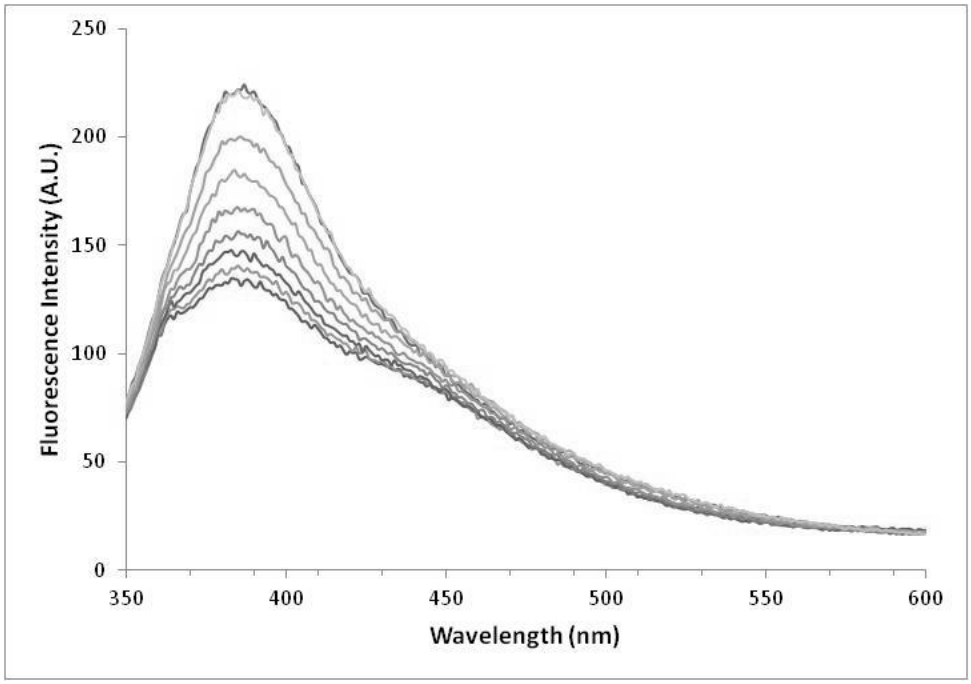

Due to the short chain length of hexanal, it was possible that the majority of the molecule was buried inside the hydrophobic cavity and there was relatively little interaction between the aldehyde and hydrazone. To explore this possibility, we synthesized the succinic dihydrazide hydrazone by reaction of the saponified open tube aldehyde with a large excess of succinic dihydrazide in DMSO (Scheme 29). The

Scheme 29 Synthesis of succinic dihydrazide hydrazone open molecular tube **68**.

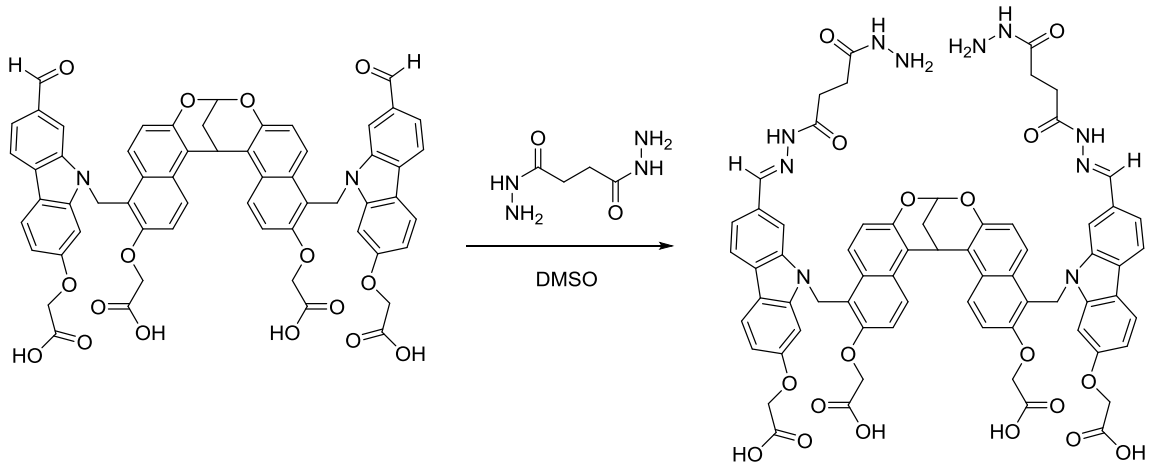

66 **68**

hypothesis was that the flexible linker now present between the fluorophore and terminal hydrazide nitrogen would allow the short hexanal to maximize its hydrophobic interaction inside the cavity while maintaining contact with the hydrazide, which could bend around towards the hydrophobic cavity, in order to form the new hydrazone. Unfortunately, the dihydrazide hydrazone sensor, while stable on its own in buffer, was not photostable in the presence of hexanal, and so no reliable data could be gathered.

6.3 Conclusions and Future Directions

The titration results for the open molecular tube hydrazone **67** show promise for the use of hydrazide- and hydrazone-bearing molecular tubes for the recognition of oxidized phospholipids. Future work on this project will include further attempts at oxidizing the aldehyde-bearing open molecular tube to the dicarboxylic acid in order to generate the original proposed sensor **47**. We will also attempt to create a protected

carbazole hydrazide, **69** (Figure 40), to attach to the naphthalene dimer core, followed by deprotection of hydrazide and esters to give the original target sensor **47**. In addition, we are also exploring alternative ways to attach hydrazines or hydrazides to the carbazole arm, as well as other possible fluorophores that would still promote binding.

Figure 40 Carbazole ester with alloc protecting group.

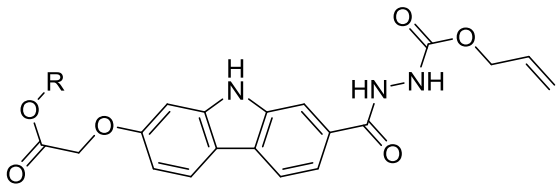

69

APPENDIX

EXPERIMENTAL PROCEDURES

Instrumentation

Absorption spectra were recorded on a Cary 1E spectrophotometer at 25 °C. Fluorescence spectra were recorded on a Shimadzu RF-5301 PC spectrofluorometer at 25 °C. NMR spectra were recorded on Bruker DRX 500 or Bruker DRX 300.

Solution preparation: Phosphoserine Sensors

Solutions for UV/Vis and fluorescence spectroscopy were prepared from a 1 mg mL^{-1} sensor stock solution in MeOH that was diluted to volume with buffer (50 mM HEPES, 100 mM NaCl, pH 7.4) until a 10 μM sensor solution was produced following removal of the solvent. For sensor 1, DMSO was added to equal 3% of the total volume to improve solubility. Analytes were measured and diluted to volume with the buffered sensor solution to keep the sensor concentration constant throughout the titration.

Solution preparation: Oxidized Phospholipid Sensors

Solutions for UV/Vis and fluorescence spectroscopy were prepared from a 1 mg mL^{-1} sensor stock solution in DMSO that was diluted to volume with buffer (10 mM citrate, no salt, pH 5.5) until a 10 μM sensor solution was produced following removal of the

solvent. Analytes were measured by volume and diluted to volume with the buffered sensor solution to keep the sensor concentration constant throughout the titration.

Quantum yields

Separate stock solutions of sensors 1 and 2 (10 μM) in buffer (50 mM HEPES, 100 mM NaCl, pH 7.4) were prepared. The solution of sensor 1 contained 3% (v/v) DMSO as a cosolvent. For quantum yields (Φ_{fl}), a 1.0 μM solution of fluorescein (absolute Φ_{fl} = 0.85) in 0.1 N NaOH (pH 13) was used as a fluorescence standard. Sensors 1 and 2 were excited at 473 nm. The slit width was 2 nm for both excitation and emission. Quantum yields were obtained in triplicate.

Binding constant calculations

The concentration of analyte was plotted against the fluorescence intensity and fit to a one-site binding isotherm.

Synthetic procedures

General methods

All reactions were carried out in dried glassware under a blanket of N_2. Before use, tetrahydrofuran and diethyl ether were distilled from sodium benzophenone ketyl while dichloromethane and triethylamine were distilled from CaH_2. NMR spectra were recorded on Bruker DRX 500 or Bruker DRX 300. IR spectra were recorded on a Nexus 670 FT-IR E.S.P.

spectrometer.

Materials

All chemicals were obtained from Sigma Aldrich, Fisher Scientific, Combi-Blocks, TCI America, or Alfa Aesar and were used without further purification. Flash chromatography was performed with 32–63 μm silica gel obtained from Dynamic Adsorbents.

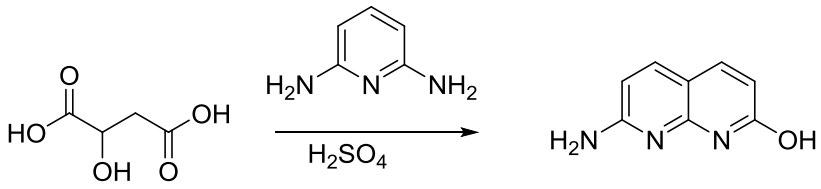

30

Compound 30:

2,6-Diaminopyridine (10.0 g, 91.6 mmol) and *d,l*-malic acid (13.5 g, 100.8 mmol) were added to a flask and cooled to 0 °C. Concentrated sulfuric acid (50 mL) was added and the mixture was warmed to room temperature, then heated to 120 °C under N_2 for 2.5 hours. The mixture was poured over ice and made basic with saturated ammonium hydroxide to pH 8, then filtered and rinsed with water. The reaction consistently produced naphthyridine **30** in greater than 90% yield.

^{1}H NMR (300 MHz, $CDCl_3$): δ 11.5 ppm (s, 1H), 7.61 ppm (d, J = 9.3 Hz, 2H), 6.73 ppm (s, 2H), 6.31 ppm (d, J = 8.5 Hz, 1H), 6.08 ppm (d, J = 9.2 Hz, 1H).

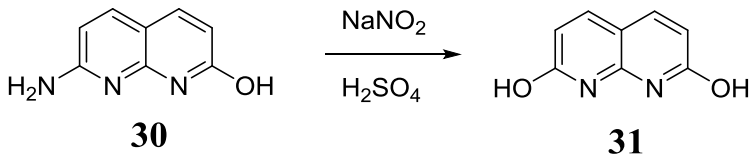

30 **31**

Compound 31:

Naphthyridine **30** (14.67 g, 91.03 mmol) and sodium nitrite (10.345 g, 149.9 mmol) were dissolved in concentrated sulfuric acid (150 mL) and stirred at room temperature for 10 minutes. The mixture was poured over ice and stirred for another 20 minutes. The reaction was made basic with sodium hydroxide (10M solution), then acidified to pH 5 with glacial acetic acid. Product was filtered and rinsed with water, followed by ethanol, and then dried under vacuum to afford diol **31** (12.59 g, 77.7 mmol, 85.3% yield).

^{1}H NMR (300 MHz, $CDCl_3$): δ 11.6 ppm (s, 2H), 7.81 ppm (d, J = 9.0 Hz, 2H), 6.34 ppm (d, J = 9.0 Hz, 2H).

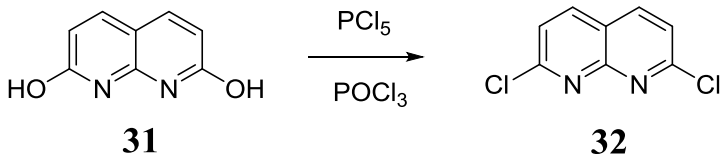

31 **32**

Compound 32:

Compound **31 (**5.2886 g, 32.81 mmol), phosphorus pentachloride (13.53 g, 64.97 mmol), and phosphorus oxychloride (6.88 mL) were added to a flask and refluxed for 2 hours. After cooling to room temperature, the mixture was poured over ice and neutralized with

sodium bicarbonate, then potassium carbonate until pH 8. The mixture was filtered, and the solid was recrystalized from acetone to give dichloride **32** as a brown solid (2.8934 g, 14.54 mmol, 44.3% yield).

^{1}H NMR (300 MHz, $CDCl_3$): δ 8.16 ppm (d, J = 8.5 Hz, 2H), 7.54 ppm (d, J = 8.5 Hz, 2H)

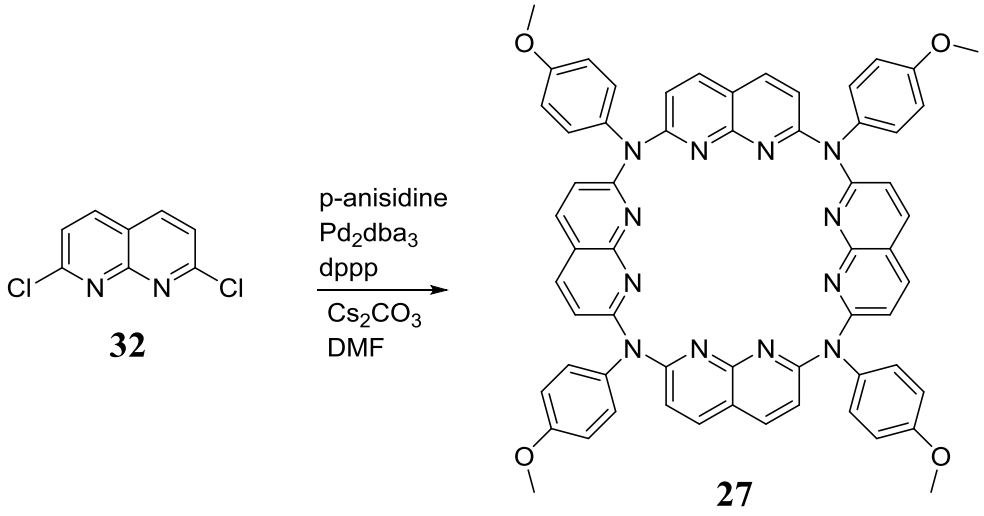

Compound 27:

In a flame-dried flask, compound **32 (**125 mg, 0.628 mmol), 4-methoxyaniline (154.7 mg, 1.256 mmol), bis(diphenylphosphino)propane (62.15 mg, 0.151 mmol), tris(dibenzylideneacetone)dipalladium (69.00 mg, 0.0753 mmol), and cesium carbonate (1.023 g, 3.136 mmol) were dissolved in dimethylformamide (30 mL). The system was flushed with N_2 and degassed by bubbling N_2 through the solution for 1 hour. In a separate flame-dried flask, more compound **32** (125 mg, 0.628 mmol) was dissolved in

DMF (30 mL) and degassed as before. The first flask was then heated to 110 °C under N_2. After six hours, the second solution was slowly added by syringe pump over 18 hours. Heating continued for another 36 hours after the last of the solution was added. The DMF was removed under reduced pressure. The product was dissolved in dichloromethane and filtered through a basic alumina plug. HPLC was performed using an acetonitrile/water solvent system with 0.5% trifluoroacetic acid. The eluted product was dissolved in dichloromethane and washed with saturated sodium bicarbonate to remove trifluoroacetic acid. The organic layer was dried with sodium sulfate and filtered, and the dichloromethane was removed under reduced pressure to afford **27** (0.0312 g, .0313 mmol, 9.97% yield).

^{1}H NMR (250 MHz, $CDCl_3$): δ 8.13 ppm (d, J = 7.5 Hz, 8H), 7.32 ppm (d, J = 8.1 Hz, 8H), 7.07 ppm (d, J = 7.0 Hz, 8H), 6.97 ppm (d, J = 8.0 Hz, 8H), 3.82 ppm (s, 12H).

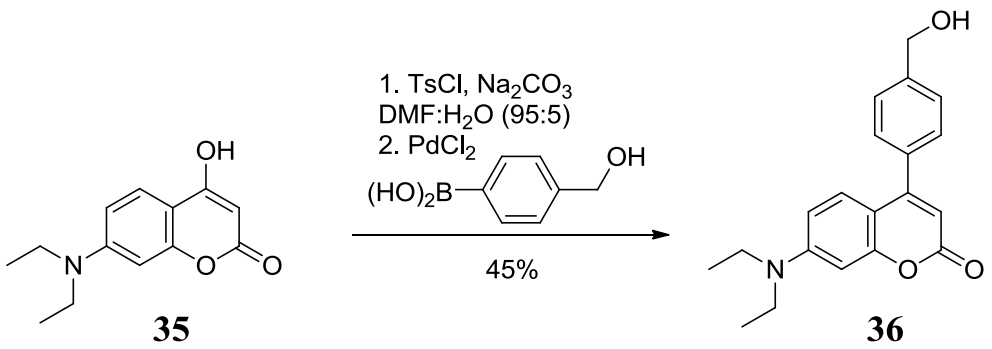

Compound 36

Compound 35 (250 mg, 1.072 mmol), Na_2CO_3 (340 mg, 3.215 mmol), and TsCl (204.4 mg, 1.072 mmol) were dissolved in 10 mL degassed DMF–H_2O (95 : 5). The solution was stirred at 60 °C for 1 h. Then 4-(hydroxymethyl)phenylboronic acid (179.2 mg, 1.179 mmol) and $PdCl_2$ (29 mg, 0.161 mmol) were added and N_2 was bubbled through for 5 min. The solution was stirred at 60 °C for 16 h. The inorganic solids were filtered off and rinsed with acetone. The solvent was removed *in vacuo* and the remaining crude material was purified by chromatography (95 : 5 CH_2Cl_2–EtOAc) to yield compound 36 (156.5 mg, 45%) as a yellow solid (mp 62 °C):

^{1}H NMR (500 MHz, $CDCl_3$) δ 7.50 (d, 2H, J = 7.5 Hz), 7.43 (d, 2H, J = 7.5 Hz), 7.23 (d, 1H, J = 9.0 Hz), 6.57 (d, 1H, J = 2.0 Hz), 6.51 (dd, 1H, J = 9.0, 2.0 Hz), 5.99 (s, 2H), 4.80 (s, 2H), 3.42 (q, 4H, J = 7.0), 1.21 (t, 6H, 7.0 Hz); **^{13}C NMR** (125 MHz, CDC^{l3}) δ 162.1, 156.8, 155.8, 150.6, 142.1, 135.5, 128.6, 127.8, 127.1, 108.5, 108.2, 107.9, 97.9, 64.8, 44.8, 12.4; **IR** (neat, cm^{-1}) 3412, 2970, 1695, 1605, 1589, 1417, 1352, 1115; **HRMS** calculated for $C_{20}H_{21}NO_3Na$ ($M + Na^+$): 346.1414. Found: 346.1414.

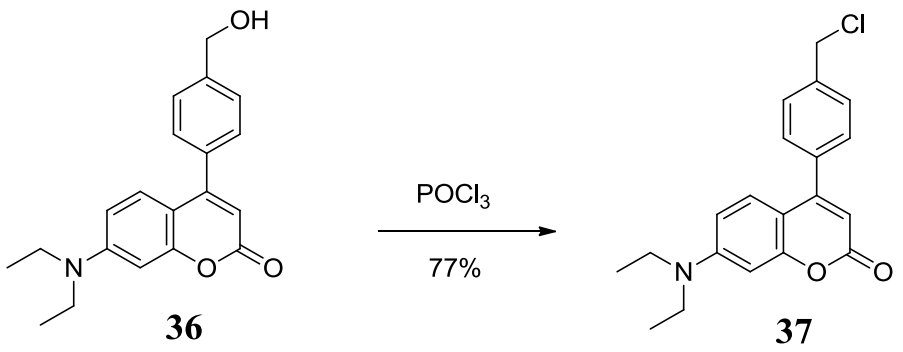

36 **37**

Compound 37

Compound 36 (100 mg, 0.309 mmol) and $POCl_3$ (3 mL) were combined in a round bottom flask and stirred at room temperature for 21 h. The mixture was poured over ice water (10 mL) and extracted with CH_2Cl_2 (10 mL × 4). The organic solvent was removed *in vacuo* and the resulting material was purified by chromatography (90 : 10 CH_2Cl_2–EtOAc) to yield compound 37 (81 mg, 77%) as a yellow oil: **^{1}H NMR** (500 MHz, $CDCl_3$) δ 7.51 (d, 2H, J = 8.0 Hz), 7.43 (d, 2H, J = 8.0 Hz), 7.22 (d, 1H, J = 9.0 Hz), 6.56 (d, 1H, J = 2.5 Hz), 6.51 (dd, 1H, J = 9.0, 2.5 Hz), 5.98 (s, 1H), 3.41 (q, 4H, J = 7.0 Hz), 1.20 (t, 6H, J = 7.0 Hz); **^{13}C NMR** (125 MHz, $CDCl_3$) δ 161.9, 156.7, 155.4, 150.6, 138.5, 136.3, 128.8, 128.7, 127.7, 108.5, 108.3, 107.6, 97.8, 45.6, 44.7, 12.4; **IR** (neat, cm^{-1}) 2970, 1708, 1614, 1593, 1524, 1417, 1356, 1115; **HRMS** calculated for $C_{20}H_{20}ClNO_2Na$ ($M + Na^+$): 364.1075. Found: 364.1077.

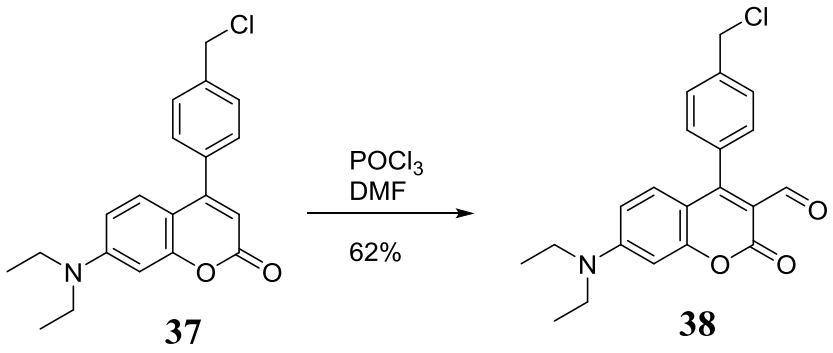

37 38

Compound 38

The Vilsmeier reagent was made by combining 2 mL $POCl_3$ and 3.6 mL DMF in a flame-dried round bottom flask at 0 °C and stirring for 30 min. In a separate flask, 143 mg of compound 37 (2.59 mmol) was dissolved in 3 mL DMF. The starting material was cooled to 0 °C and 3 mL of the Vilsmeier reagent was added dropwise. The reaction was brought to room temperature and stirred for 40 h. The mixture was poured over ice water (30 mL), extracted with CH_2Cl_2 (20 mL × 6), the organic layers combined and dried over Na_2SO_4, and the solvent removed in vacuo. Purification via column chromatography (95 : 5 CH_2Cl_2–EtOAc) yielded compound 38 as a yellow oil (97 mg, 62%): **^{1}H NMR** (500 MHz, $CDCl_3$) δ 9.89 (s, 1H), 7.54 (d, 2H, J = 8.0 Hz), 7.26 (d, 2H, J = 8.0 Hz), 6.94 (d, 1H, J = 9.5 Hz), 6.49–6.53 (m, 2H), 4.68 (s, 2H), 3.45 (q, 4H, J = 7.0 Hz), 1.23 (t, 6H, J = 7.0 Hz); **^{13}C NMR** (125 MHz, $CDCl_3$) δ 188.2, 160.8, 160.1, 157.7, 153.1, 138.3, 133.4, 131.0, 128.6, 128.5, 112.0, 109.8, 108.9, 97.0, 45.7, 45.2, 12.4; **IR** (neat, cm^{-1}) 1614, 1559, 1494, 1417, 1352; **HRMS** calculated for $C_{21}H_{20}ClNO_3Na$ ($M + Na^+$): 392.1024. Found: 392.1022.

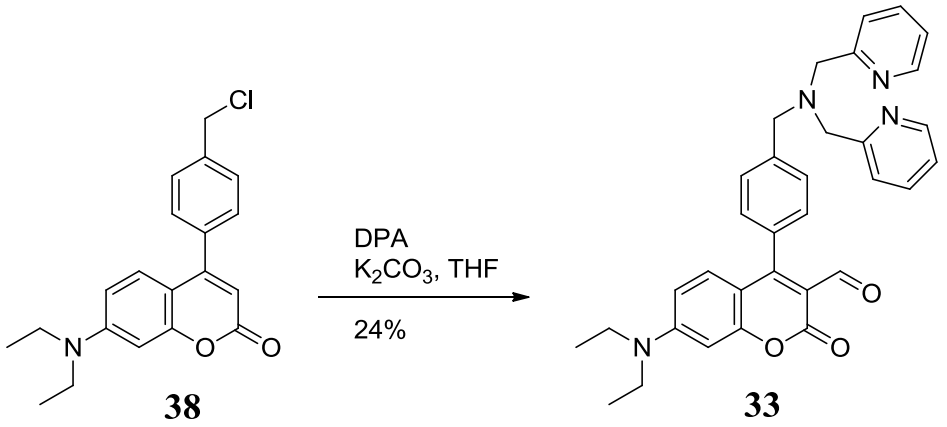

Compound 33

Compound 38 (102 mg, 0.276 mmol), di(2-picolyl)amine (55 μL, 0.290 mmol), K_2CO_3 (114 mg, 0.828 mmol), and 7 mL of THF were combined in a round bottom flask and stirred at 55 °C for 21 h. The mixture was filtered and rinsed with acetone. The filtrate solvent was removed in vacuo and the remaining residue was purified via column chromatography (100% CH_2Cl_2 → 100% EtOAc → 80 : 20 EtOAc–MeOH) to yield sensor 33 as a yellow oil (54 mg, 47%). **^{1}H NMR** (500 MHz, $CDCl_3$) δ 9.76 (s, 1H) 8.55 (d, 2H, J = 5.0 Hz), 7.69 (td, 2H, J = 7.5, 1.5 Hz), 7.61 (d, 2H, J = 8.0 Hz), 7.54 (d, 2H, J = 8.0 Hz), 7.21 (d, 2H, J = 8.0 Hz), 7.17 (m, 2H), 6.93 (d, 1H, J = 9.5 Hz), 6.45–6.51 (m, 2H), 3.88 (s, 4H), 3.80 (s, 2H), 3.43 (q, 4H, J = 7.0 Hz), 1.21 (t, 6H, J = 7.0 Hz); **^{13}C NMR** (125 MHz, $CDCl_3$) δ 188.3, 162.2, 159.5, 159.4, 157.7, 153.0, 148.9, 140.2, 136.5, 131.5, 130.9, 128.7, 128.5, 122.8, 122.0, 112.2, 109.6, 108.9, 96.9, 60.1, 58.1, 45.1, 12.4; **IR** (neat, cm^{-1}) 1746, 1611, 1495, 1422, 1356, 1133, 731; **HRMS** calculated for $C_{33}H_{32}N_4O_3Na$ ($M + Na^+$): 555.2367. Found: 555.2366.

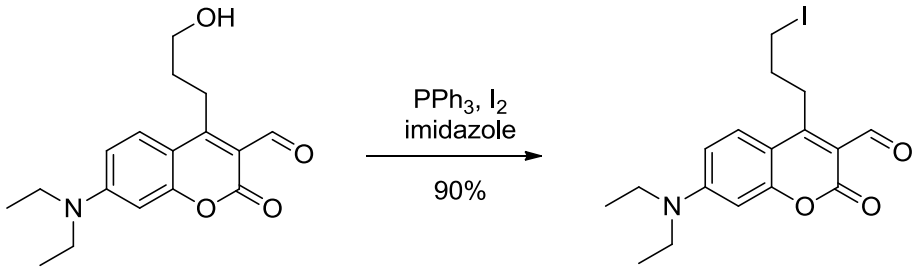

39 **40**

Compound 40

Compound 39 (0.0412 g, 0.1358 mmol), iodine (0.0655 g, 0.2580 mmol), triphenylphosphine (0.0641 g, 0.2444 mmol) and imidazole (0.0185 g, 0.2716 mmol) were dissolved in dichloromethane (7.0 mL) and stirred at room temperature for 2 h. The mixture was filtered and column chromatography was performed twice on silica with 9 : 1 CH_2Cl_2–EtOAc to give compound 40 (48.9 mg, 90%) as a yellow solid (decomp 138–141 °C). **^{1}H NMR** (300 MHz, $CDCl_3$) δ 10.35 (s, 1H), 7.73 (d, 1H, J = 9.6 Hz), 6.69 (dd, 1H, J = 9.3, 4.5 Hz), 6.47 (d, 1H, J = 2.7 Hz), 3.33–3.52 (m, 8H), 2.05–2.15 (m, 2H), 1.26 (t, 6H, J = 4.2 Hz); **^{13}C NMR** (75 MHz, $CDCl_3$) δ 190.9, 162.9, 161.5, 157.6, 152.8, 128.6, 111.8, 110.1, 108.4, 97.3, 45.1, 33.5, 28.9, 12.5, 6.8; **IR** (neat, cm^{-1}) 2913, 1716, 1671, 1614, 1556, 1503, 1454, 1352; **HRMS** calculated for $C_{17}H_{20}INO_3Na$ ($M + Na^+$): 436.0380. Found: 436.0372.

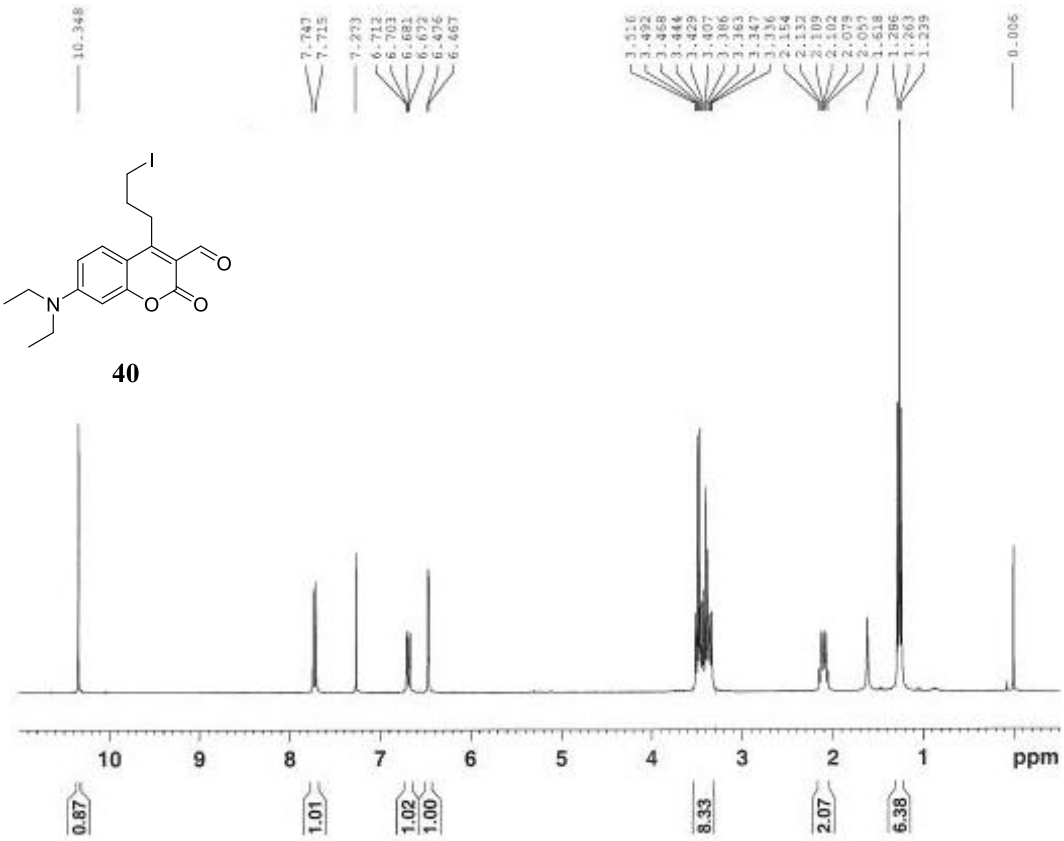
10.348
7.747
7.715
7.273
6.713
6.703
6.681
6.672
6.476
6.467
3.516
3.492
3.468
3.444
3.429
3.407
3.386
3.363
3.347
3.336
2.154
2.132
2.109
2.102
2.079
2.057
1.618
1.286
1.263
1.239
0.006
I
O
N
O
O
10
9
8
7
6
5
4
3
2
1
ppm
0.87
1.01
1.02
1.00
8.33
2.07
6.38

40

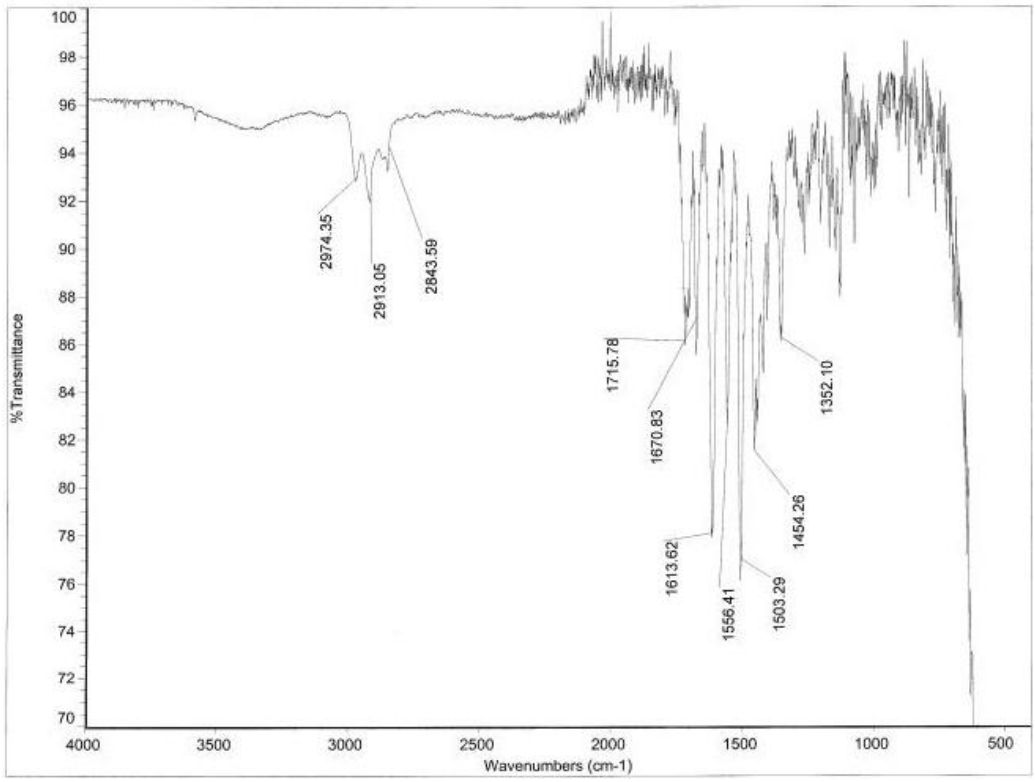
%Transmittance
Wavenumbers (cm-1)
2974.35
2913.05
2843.59
1715.78
1670.83
1613.62
1556.41
1503.29
1454.26
1352.10

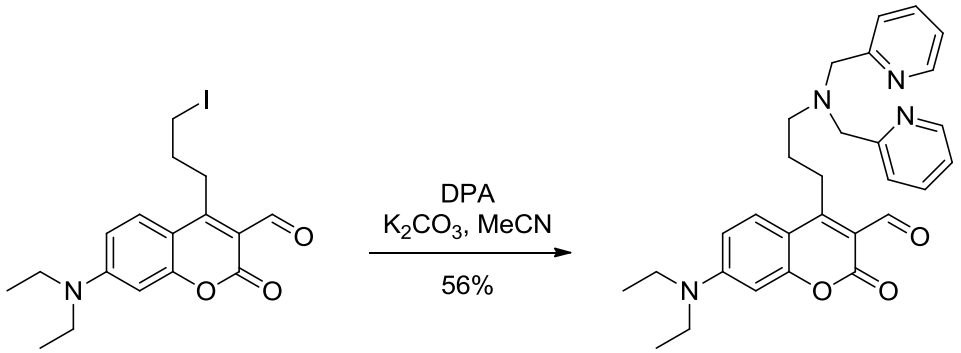

40 **34**

Compound 34

In a flame-dried flask, compound 40 (0.0485 g, 0.1174 mmol), potassium carbonate (0.0243 g, 0.1761 mmol), and di(2-picolyl)amine (31.7 μL, 0.1761 mmol) were dissolved in acetonitrile (4.1 mL) and the flask was flushed with N_2. The mixture was stirred at room temperature for 60 h. Column chromatography on silica with 1 : 1 CH_2Cl_2–EtOAc gave sensor 34 (24.1 mg, 56%) as a yellow solid (mp 109 °C). **^{1}H NMR** (300 MHz, $CDCl_3$) δ 10.34 (s, 1H), 8.55 (d, 2H, J = 4.2 Hz), 7.56–7.71 (m, 5H), 7.14–7.19 (m, 2H), 6.52 (dd, 1H, J = 5.7, 2.7 Hz), 6.44 (d, 1H, J = 2.7 Hz); **^{13}C NMR** (75 MHz, $CDCl_3$) δ 190.7, 163.8, 163.1, 159.6, 157.5, 152.6, 149.0, 136.4, 128.7, 123.0, 121.9, 111.7, 109.8, 108.5, 97.2, 60.2, 54.3, 45.0, 27.8, 25.8, 12.4; **IR** (neat, cm^{-1}) 2970, 2921, 1712, 1676, 1615, 1559, 1508, 1452, 1355, 1148, 1131; **HRMS** calculated for $C_{29}H_{32}N_4O_3Na$ ($M + Na^+$): 507.2367. Found: 507.2357.

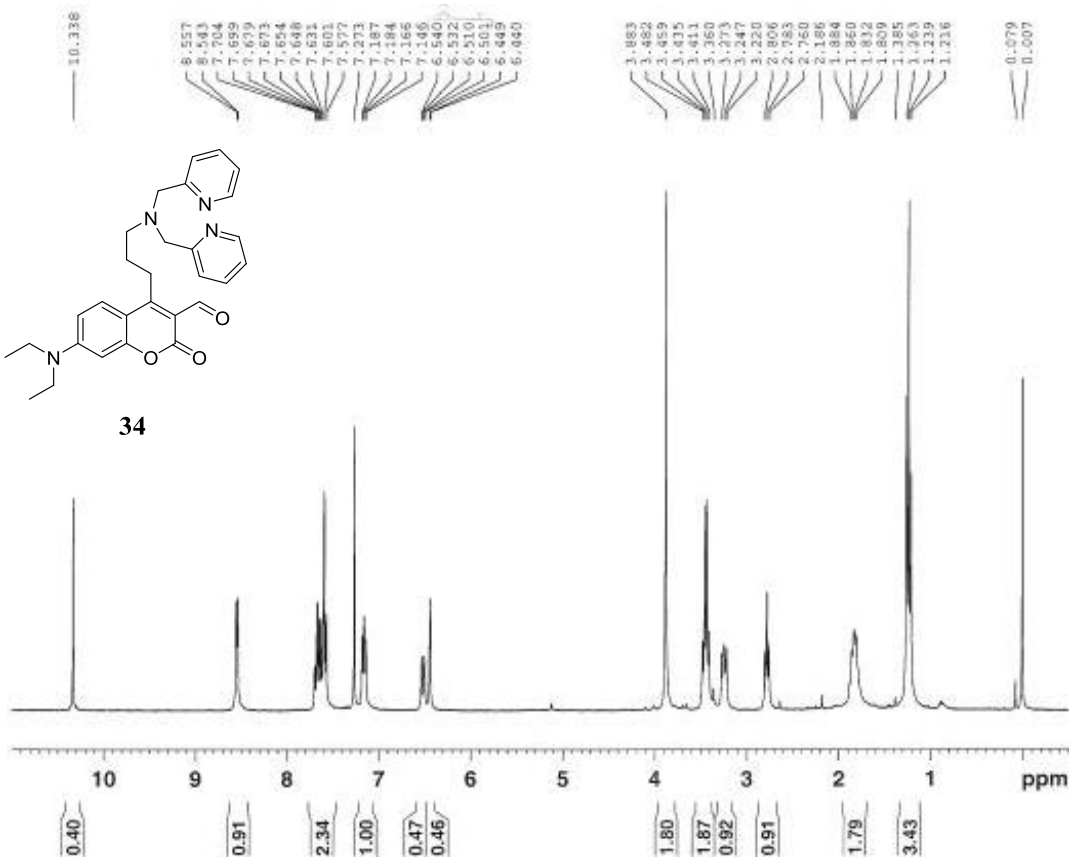
10.338
8.557
8.543
7.704
7.699
7.679
7.673
7.654
7.648
7.631
7.601
7.577
7.273
7.187
7.184
7.166
7.146
6.540
6.532
6.510
6.501
6.449
6.440
3.883
3.482
3.459
3.435
3.411
3.360
3.273
3.247
3.220
2.806
2.783
2.760
2.186
1.884
1.860
1.832
1.809
1.385
1.261
1.239
1.216
0.079
0.007
N
N
N
O
O
O
10
9
8
7
6
5
4
3
2
1
ppm
0.40
0.91
2.34
1.00
0.47
0.46
1.80
1.87
0.92
0.91
1.79
3.43

34

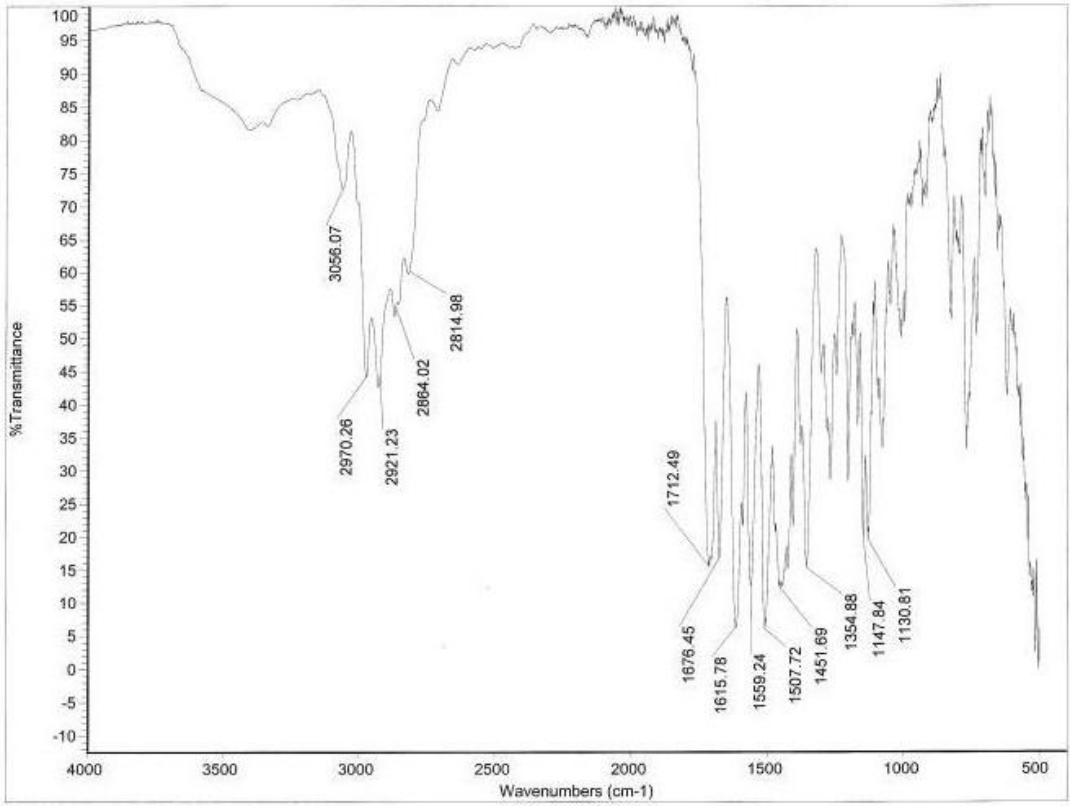
%Transmittance
100
95
90
85
80
75
70
65
60
55
50
45
40
35
30
25
20
15
10
5
0
-5
-10
3056.07
2970.26
2921.23
2864.02
2814.98
1712.49
1676.45
1615.78
1559.24
1507.72
1451.69
1354.88
1147.84
1130.81
4000
3500
3000
2500
2000
1500
1000
500
Wavenumbers (cm-1)

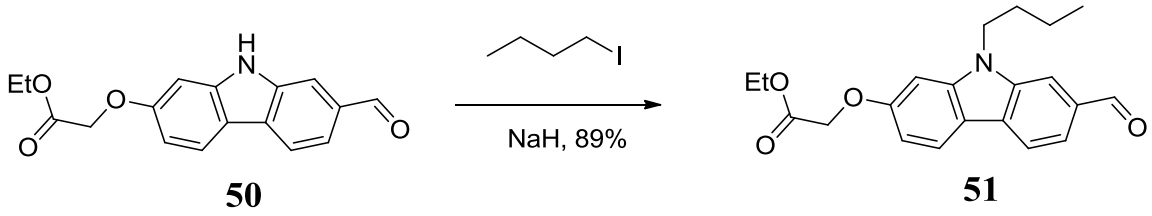

50 **51**

Compound 51

In a flame-dried flask, compound 50 (0.0422 g, 0.142 mmol), sodium hydride (60% by mass, suspended in mineral oil, 0.0057 g, 0.142 mmol), and 5 mL DMF were mixed and the flask was flushed with N_2. After 30 minutes, 1-iodobutane (32.3 μL, 0.284 mmol) was added via syringe and the mixture was stirred at room temperature for 12 hours. The flask was then cooled to 0 °C and the reaction was quenched with saturated ammonium chloride solution. Extraction with CH_2Cl_2 followed by column chromatography on silica with 100% CH_2Cl_2 gave compound 51 (45.9 mg, 92%) as a yellow solid (mp 108-111 °C). **^{1}H NMR** (300 MHz, $CDCl_3$) δ 10.10 (s, 1H), 8.04 (d, 1H, J = 7.8 Hz), 7.98 (d, 1H, J = 9.3 Hz), 7.86 (s, 1H), 7.68 (d, 1H, J = 7.8 Hz), 6.85-6.88 (m, 2H), 4.74 (s, 2H), 4.20-4.34 (m, 4H), 1.81 (m, 2H), 1.25-1.44 (m, 5H), 0.93 (t, 3H, J = 7.4); **^{13}C NMR** (75 MHz, $CDCl_3$) δ; 192.0, 168.8, 158.5, 143.5, 140.3, 132.9, 128.2, 122.4, 121.8, 119.6, 116.7, 109.1, 108.2, 94.7, 65.9, 61.4, 43.0, 30.9, 20.5, 14.2, 13.8; **IR** (neat, cm^{-1}) 2954, 2929, 2868, 1753, 1671, 1622, 1434, 1160.

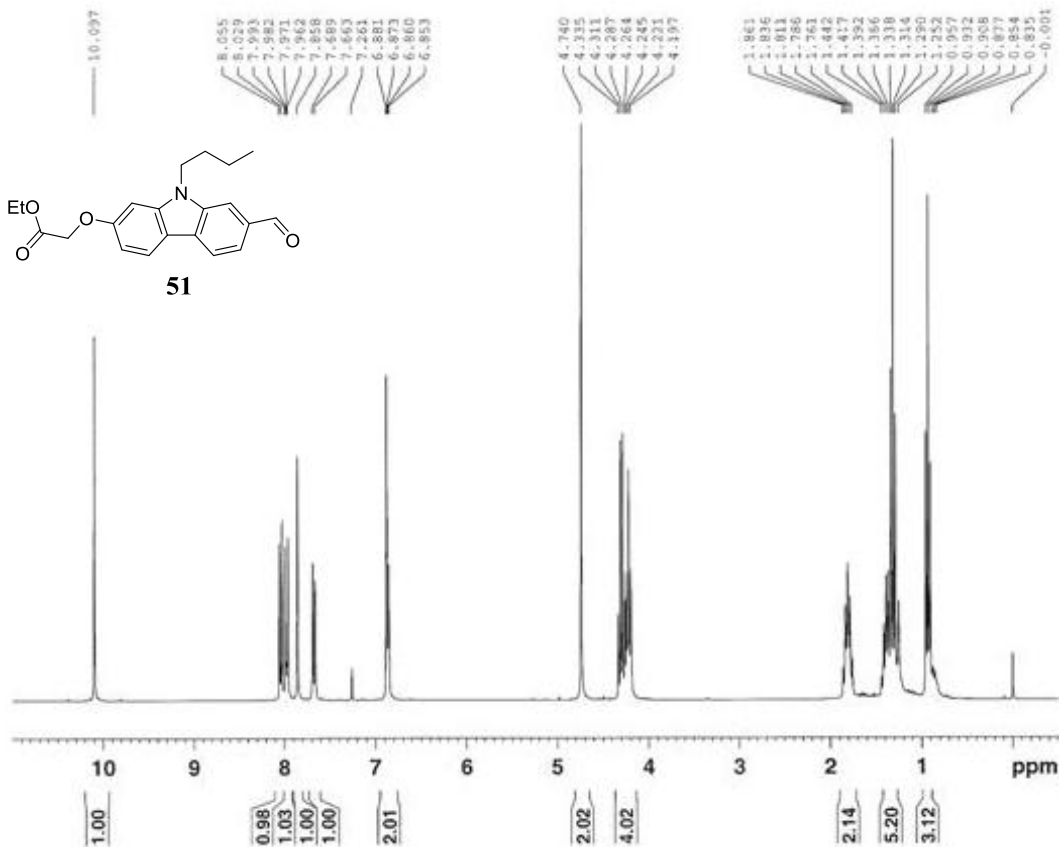
10.097
8.055
8.029
7.993
7.982
7.971
7.962
7.858
7.689
7.663
7.261
6.881
6.873
6.860
6.853
4.740
4.335
4.311
4.287
4.264
4.245
4.231
4.197
1.861
1.836
1.811
1.786
1.761
1.442
1.417
1.392
1.366
1.338
1.314
1.290
1.252
0.957
0.932
0.908
0.877
0.854
0.833
-0.001
EtO
O
O
N
O
10
9
8
7
6
5
4
3
2
1
ppm
1.00
0.98
1.03
1.00
1.00
2.01
2.02
4.02
2.14
5.20
3.12

51

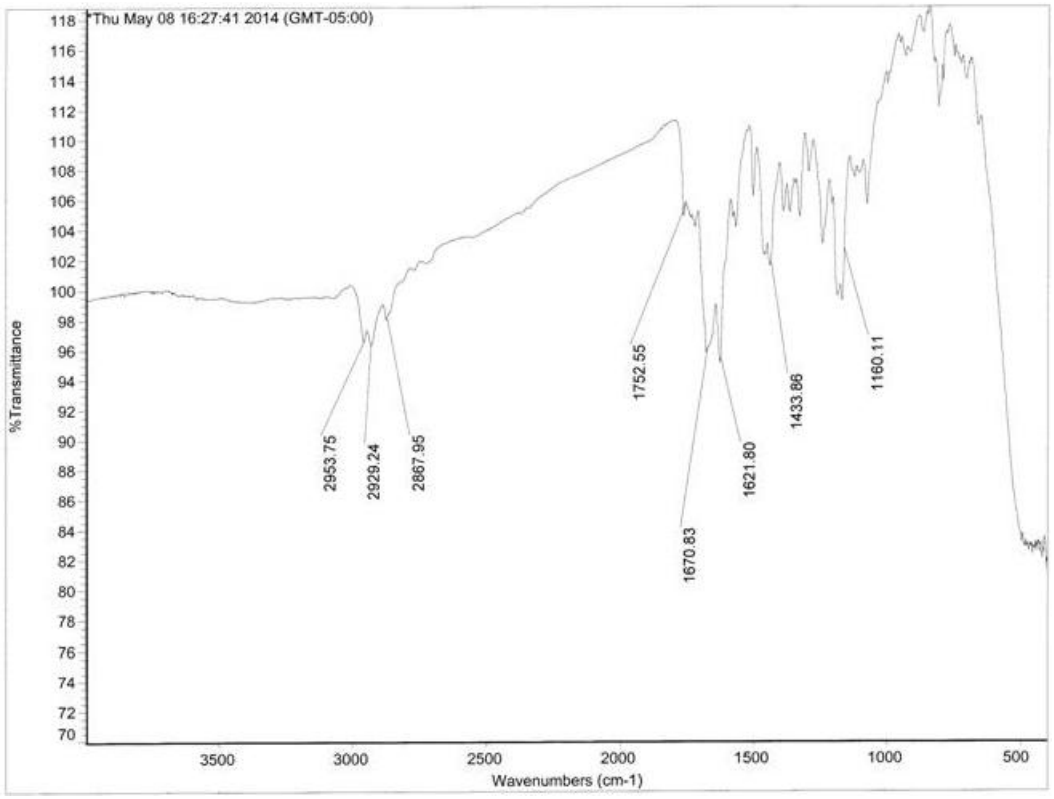
Thu May 08 16:27:41 2014 (GMT-05:00)
%Transmittance
Wavenumbers (cm-1)
2953.75
2929.24
2867.95
1752.55
1670.83
1621.80
1433.86
1160.11

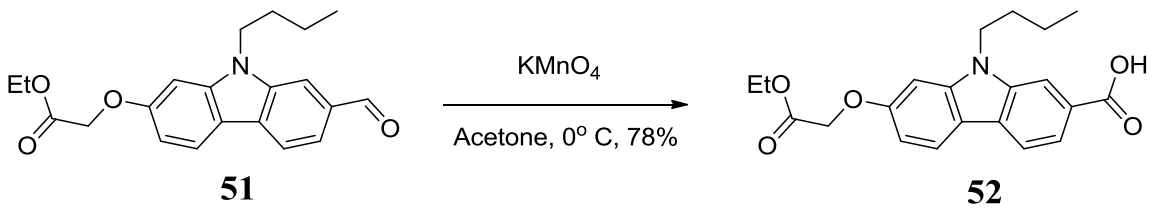

51 **52**

Compound 52

Compound 51 (29.2 mg, 0.826 mmol) was dissolved in 0.5 mL of acetone in a 2 mL vial and cooled to 0 °C. Potassium permanganate (19.6 mg, 0.124 mmol) was added to the vial and rinsed down with another 0.5 mL of acetone. The reaction was stirred at 0 °C for 4 hours, then diluted with ethyl acetate and washed with a 10% aqueous solution of acetic acid. The organic phase was dried with sodium sulfate and filtered to give Compound 52 (23.9 mg, 78%) as a pale yellow solid (decomp 171 °C). **^{1}H NMR** (300 MHz, $CDCl_3$) δ 8.17 (s, 1H), 7.98-8.06 (m, 3H), 6.88-6.93 (m, 2H), 4.77 (s, 1H), 4.28-4.35 (m, 4H), 1.84 (m, 2H), 1.38-1.46 (m, 2H), 1.33 (t, 3H, J = 7.2), 0.97 (t, 3H, J = 7.4); **^{13}C NMR** (75 MHz, $CDCl_3$) δ 173.1, 169.0, 158.2, 143.2, 140.0, 127.4, 125.1, 122.2, 121.0, 119.2, 116.9, 110.9, 108.0, 94.7, 66.0, 61.5, 43.0, 31.0, 20.5, 14.2, 13.9; **IR** (neat, cm^{-1}) 3432, 2954, 2925, 2848, 1752, 1646, 1601, 1385, 1197, 1070.

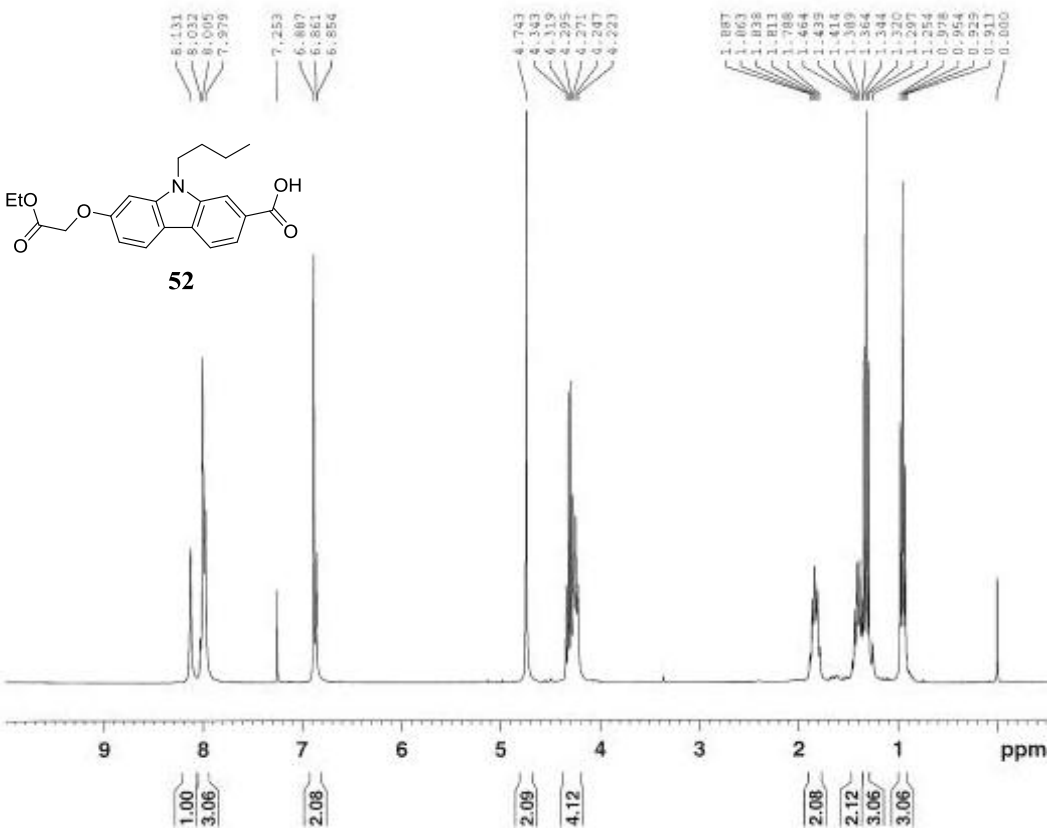
8.131
8.032
8.005
7.979
7.253
6.867
6.861
6.854
4.743
4.343
4.319
4.295
4.271
4.247
4.223
1.887
1.863
1.838
1.813
1.788
1.464
1.439
1.414
1.389
1.364
1.344
1.320
1.297
1.254
0.978
0.954
0.929
0.913
0.000
EtO
O
O
N
OH
O
52
9
8
7
6
5
4
3
2
1
ppm
1.00
3.06
2.08
2.09
4.12
2.08
2.12
3.06
3.06

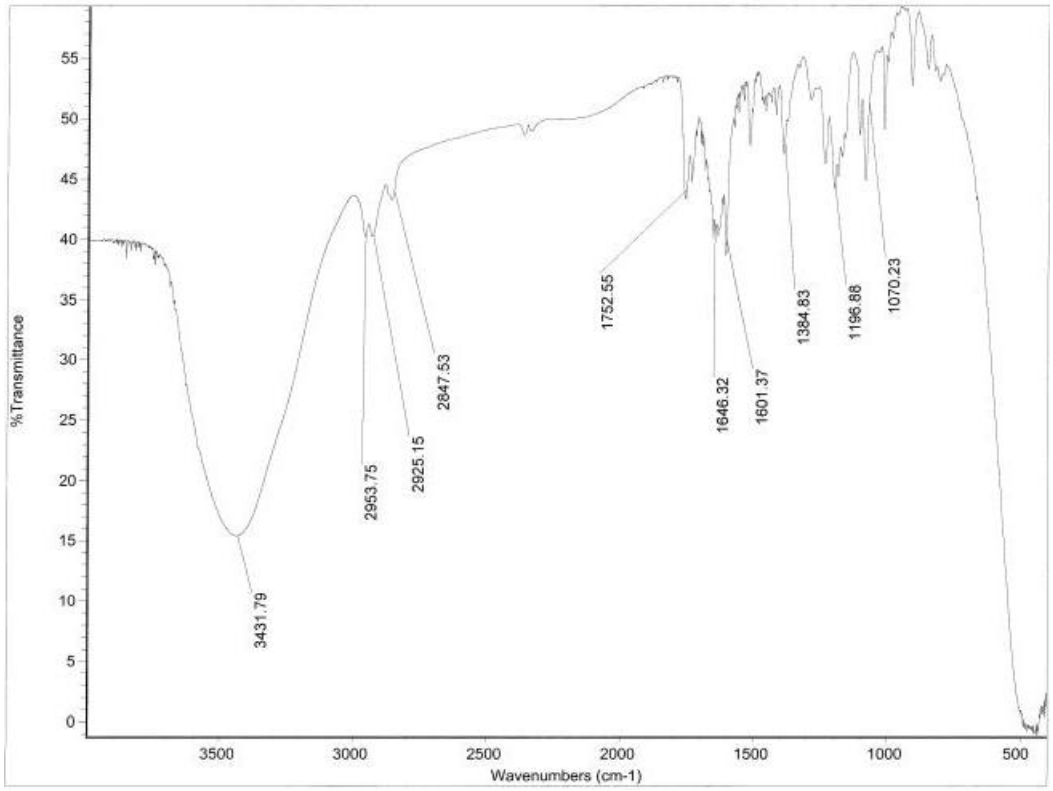
%Transmittance
Wavenumbers (cm-1)
3431.79
2953.75
2925.15
2847.53
1752.55
1646.32
1601.37
1384.83
1196.88
1070.23

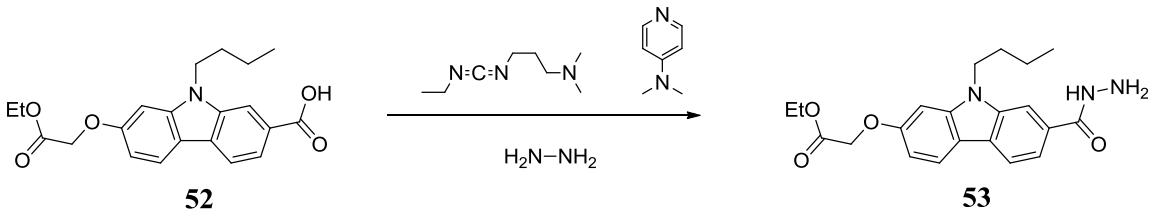

Compound 53

Compound 52 (22.2 mg, 0.0601 mmol), EDC (17.2 mg, 0.0901 mmol) and dimethylaminopyridine (11.0 mg, 0.0901 mmol) were dissolved in 3 mL of dichloromethane and cooled to 0 °C for 1.5 hours. Anhydrous hydrazine (3.0 μL, 0.0721 mmol) was added and the reaction was stirred for 1 hour at 0 °C. The mixture was washed with brine, dried with sodium sulfate and filtered through a plug of silica with 1:1 CH_2Cl_2/EtOAc to provide compound 53 (6.4 mg, 28%) as an off-white solid.

^{1}H NMR (500 MHz, $CDCl_3$) δ 7.97-8.01 (m, 2H), 7.94 (s, 1H), 7.69 (dd, 1H, J = 1.3, 8.3 Hz), 6.88-6.90 (m, 2H), 4.76 (s, 2H), 4.32 (q, 2H, J = 7.2 Hz), 4.17 (t, 2H, J = 7.3), 1.77-1.83 (m, 2H), 1.30-1.41 (m, 5H), 0.92 (t, 3H, J = 7.3).

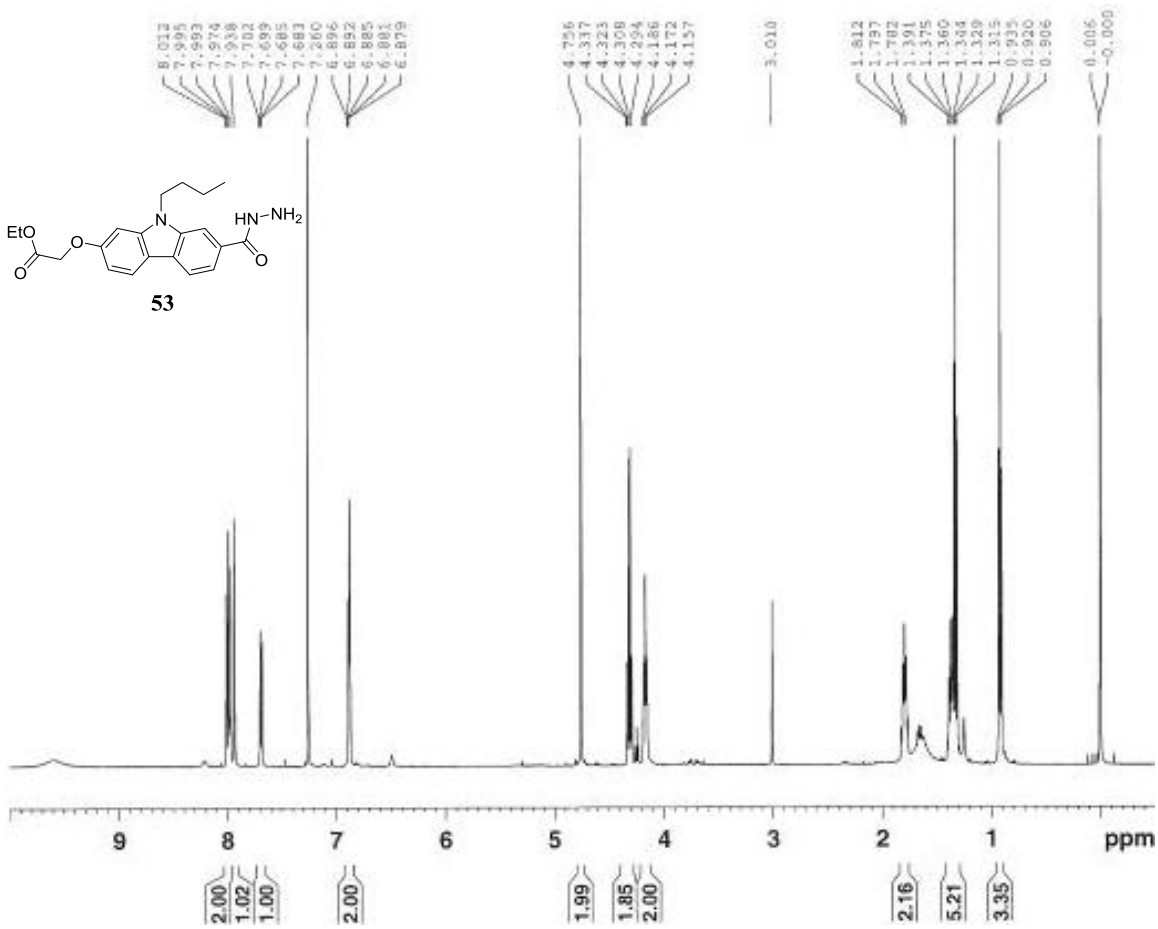
8.013
7.995
7.993
7.974
7.938
7.702
7.699
7.685
7.683
7.200
6.896
6.892
6.885
6.881
6.879
4.756
4.337
4.323
4.308
4.294
4.186
4.172
4.157
3.010
1.812
1.797
1.782
1.391
1.375
1.360
1.344
1.329
1.315
0.935
0.920
0.906
0.006
-0.000
EtO
O
O
N
HN–NH2
O
53
9
8
7
6
5
4
3
2
1
ppm
2.00
1.02
1.00
2.00
1.99
1.85
2.00
2.16
5.21
3.35

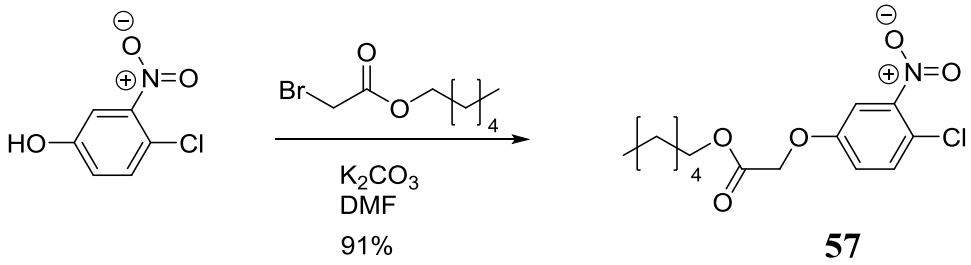

57

Compound 57

4-Chloro-3-nitropenol (778 mg, 4.482 mmol), hexyl bromoacetate (1.500 g, 6.723 mmol) and 40 mL DMF were combined in a round bottom flask and stirred at room temperature. Potassium carbonate (929 mg, 6.723 mmol) was added and the flask was flushed with N_2. After 14 hours the majority of the DMF was removed under reduced pressure, the mixture was dissolved in CH_2Cl_2 and extracted with 10% HCl. Column chromatography on silica gel with 1:1 hexanes:CH_2Cl_2 gave compound 57 (1.29 g, 91%) as a yellow oil. **^{1}H NMR** (300 MHz, $CDCl_3$) δ 7.45 (d, 1H, J = 9.0), 7.40 (d, 1H, J = 3.0), 7.10 (dd, 1H, J = 3.0, 9.0), 4.68 (s, 2H), 4.21 (t, 2H, J = 6.8), 1.61-1.70 (m, 2H), 1.29-1.33 (m, 6H), 0.90 (m, 3H); **^{13}C NMR** (75 MHz, $CDCl_3$) δ 167.7, 156.6, 148.0, 132.5, 120.3, 119.3, 111.5, 65.9, 65.6, 31.2, 28.4, 25.4, 22.4, 13.9; **IR** (neat, cm^{-1}) 3536, 3093, 2958, 2925, 2852, 1748, 1536, 1482, 1352, 1307, 1201, 1078, 805; **HRMS** calculated for $C_{14}H_{18}ClNO_5Na$ ($M + Na^+$): 338.07657. Found: 338.07656.

.

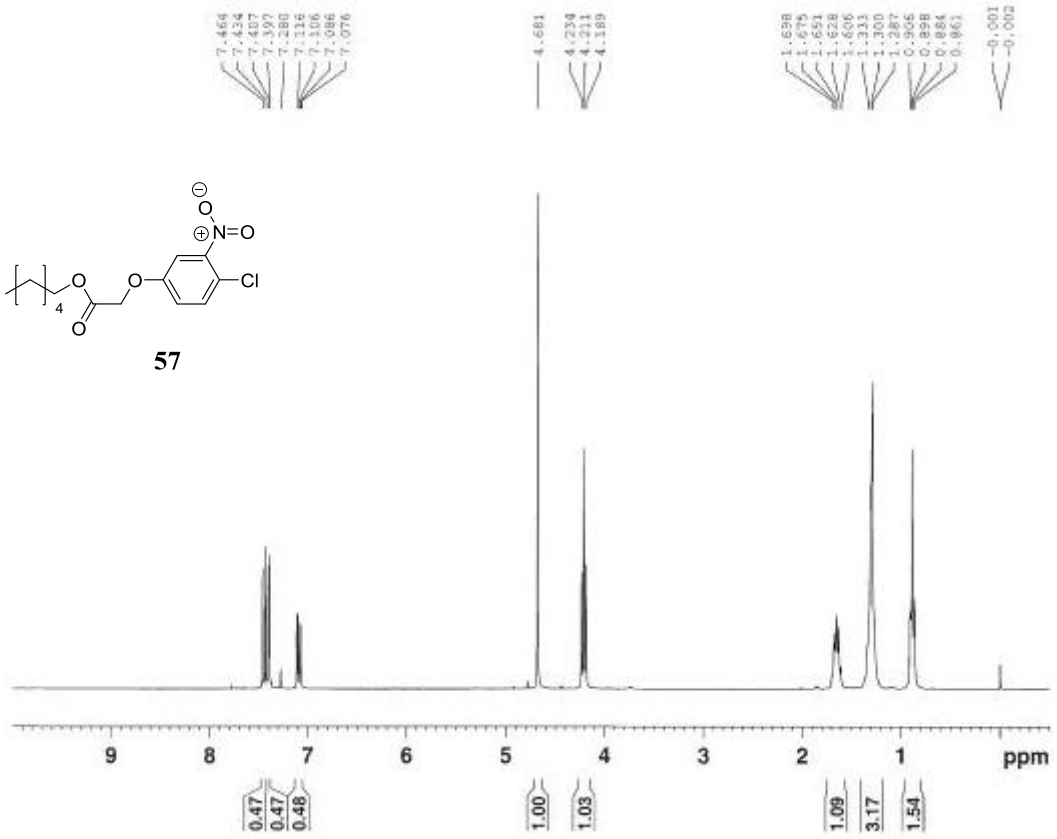
7.464
7.434
7.407
7.397
7.280
7.116
7.106
7.086
7.076
4.681
4.234
4.211
4.189
1.698
1.675
1.651
1.628
1.606
1.333
1.300
1.287
0.906
0.898
0.884
0.861
-0.001
-0.002
9
8
7
6
5
4
3
2
1
ppm
0.47
0.47
0.48
1.00
1.03
1.09
3.17
1.54

57

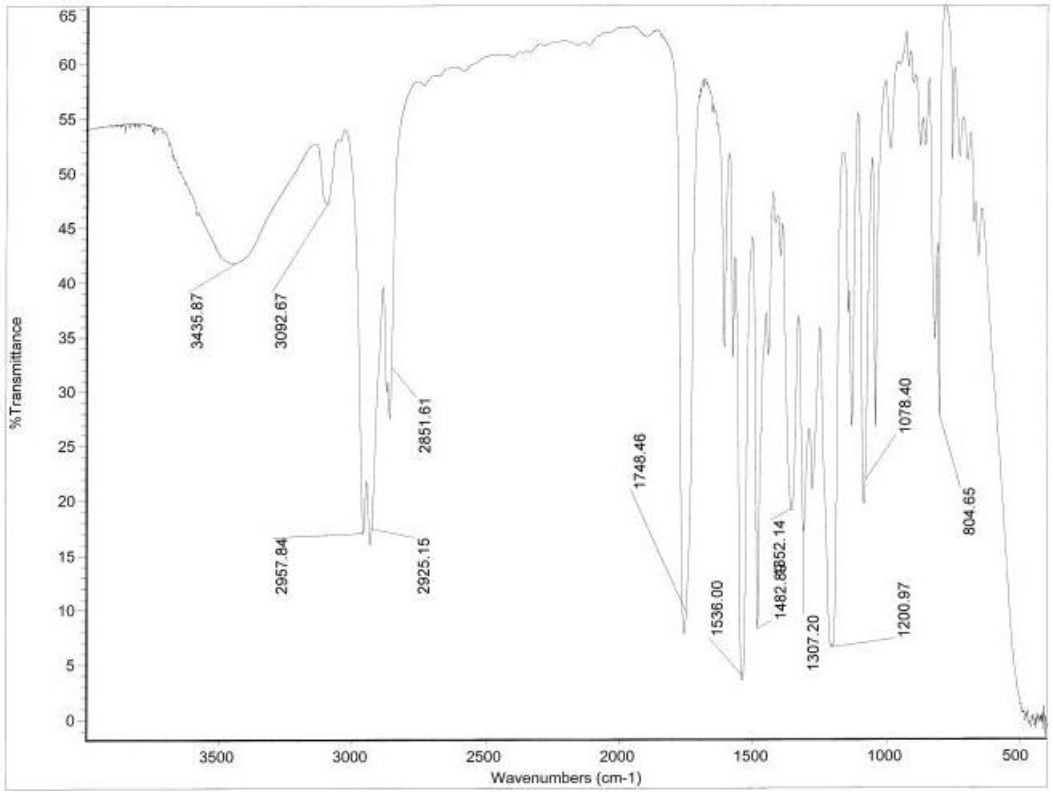
%Transmittance
Wavenumbers (cm-1)
3435.87
3092.67
2957.84
2925.15
2851.61
1748.46
1536.00
1482.68
1452.14
1307.20
1200.97
1078.40
804.65

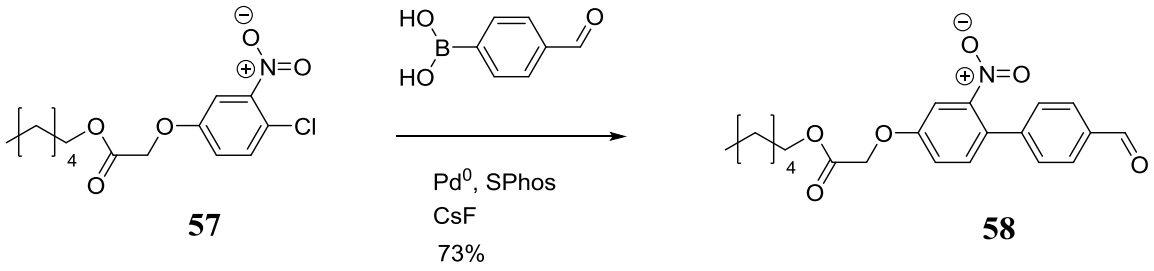

57 **58**

Compound 58

Compound 57 (320 mg, 1.02 mmol), 4-formylphenylboronic acid (244 mg, 1.63 mmol), tris(dibenzylideneacetone)dipalladium (27.9 mg, 0.0305 mmol), SPhos (56.7 mg, 0.138 mmol), and cesium fluoride (401 mg, 2.64 mmol) were added to a sealed tube capped with a rubber septum, evacuated and back-filled with N_2. THF (14 mL) was added by syringe and the tube was sealed with a screw cap. The mixture was heated at 100 °C for 46 hours, cooled to room temperature and filtered through a silica plug, which was then rinsed with 20% diethyl ether in dichloromethane. The resulting solution was dried under reduced pressure and column chromotography was performed on silica with DCM to yield compound 58 (284 mg, 73%) as an orange oil. **^{1}H NMR** (500 MHz, $CDCl_3$) δ 10.09 (s, 1H), 7.95 (d, 2H, J = 8.0 Hz), 7.49 (d, 1H, J = 2.5), 7.47 (d, 2H, J = 8.0), 7.39 (d, 1H, J = 8.5 Hz), 7.24 (dd, 1H, J = 2.5, 8.5 Hz), 4.77 (s, 2H), 4.27 (t, 2H, J = 6.8 Hz), 1.69-1.72 (m, 2H), 1.33-1.37 (m, 6H), 0.92 (t, 3H, J = 7 Hz).

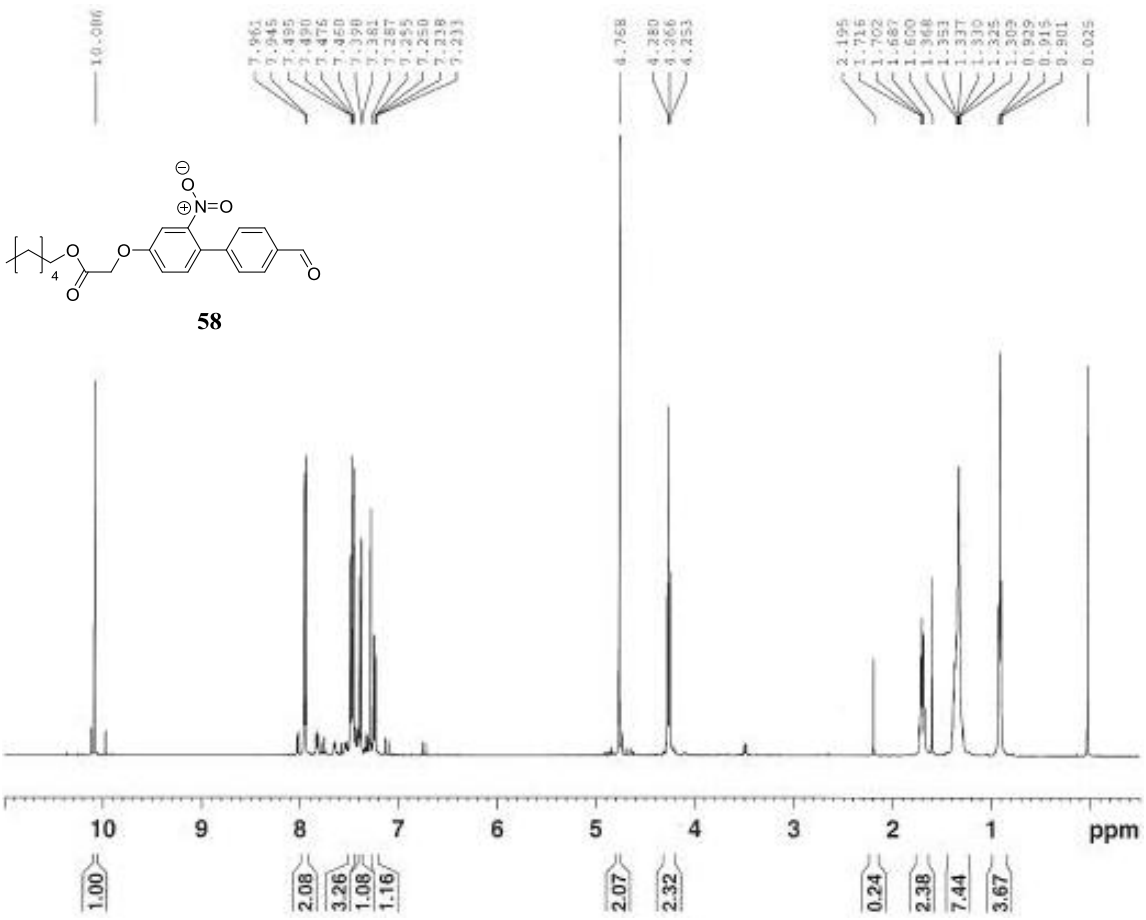
10.086
7.961
7.945
7.495
7.490
7.476
7.460
7.398
7.381
7.287
7.255
7.250
7.238
7.233
4.758
4.280
4.266
4.253
2.195
1.715
1.702
1.687
1.600
1.368
1.353
1.337
1.330
1.325
1.309
0.939
0.915
0.901
0.025
10
9
8
7
6
5
4
3
2
1
ppm
1.00
2.08
3.26
1.08
1.16
2.07
2.32
0.24
2.38
7.44
3.67

58

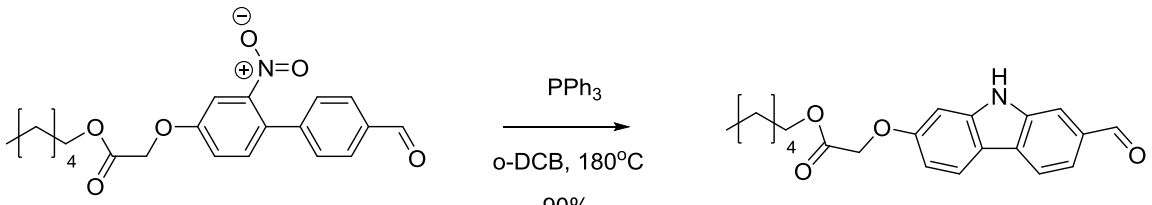

58 **59**

Compound 59

Compound 58 (269 mg, 0.698 mmol), and triphenylphosphine (458 mg, 1.74 mmol) were dissolved in 7 mL of o-dichlorobenzene. The flask was fitted with a condenser and the system flushed with N_2. The mixture was heated at reflux for 16 hours, cooled to room temperature and poured directly onto a silica gel column and chromatographed with 0 to 5% diethyl ether:dichloromethane to afford compound 59 (221 mg, 90%) as a pale yellow solid (mp 114-116 °C). **^{1}H NMR** (500 MHz, $CDCl_3$) δ 10.08 (s, 1H), 8.54 (s, 1H), 8.05 (d, 1H, J = 8.0 Hz), 7.96 (d, 1H, J = 8.5), 7.91 (s, 1H), 7.72 (d, 1H, J = 8.0), 6.89-6.93 (m, 2H), 4.73 (s, 2H), 4.23 (t, 2H, J = 6.8), 1.62-1.68 (m, 2H), 1.21-1.33 (m, 6H), 0.84 (t, 3H, J = 7.0 Hz); **^{13}C NMR** (75 MHz, $CDCl_3$) δ 192.4, 169.0, 158.4, 142.5, 139.2, 133.1, 128.6, 122.3, 122.0, 119.6, 117.0111.4, 109.3, 95.9, 65.7, 65.6, 31.2, 28.4,25.3, 22.4, 13.8; **IR** (neat, cm^{-1}) 3346, 2950, 2925, 2852, 1740, 1687, 1626, 1467, 1426, 1307, 1234, 1189, 792; **HRMS** calculated for $C_{21}H_{23}NO_4Na$ ($M + Na^+$): 376.15193. Found: 376.15185.

.

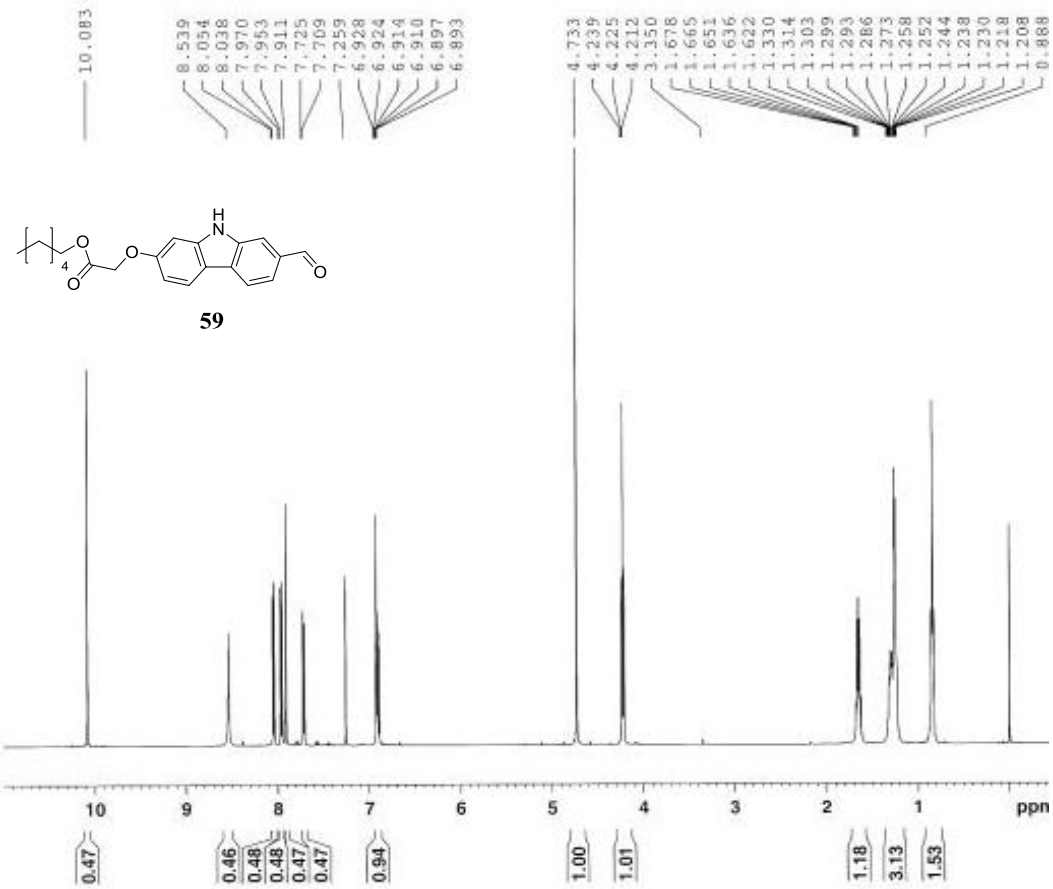
10.083
8.539
8.054
8.038
7.970
7.953
7.911
7.725
7.709
7.259
6.928
6.924
6.914
6.910
6.897
6.893
4.733
4.239
4.225
4.212
3.350
1.678
1.665
1.651
1.636
1.622
1.330
1.314
1.303
1.299
1.293
1.286
1.273
1.258
1.252
1.244
1.238
1.230
1.218
1.208
0.888
10
9
8
7
6
5
4
3
2
1
ppm
0.47
0.46
0.48
0.48
0.47
0.47
0.94
1.00
1.01
1.18
3.13
1.53

59

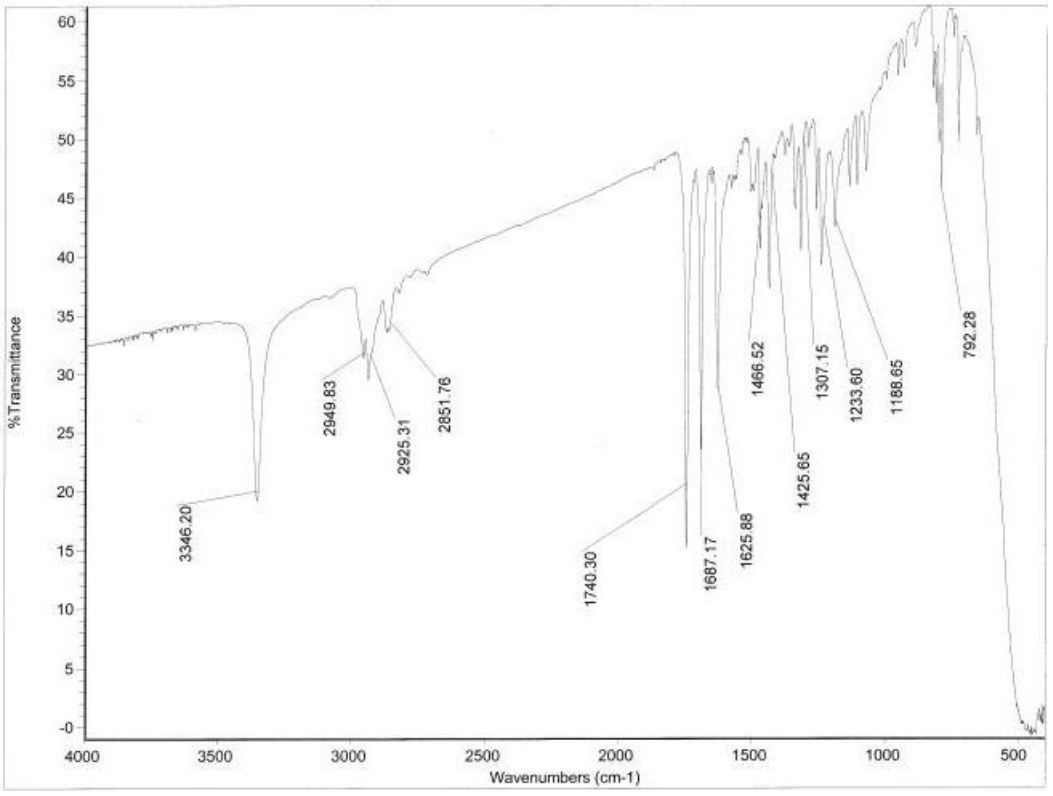
%Transmittance
Wavenumbers (cm-1)
3346.20
2949.83
2925.31
2851.76
1740.30
1687.17
1625.88
1466.52
1425.65
1307.15
1233.60
1188.65
792.28

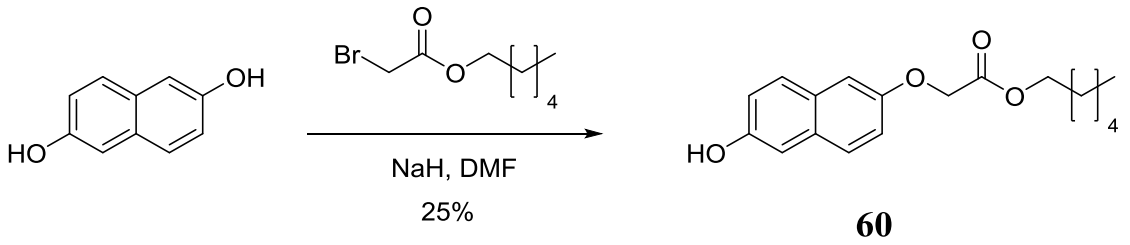

60

Compound 60

2,6-Dihydroxynaphthalene (3.00 g, 18.7 mmol) and sodium hydride (60% by mass, suspended in mineral oil, 644 mg, 16.1 mmol) were dissolved in 90 mL DMF and the flask was flushed with N_2 for 30 minutes. Hexyl bromoacetate was added by syringe and the mixture was stirred at room temperature for 10 hours. DMF was removed under reduced pressure and column chromatography was performed on silica gel with 0 to 3% diethyl ether in dichloromethane to afford compound 60 (1.43 g, 25%) as brown solid (mp 83-86 °C). **^{1}H NMR** (300 MHz, $CDCl_3$) δ 7.47-7.55 (m, 2H), 7.14 (dd, 1H, J = 2.4, 9.0), 7.04-7.08 (m, 2H), 7.00 (d, 1H, J = 2.4), 5.93 (s, 1H), 4.72 (s, 2H), 4.23 (t, 2H, J = 6.8), 1.60-1.69 (m, 2H), 1.24-1.35 (m, 6H), 0.85 (t, 3H, J = 6.4 Hz); **^{13}C NMR** (75 MHz, $CDCl_3$) δ 169.7, 154.1, 152.4, 130.4, 129.2, 128.4, 128.1, 119.0, 118.4, 109.7, 107.4, 65.7, 65.5, 31.3, 28.5, 25.4, 22.5, 13.9; **IR** (neat, cm^{-1}) 3407, 2954, 2925, 2852, 1736, 1605, 1511, 1393, 1213, 1111, 1066, 850; **HRMS** calculated for $C_{18}H_{22}O_4Na$ ($M + Na^+$): 325.14103. Found: 325.14111.

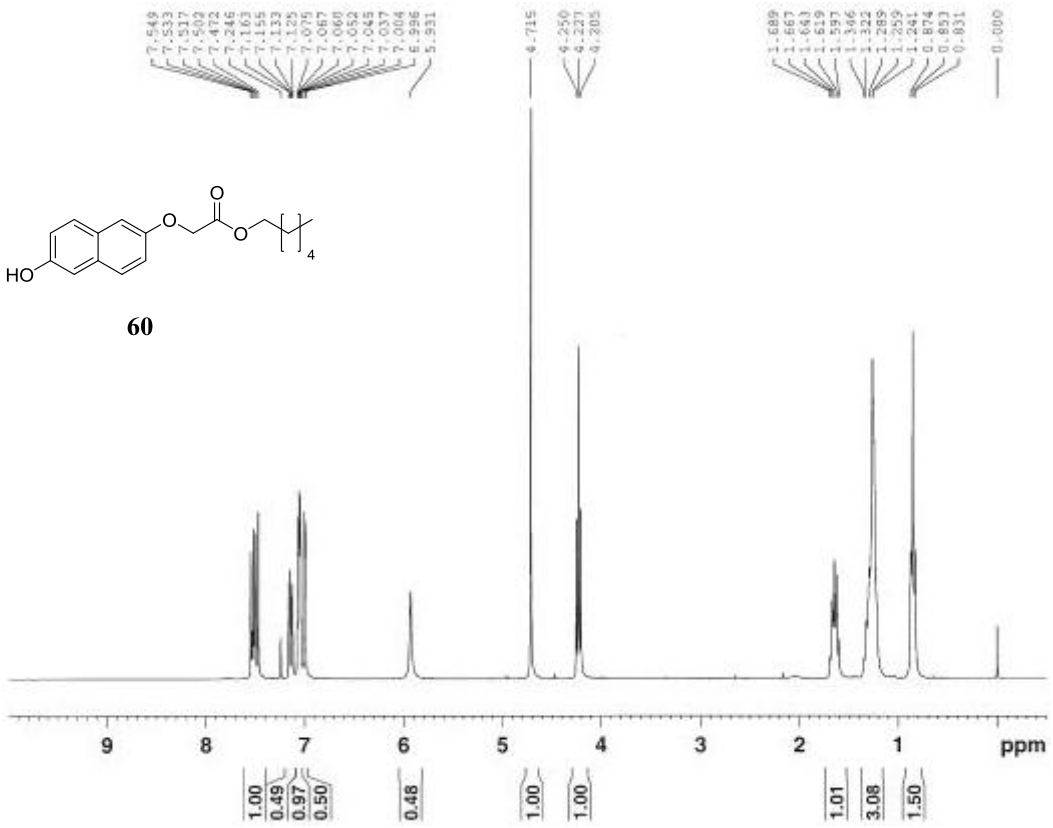
HO
O
O
O
4
9
8
7
6
5
4
3
2
1
ppm

60

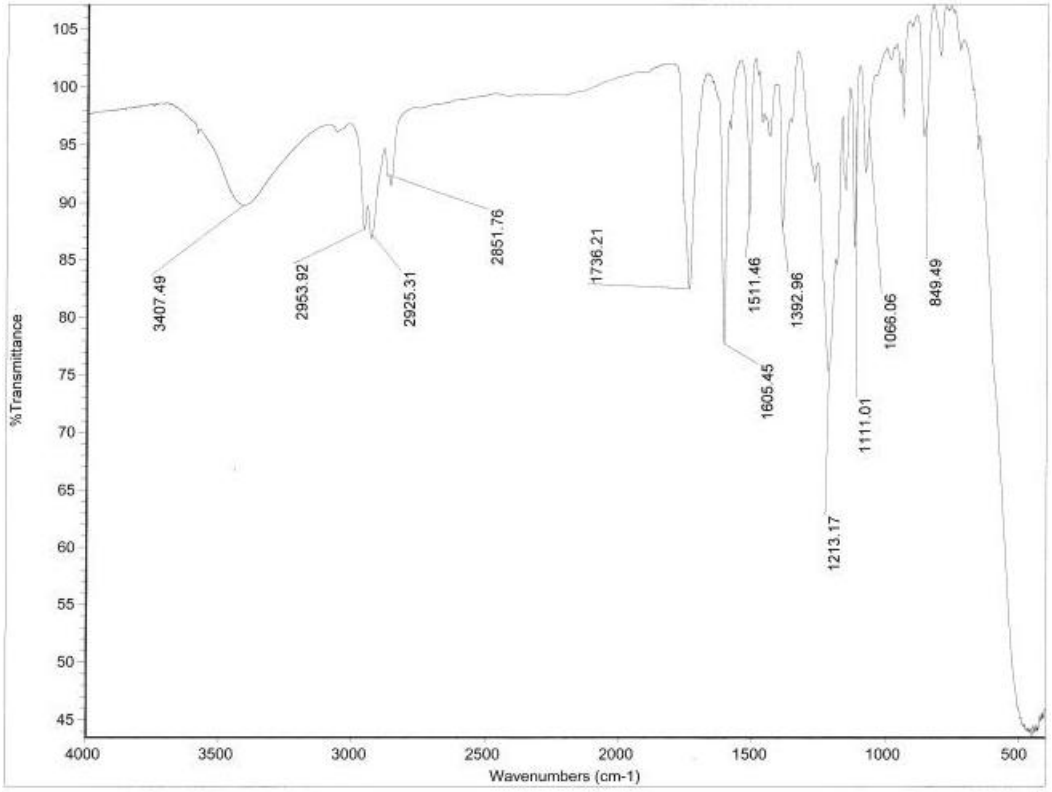
%Transmittance
Wavenumbers (cm-1)
3407.49
2953.92
2925.31
2851.76
1736.21
1605.45
1511.46
1392.96
1213.17
1111.01
1066.06
849.49

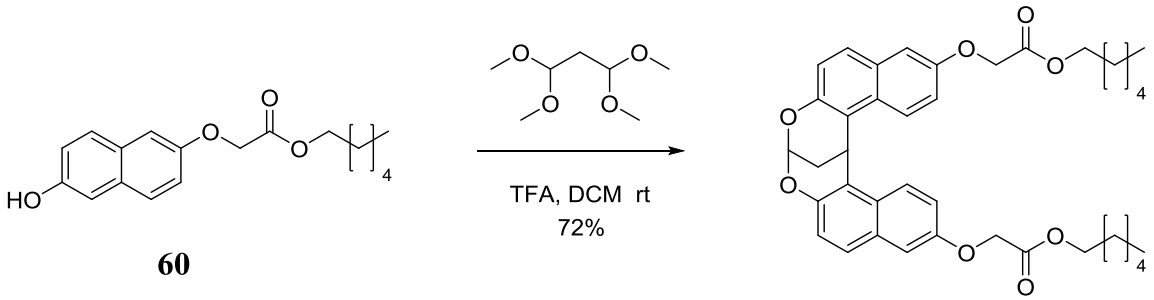

60 **61**

Compound 61

Compound 60 (1.43 g, 4.73 mmol) was dissolved in 11 mL of nitromethane and 4 mL of dichloromethane and flushed with N_2. 4 mL trifluoroacetic acid was added by syringe, then 470 μL of 1,1,3,3-tetramethoxypropane was added dropwise over 30 minutes. The solution was stirred at room temperature for 6 hours. Ice was added to the flask, followed by saturated sodium bicarbonate solution until a pH of 8 was reached. The product was extracted from the mixture with dichloromethane, dried over sodium sulfate, filtered and then purified by column chromatography on silica in DCM to yield compound 61 (1.09 g, 72%) as a yellow solid (mp 85 °C). **^{1}H NMR** (300 MHz, $CDCl_3$) δ 8.40 (d, 2H, J = 9.3), 7.39 (d, 2H, J = 8.7), 7.28 (dd, 2H, J = 2.7, 9.3), 7.08 (d, 2H, J = 9.0), 6.95 (d, 2H, J = 2.7), 6.19 (s, 1H), 5.15 (s, 1H), 4.64 (s, 4H), 4.17 (t, 4H, J = 6.6), 2.31 (s, 2H), 1.56-1.77 (m, 4H), 1.20-1.28 (m, 12H), .79-.88 (m, 6H); **^{13}C NMR** (75 MHz, $CDCl_3$) δ 169.0, 154.0, 148.9, 130.4, 127.3, 126.8, 124.4, 119.0, 118.7, 118.4, 108.6, 91.4, 65.5, 65.4, 31.3, 28.5, 26.7, 25.4, 22.8, 22.4, 13.9; **IR** (neat, cm^{-1}) 2958, 2929, 2868,1753, 1671, 1626, 1454, 1172; **HRMS** calculated for $C_{39}H_{44}O_8Na$ ($M + Na^+$):663.29294. Found: 663.29210.

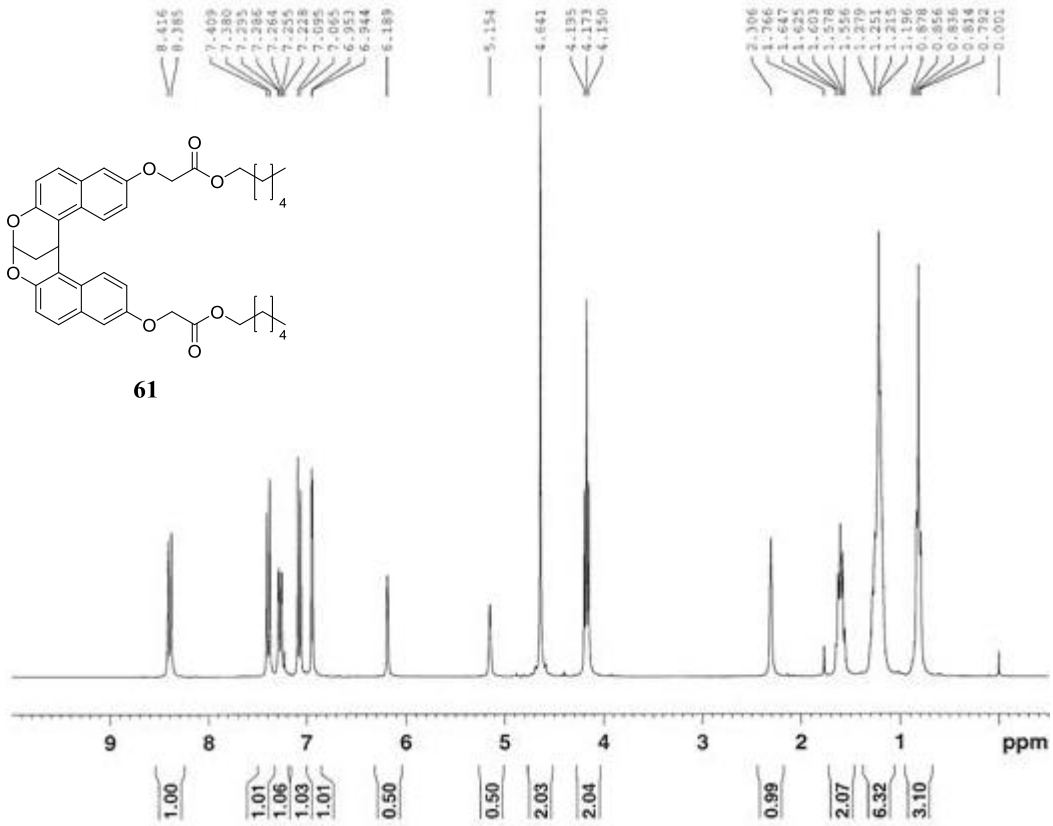
8.416
8.385
7.409
7.380
7.295
7.286
7.264
7.255
7.228
7.095
7.065
6.953
6.944
6.189
5.154
4.641
4.135
4.173
4.150
2.306
1.766
1.647
1.625
1.603
1.578
1.556
1.379
1.251
1.215
1.196
0.878
0.856
0.836
0.814
0.792
0.001
9
8
7
6
5
4
3
2
1
ppm
1.00
1.01
1.06
1.03
1.01
0.50
0.50
2.03
2.04
0.99
2.07
6.32
3.10

61

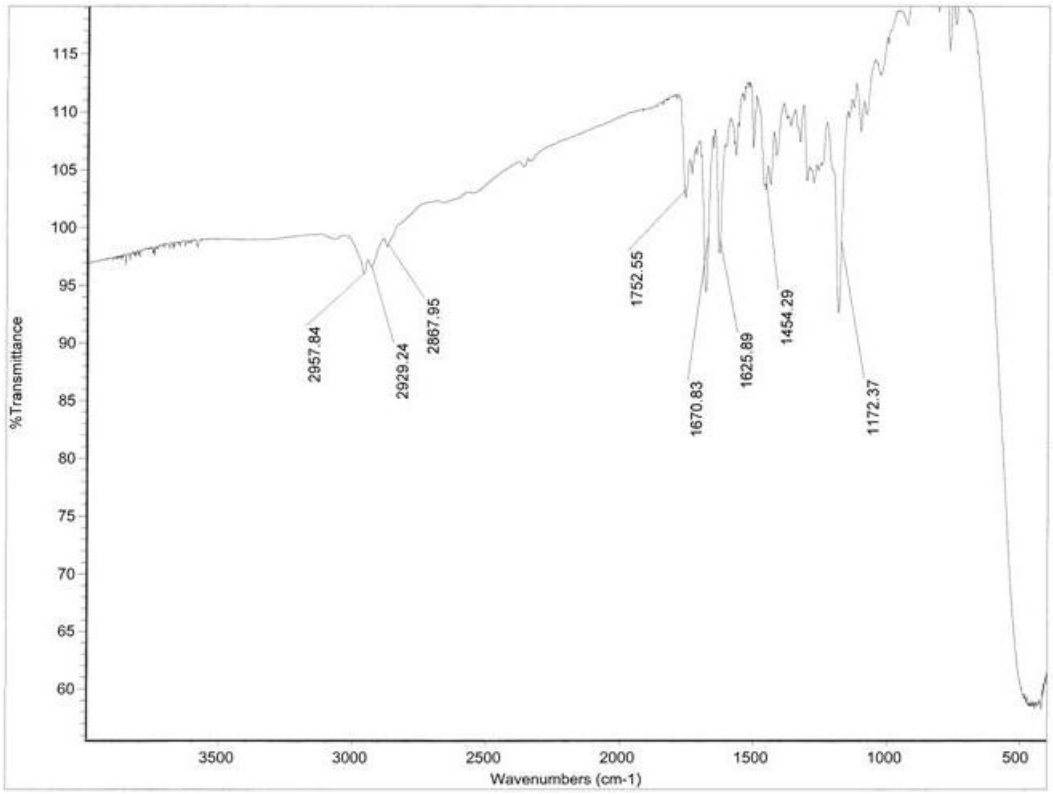
%Transmittance
115
110
105
100
95
90
85
80
75
70
65
60
2957.84
2929.24
2867.95
1752.55
1670.83
1625.89
1454.29
1172.37
3500
3000
2500
2000
1500
1000
500
Wavenumbers (cm-1)

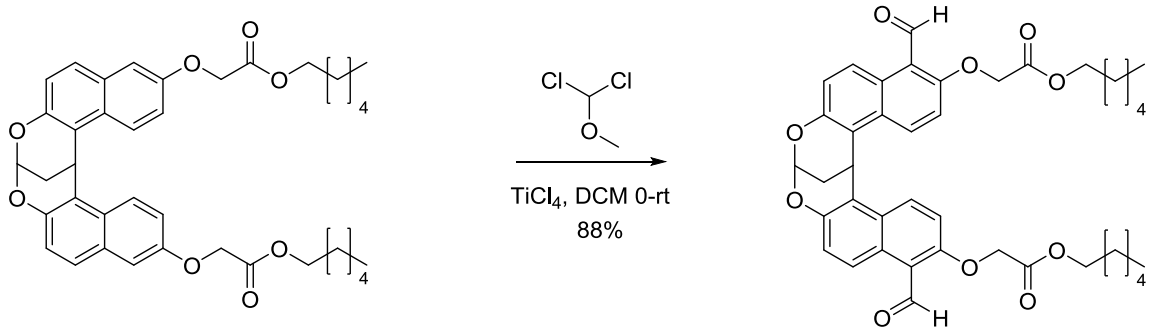

61 **62**

Compound 62

Compound 61 (4.28 g, 6.68 mmol) and 1,1-dichloromethyl methyl ether (2.4 mL, 27 mmol) were dissolved in 75 mL of dichloromethane and the flask was flushed with nitrogen gas and cooled to 0 °C. 27 mL of a 1.0 M solution of $TiCl_4$ was added via syringe and the mixture was stirred at 0 °C for 15 hours while slowly warming to room temperature. The reaction mixture was cooled to 0 °C and quenched with a saturated solution of sodium bicarbonate. The mixture was extracted with DCM, dried over Na_2SO_4, and columned in 0 to 3% diethyl ether in DCM to yield compound 62 (4.09 g, 88%) as a yellow solid (decomp 102 °C). **^{1}H NMR** (300 MHz, $CDCl_3$) δ 10.84 (s, 2H), 9.03 (d, 2H, J = 9.6), 8.57 (d, 2H, J = 9.6), 7.25 (d, 2H, J = 8.4), 7.16 (d, 2H, J = 9.6), 6.22 (s, 1H), 5.14 (s, 1H), 4.79 (s, 4H), 4.17 (t, 4H, J = 6.9), 2.37 (s, 2H), 1.55-1.64 (m, 4H), 1.18-1.27 (m, 12H), .079-.083 (m, 6H); **^{13}C NMR** (75 MHz, $CDCl_3$) δ 191.9, 168.3, 160.0, 149.5, 130.6, 127.6, 126.7, 125.5, 122.0, 118.4, 113.5, 91.1, 66.4, 65.8, 31.2, 28.4, 26.6, 25.4, 22.7, 22.4, 13.9; **IR** (neat, cm^{-1}) 2958, 2929, 2860, 1748, 1675, 1589, 1524, 1385, 1201, 1054, 907, 817; **HRMS** calculated for $C_{41}H_{44}O_{10}Na$ ($M + Na^+$): 719.28267. Found: 719.28190.

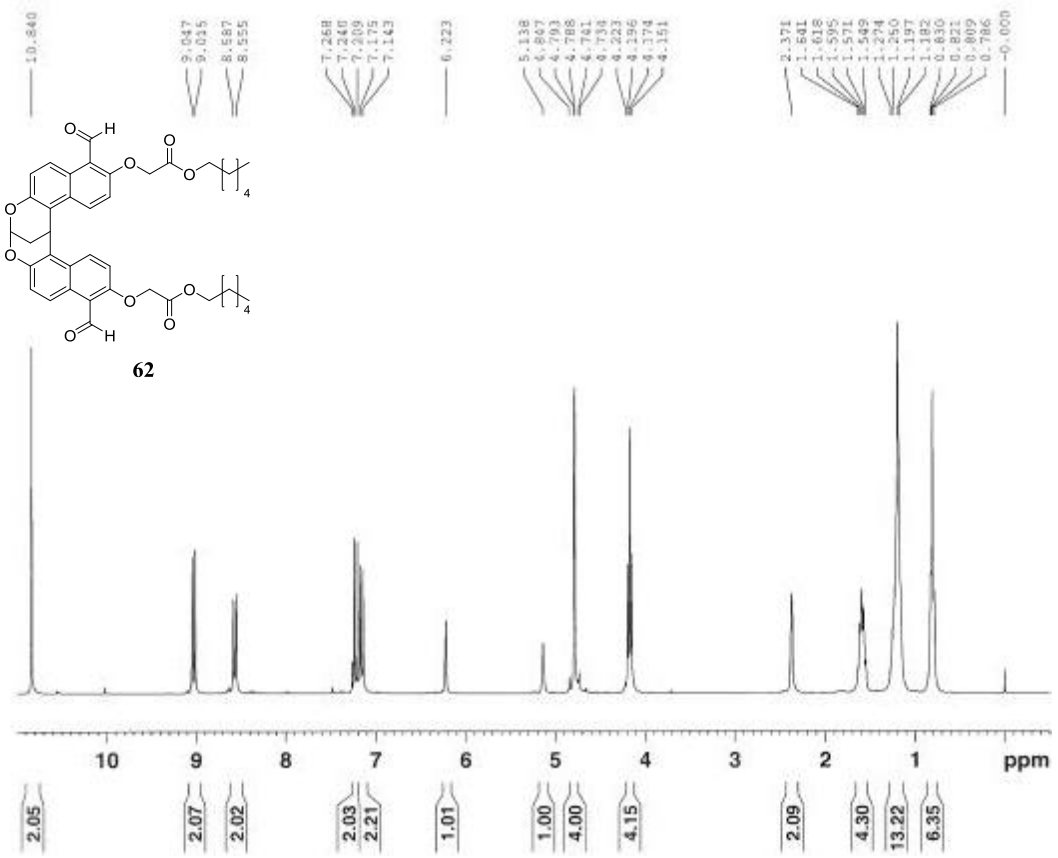
10.840
9.047
9.045
8.587
8.555
7.268
7.240
7.209
7.175
7.143
6.223
5.138
4.867
4.793
4.788
4.761
4.734
4.223
4.196
4.174
4.151
2.371
1.641
1.618
1.595
1.571
1.549
1.274
1.250
1.197
1.182
0.830
0.821
0.809
0.786
-0.000
10
9
8
7
6
5
4
3
2
1
ppm
2.05
2.07
2.02
2.03
2.21
1.01
1.00
4.00
4.15
2.09
4.30
13.22
6.35

62

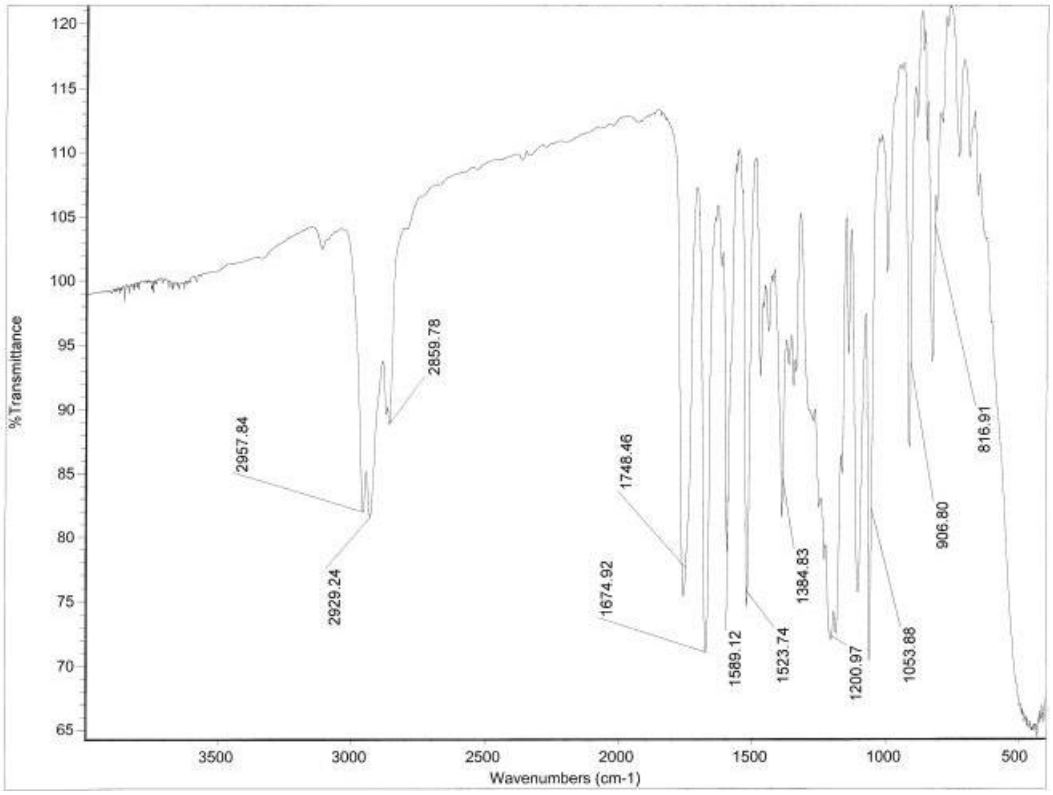
%Transmittance
Wavenumbers (cm-1)
2957.84
2929.24
2859.78
1748.46
1674.92
1589.12
1523.74
1384.83
1200.97
1053.88
906.80
816.91

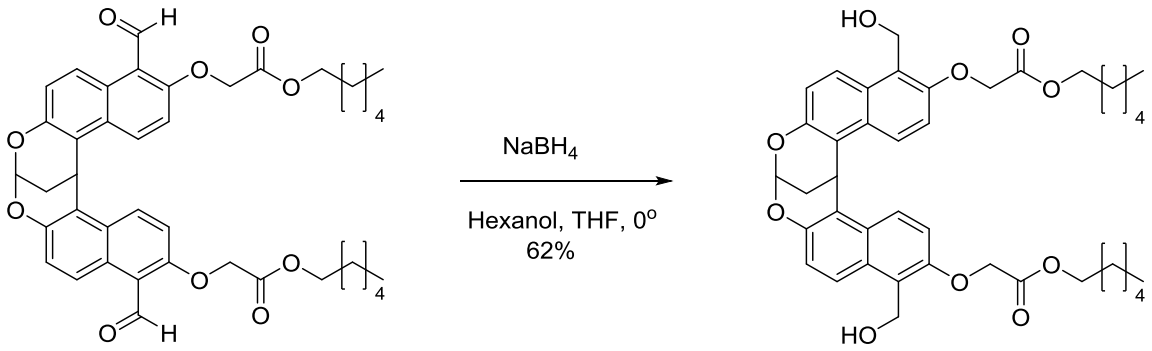

62 **63**

Compound 63

Compound 62 (1.67 g, 2.39 mmol) was dissolved in 40 mL THF and 40 mL 1-hexanol and cooled to 0 °C. $NaBH_4$ (226 mg, 5.98 mmol) was added and the mixture was stirred at 0 °C for 25 minutes, then quenched at 0 °C with a saturated solution of NH_4Cl and warmed to room temperature. The product was extracted with DCM, dried over Na_2SO_4 and filtered, and then purified by column chromatography on silica with 0-30% Et_2O/DCM to yield compound 63 (1.05 g, 62%) as a yellow-brown solid. **^{1}H NMR** (300 MHz, $CDCl_3$) δ 8.49 (d, 2H, J = 9.3), 7.99 (d, 2H, J = 9.2 Hz), 7.22-7.26 (m, 4H), 6.27 (s, 1H), 5.28 (s, 1H), 5.10-5.15 (m, 4H), 4.81 (d, 4H, J = 4.8), 4.14 (t, 4H, J = 6.8 Hz), 2.43 (s, 2H), 1.56-1.60 (m, 4H), 1.24 (s, 12H), 0.82-0.85 (m, 6H); **HRMS** calculated for $C_{41}H_{48}O_{10}Na$ ($M + Na^+$): 723.31397. Found: 723.31323.

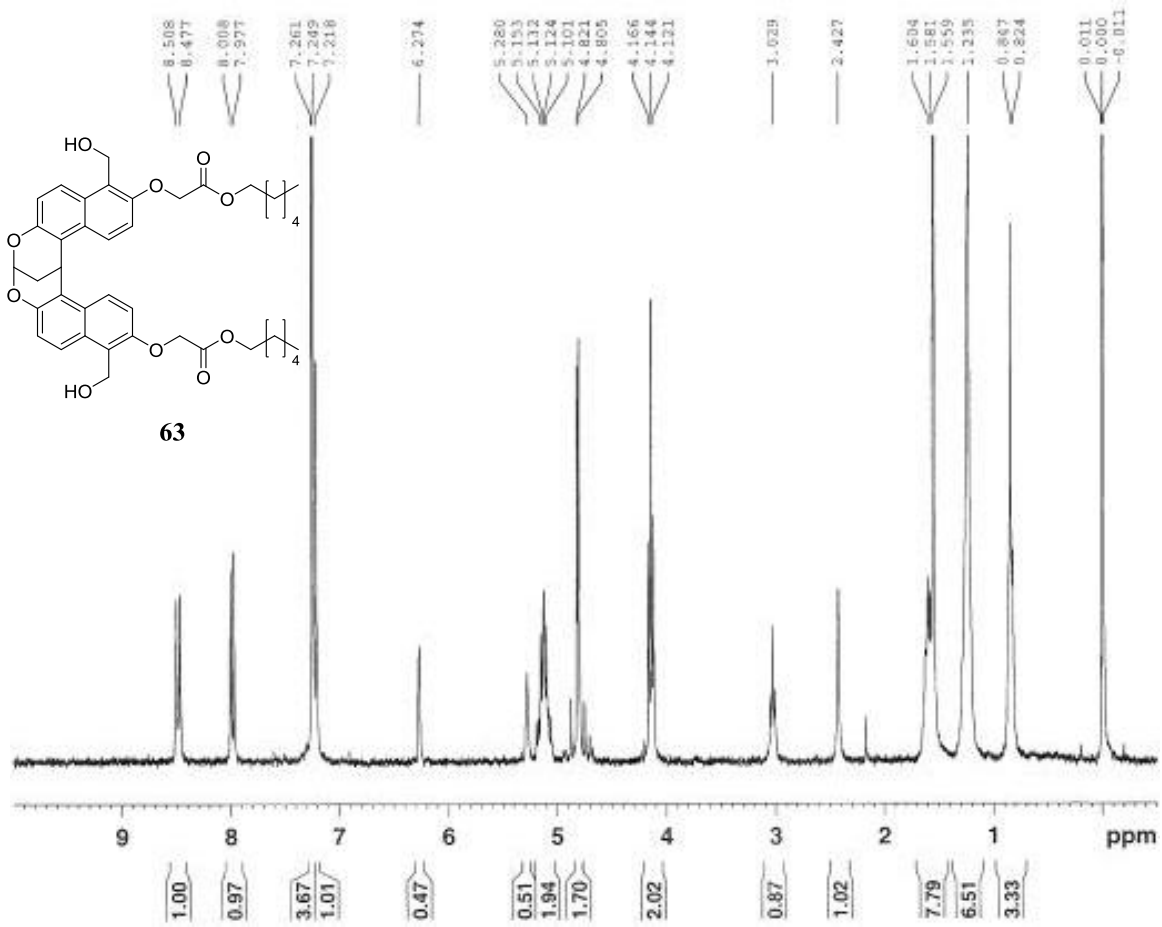
8.508
8.477
8.008
7.997
7.261
7.249
7.218
6.274
5.280
5.193
5.132
5.124
5.101
4.821
4.805
4.166
4.144
4.121
3.029
2.427
1.604
1.581
1.559
1.335
0.867
0.824
0.011
0.000
-0.011
HO
O
O
O
O
4
O
O
O
O
4
HO
9
8
7
6
5
4
3
2
1
ppm
1.00
0.97
3.67
1.01
0.47
0.51
1.94
1.70
2.02
0.87
1.02
7.79
6.51
3.33

63

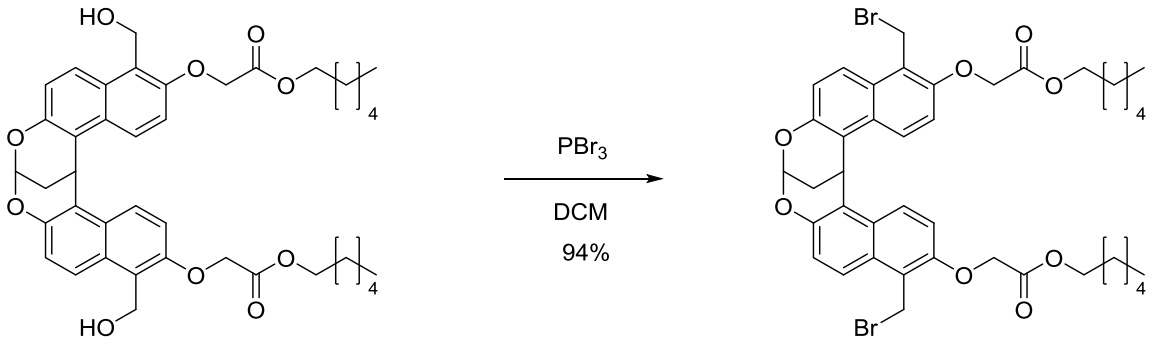

63 **64**

Compound 64

Compound 63 (1.05 g, 1.49 mmol) was dissolved in DCM and flushed with N_2. PBr_3 (354 μL, 3.73 mmol) was added dropwise via syringe, and the mixture was stirred at room temperature for 6 hours. The mixture was cooled to 0 °C and quenched with saturated sodium bicarbonate solution, and then extracted with DCM, dried over Na_2SO_4 and filtered. The DCM was removed under reduced pressure to yield compound 64 (1.16 g, 94%) as a brown solid (mp 62 °C). **^{1}H NMR** (300 MHz, $CDCl_3$) δ 8.49 (d, 2H, J = 9.6), 7.85 (d, 2H, J = 9.3), 7.30 (d, 2H, J = 9.6), 7.19 (d, 2H, J = 9.3), 6.28 (s, 1H), 5.26 (s, 1H), 5.06 (dd, 4H, J = 10.2, 27.2), 4.82 (s, 4H), 4.19 (t, 4H, J = 6.6), 2.42 (s, 2H), 1.57-1.64 (m, 4H), 1.20-1.25 (m, 12H), 0.80-0.84 (m, 6H); **^{13}C NMR** (75 MHz, $CDCl_3$) δ 169.0, 151.8, 149.4, 128.5, 127.4, 125.1, 123.5, 121.0, 120.0, 118.9, 114.4, 91.3, 66.9, 65.6, 31.3, 28.5, 26.8, 25.5, 24.7, 23.0, 22.5, 13.9; **IR** (neat, cm^{-1}) 3428, 2958, 2921, 2852, 1753, 1638, 1593, 1201, 1074; **HRMS** calculated for $C_{41}H_{46}Br_2O_8Na$ ($M + Na^+$): 847.14517. Found: 847.14414.

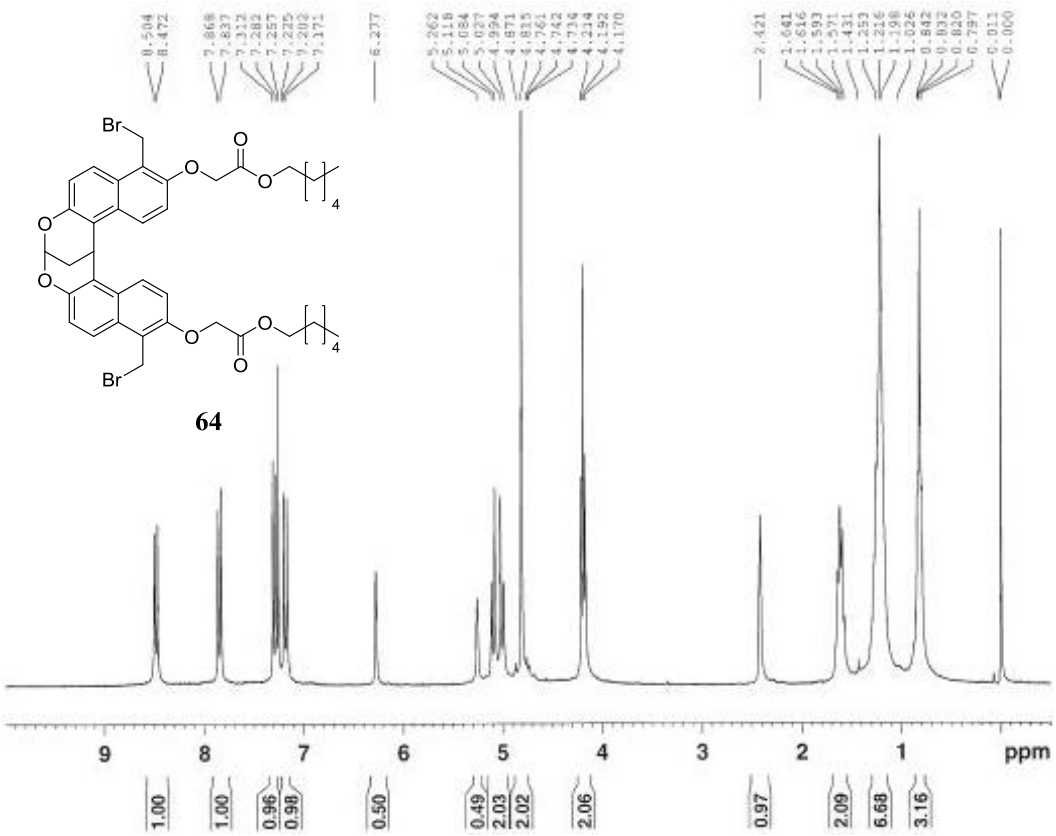
Br
O
O
O
O
4
O
O
O
O
4
Br
64
9
8
7
6
5
4
3
2
1
ppm
1.00
1.00
0.96
0.98
0.50
0.49
2.03
2.02
2.06
0.97
2.09
6.68
3.16

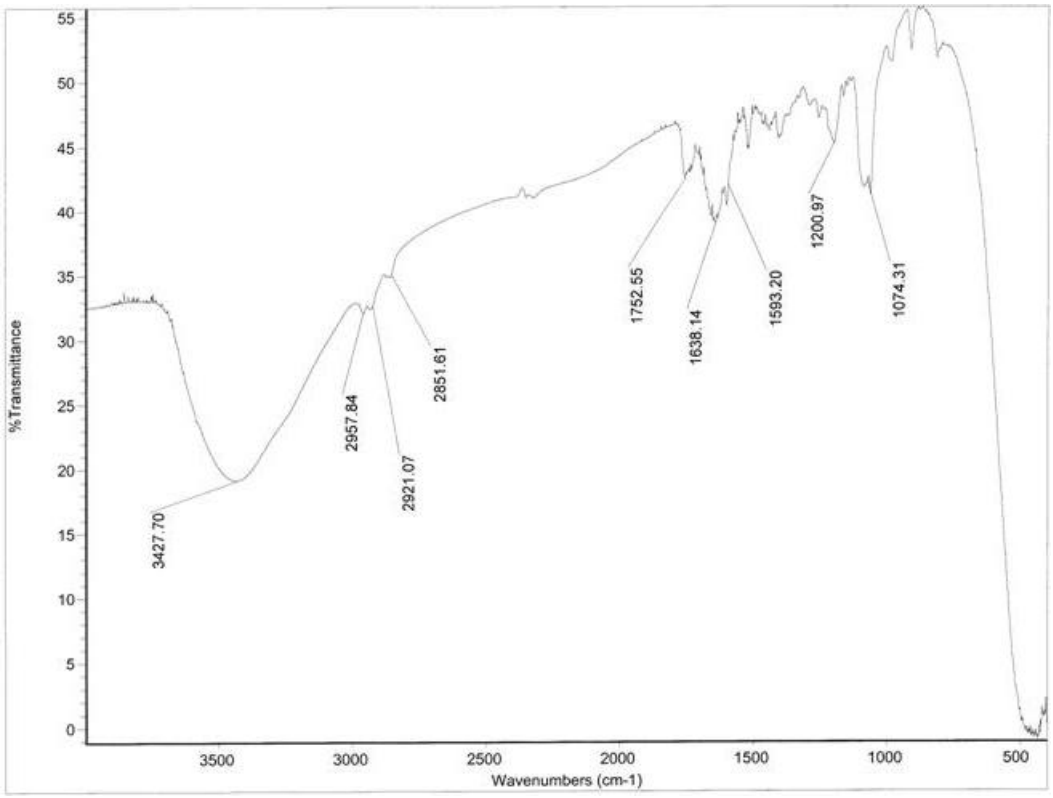
%Transmittance
Wavenumbers (cm-1)
3427.70
2957.84
2921.07
2851.61
1752.55
1638.14
1593.20
1200.97
1074.31

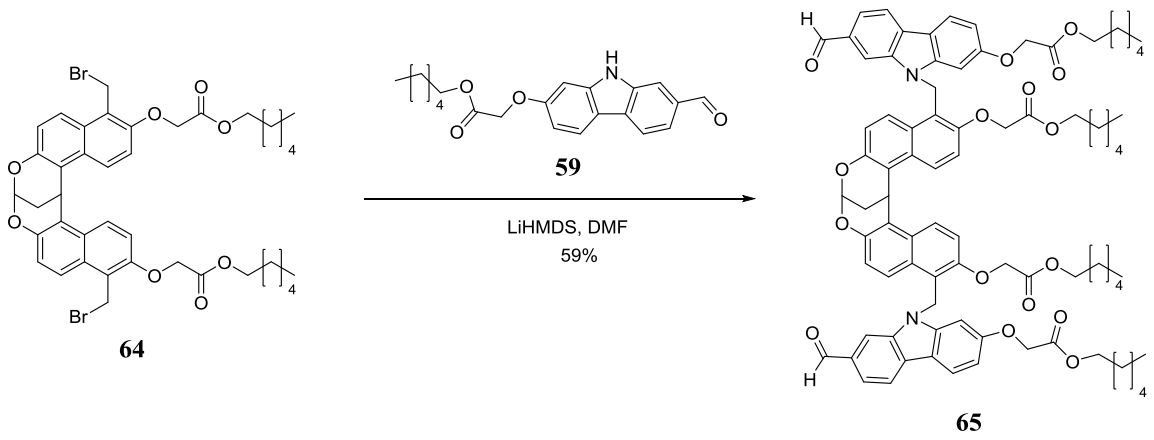

Compound 65

Compound 59 (101 mg, 0.287 mmol) as dissolved in 11 mL of DMF and flushed with N_2. A 1.0 M solution of LiHMDS in THF (252 µL, 0.252 mmol) was added by syringe and the mixture was stirred for 15 minutes. Compound 64 (94.8 mg, 0.115 mmol) was dissolved in 4 mL of DMF and added by syringe, and the flask that contained compound 64 was rinsed with 1 mL DMF which was also added to the reaction mixture by syringe. The reaction was stirred at room temperature for 17 hours. DMF was removed under reduced pressure and the mixture was purified by column chromatography on silica (0-10% Et_2O/DCM). The product was dried and rinsed with acetone to wash away remaining impurities to yield compound 65 (92.7 mg, 59% yield) as an off-white solid. **^{1}H NMR** (500 MHz, $CDCl_3$) δ 9.99 (s, 2H), 8.55 (d, 2H, J = 9.5 Hz), 8.01 (d, 2H, J = 8.0), 7.93 (d, 2H, J = 8.5 Hz), 7.80 (s, 2H), 7.65 (d, 2H, J = 8.0 Hz), 7.32 (d, 4H, J = 9.5 Hz), 6.78-6.88 (m, 6H), 6.13 (s, 1H), 5.29 (s, 4H), 5.20 (s, 1H), 4.76 (s, 4H), 4.57 (s, 4H), 4.10-4.15 (m, 4H), 4.00-4.03 (m, 4H), 2.30 (s, 2H), 1.54-1.55 (m, 4H), 1.41 (s, 4H), 1.21-1.26 (m, 12H), 1.09-1.12 (m, 12H), 0.79-083 (m, 6H), 0.74-0.76 (m, 6H).

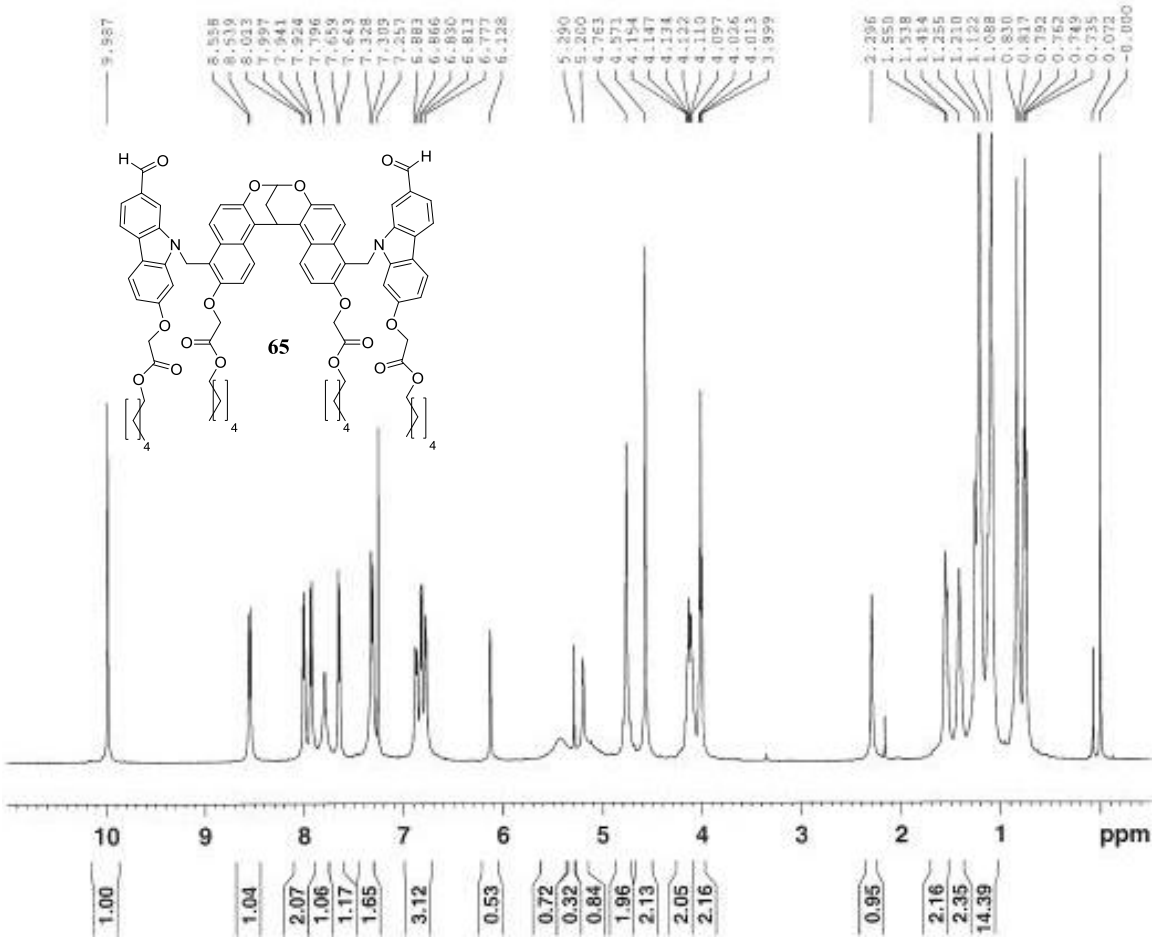
9.987
8.538
8.519
8.013
7.997
7.941
7.924
7.796
7.659
7.643
7.328
7.309
7.257
6.883
6.866
6.830
6.813
6.777
6.128
5.290
5.200
4.763
4.571
4.154
4.147
4.134
4.122
4.110
4.097
4.026
4.013
3.999
2.296
1.550
1.538
1.414
1.255
1.210
1.122
1.088
0.830
0.817
0.792
0.762
0.749
0.735
0.072
-0.000
65
10
9
8
7
6
5
4
3
2
1
ppm
1.00
1.04
2.07
1.06
1.17
1.65
3.12
0.53
0.72
0.32
0.84
1.96
2.13
2.05
2.16
0.95
2.16
2.35
14.39

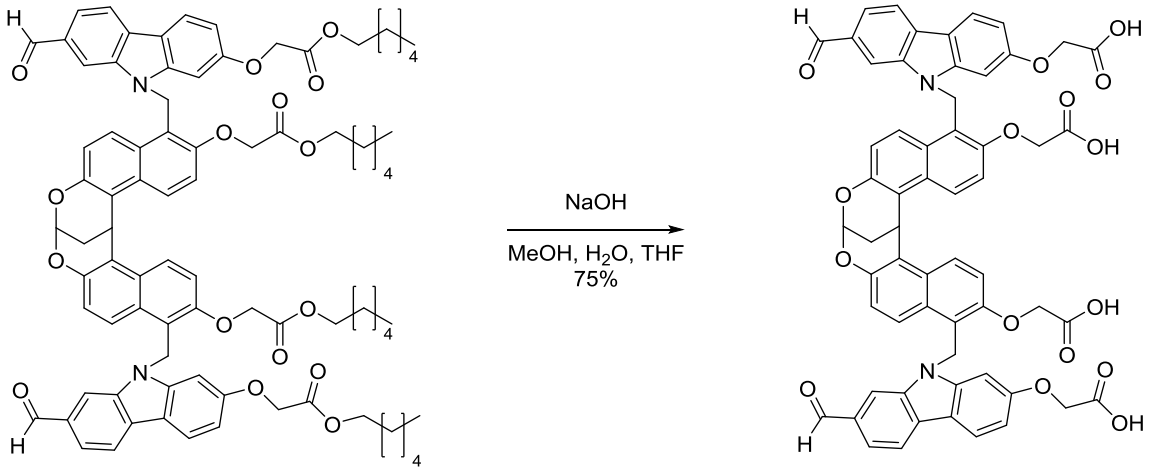

65 **66**

Compound 66

Compound 65 (27.6 mg, .0201 mmol) was dissolved in 4 mL of THF, 3 mL of MeOH was added, then 2 mL of a 2M solution of aqueous NaOH. The mixture was stirred at room temperature for 13 hours. The solvent was removed by blowing N_2 over it. The solid was suspended in 5 mL of 1M HCl, centrifuged and the liquid was decanted. The solid was again suspended in 1M HCl, centrifuged and the liquid decanted twice more, and then the same suspension/centrifugation process was followed two times each for methanol, THF, and methylene chloride to yield compound 66 (0.15 g, 75%) as a pale yellow solid. **^{1}H NMR** (500 MHz, d_6-DMSO) δ 9.97 (s, 2H), 8.79 (d, 2H, J = 9.5 Hz), 8.09-8.16 (m, 6H), 7.62 (d, 4H, J = 8.5 Hz), 7.52 (d, 2H, J = 9.5 Hz), 7.34 (d, 2H, J = 1.6 Hz), 6.90 (d, 2H, J = 9.0 Hz), 6.85 (dd, 2H, J = 1.6, 8.5 Hz), 6.22 (s, 1H), 6.01-6.04 (m, 4H), 5.55 (s, 1H), 5.01 (s, 4H), 2.26 (s, 2H).

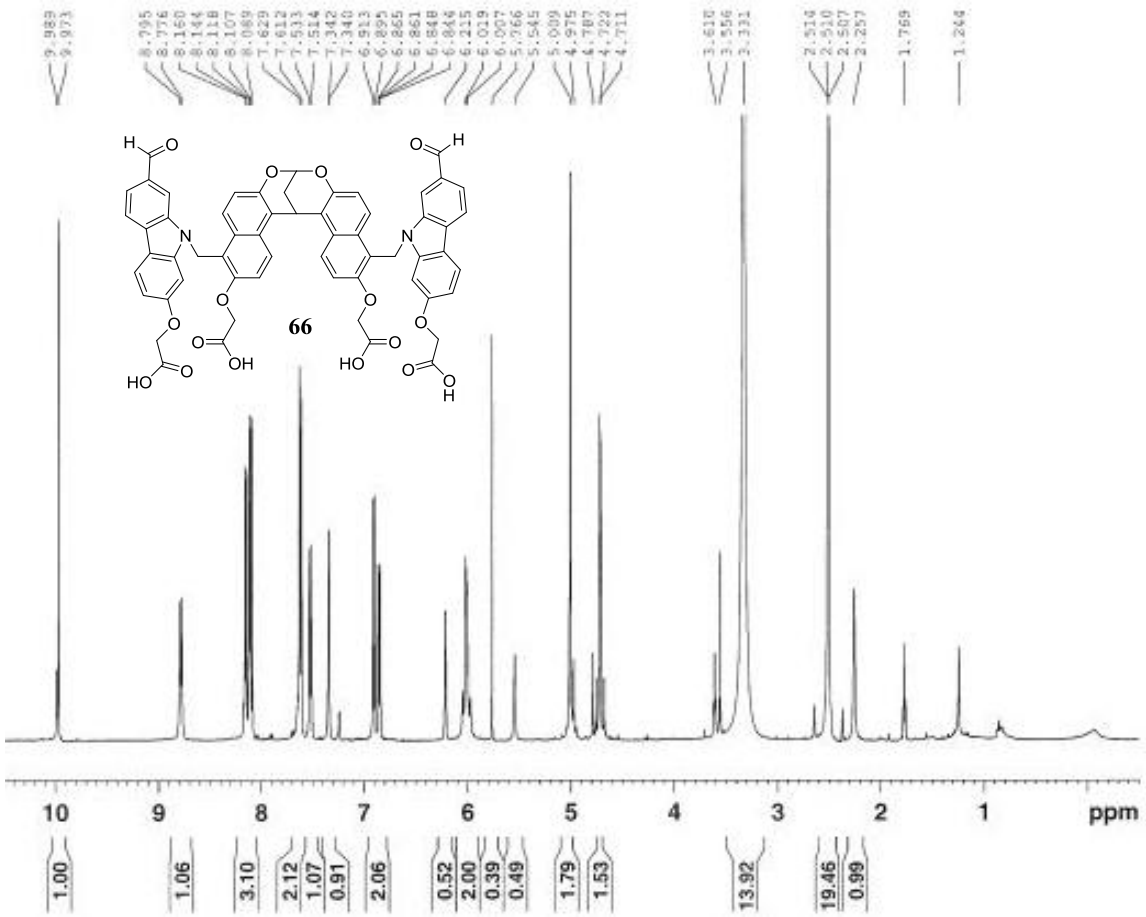
9.989
9.973
8.795
8.776
8.160
8.144
8.118
8.107
8.069
7.629
7.612
7.533
7.514
7.342
7.340
6.913
6.895
6.865
6.861
6.848
6.844
6.215
6.019
6.007
5.766
5.545
5.009
4.975
4.787
4.722
4.711
3.610
3.556
3.331
2.514
2.510
2.507
2.257
1.769
1.244
66
10
9
8
7
6
5
4
3
2
1
ppm
1.00
1.06
3.10
2.12
1.07
0.91
2.06
0.52
2.00
0.39
0.49
1.79
1.53
13.92
19.46
0.99

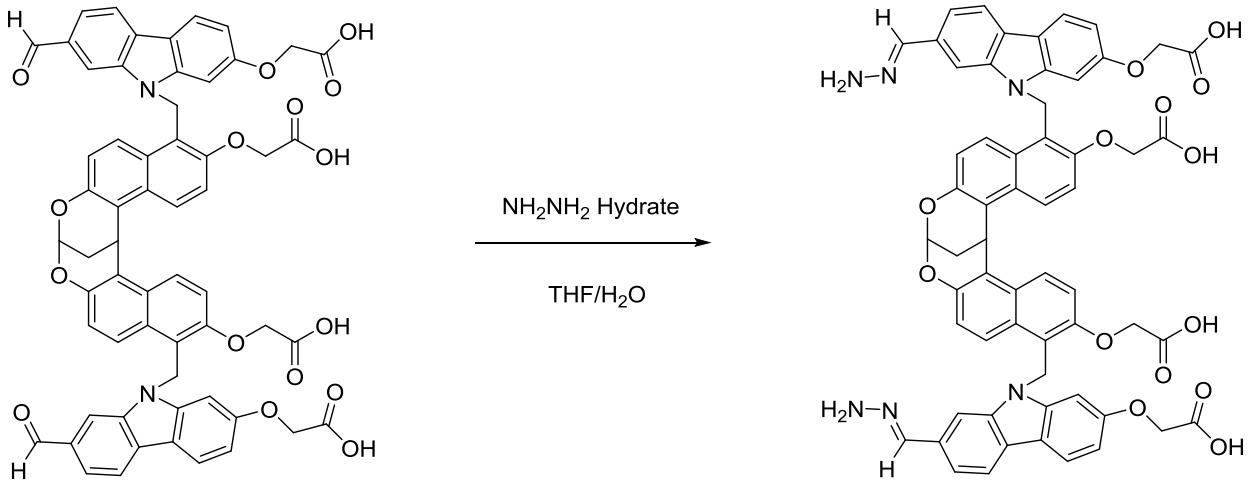

66 **67**

Compound 67

Compound 66 (7.9 mg, 0.0076 mmol) was dissolved in 0.5 mL of DMSO and 0.1 mL of hydrazine hydrate, 85% in water, and 1 drop of HCl were added. The reaction mixture was stirred for 13 hours and the DMSO was removed by blowing nitrogen over it. The solid was suspended in 1 mL of 1M HCl, centrifuged and the liquid was decanted. The solid was again suspended in 1M HCl, centrifuged and the liquid decanted twice more, and then the same suspension/centrifugation process was followed three times each for methanol, THF, and methylene chloride to yield compound 67 (6.1 mg) as a white solid that is insoluble in anything except basic water and acidic DMSO.

REFERENCES

1. Steed, J. W.; Atwood, J. L. *Supramolecular chemistry*; 2nd ed.; Wiley: Chichester, UK, 2009.
2. Rebek, J., Jr. *Angew. Chem. Int. Ed. Engl.* **1990**, *29*, 245-255.
3. Pedersen, C. J. *J. Am. Chem. Soc.* **1967**, *89*, 7017-7036.
4. Bell, T. W.; Santora, V. J. *J . Am. Chem. Soc*. **1992**, *114*, 8300-8302.
5. Bell, T. W.; Hou, Z. *Angew. Chem. Int. Ed. Engl.* **1997**, *36*, 1536-1538.
6. Schrader, T. *Chem. Eur. J.* **1997**, *3*, 1537-1541.
7. Eliseev, A. V.; Nelen, M. I. *J. Am. Chem. Soc.* **1997**, *119*, 1147-1148.
8. Bell, T. W.; Khasanov, A. B.; Drew, M. G. B.; Filikov, A.; James, T. L. *Angew. Chem. Int. Ed. Engl.* **1999**, *38*, 2543-2547.
9. *Meot-Ner, M. J. Am. Chem. Soc.* **1983**, *105*, 4912–4915.
10. Chatterjee, T.; Sarma, M.; Das, S. K. *Cryst. Growth Des.* **2010**, *10*, 3149–3163.
11. Kolthoff, I. M.; Chantooni, M. K.; Wang, W. J. *Anal. Chem.* **1983**, *55*, 1202-1204.
12. Gokel, G. W.; Leevy, W. M.; Weber, M. E. *Chem. Rev.* **2004**, *104*, 2723–2750.
13. Saenger, W. *Angew. Chem. Int. Ed. Engl.* **1980**, *19*, 344-362.
14. Wu, X.; Li, Z.; Chen, X.-X.; Fossey, J. S.; James, T. D.; Jiang, Y.-B. *Chem. Soc. Rev.* **2013**, *42*, 8032-8048.
15. Centers for Disease Control and Prevention. National Diabetes Fact Sheet: National Estimates and General Information on Diabetes and Prediabetes in the

United States, 2011. Atlanta, GA: U.S. Department of Health and Human Services, Centers for Disease Control and Prevention, 2011.

16. Tsukagoshi K.; Shinkai, S. *J. Org. Chem.* **1991**, *56*, 4089-4091.
17. Klockow, J. L; Hettie, K. S.; Glass, T. E. *ACS Chem. Neurosci*. **2013**, *4*, 1334-1338.
18. Klockow, J. L.; Glass, T. E. *Org. Lett.* **2013**, *15*, 235-237.
19. Kruppa, M.; König, B. *Chem. Rev.* **2006**, *106*, 3520-3560.
20. Skoog, D. A.; Holler, F. J.; Nieman, T. A. *Principles of Instrumental Analysis;* 5th ed.**;** Brooks/Cole: Stanford, Connecticut, 1997.
21. Lakowicz, J. R. *Principles of fluorescence spectroscopy*; 3rd ed.; Springer: New York, 2006.
22. Fletcher, K. A.; Storey, I. A.; Hendricks, A. E.; Pandey, S.; Pandey, S. *Green Chem.* **2001**, *3*, 210-215.
23. Carlotti, B.; Spalletti, A.; Sindler-Kulyk, M.; Elisei, F. *Phys. Chem. Chem. Phys*. **2011**, **13**, 4519-4528.
24. Mukherjee, S.; Chattopadhyay, A.; Samanta, A.; Soujanya, T. *J. Phys. Chem.* **1994**, *98*, 2809-2812.
25. Kucherak, O. A.; Oncul, S.; Darwich, Z.; Yushchenko, D. A.; Arntz, Y.; Didier, P.; Mely, Y.; Klymchenko, A. S. *J. Am. Chem. Soc.* **2010**, *132*, 4907-4916.
26. Prifti, E.; Reymond, L.; Umebayashi, M.; Hovius, R.; Riezman, H.; Johnsson, K. *ACS Chem. Biol.* **2014**, *9*, 606-612.
27. Signore, G.; Nifosi, R.; Albertazzi, L.; Storti, B.; Bizzarri, R. *J. Am. Chem. Soc.* **2010**, *132*, 1276-1288.

28. Li, X.; Gao, X.; Shi, W.; Ma, H. *Chem. Rev.* **2014**, *114*, 590-659.

29. Martinez-Manez, R.; Sancenon, F. *Chem. Rev.* **2003**, *103*, 4419-4476.

30. de Silva, A. P.; Gunaratne, H. Q. N.; Gunnlaugsson, T.; Huxley, A. J. M.; McCoy, C. P.; Rademacher, J. T.; Rice, T. E. *Chem. Rev.* **1997**, *97*, 1515-1556.

31. Wu, M.-Y.; He, T.; Li, K.; Wu, M.-B.; Huang, Z.; Yu, X.-Q. *Analyst*, **2013**, *138*, 3018-3025.

32. Baldridge, A.; Solntsev, K. M.; Song, C.; Tanioka, T.; Kowalik, J.; Hardcastle, K.; Tolbert, L. M. *Chem. Commun.* **2010**, *46*, 5686-5688.

33. Geddes, C. D. *Dyes Pigments*, **2000**, *45*, 243–251.

34. Wang, T.; Douglass, E. F., Jr.; Fitzgerald, K. J; Spiegel, D. A. *J. Am. Chem. Soc.* **2013**, *135*, 12429-12433.

35. Garrett, R. H.; Grisham, C. M. *Biochemistry*; 3rd ed.; Brooks/Cole: Belmont, California 2005.

36. Gunstone, F. D.; Harwood, J. L.; Dijkstra, A. J. *Lipid Handbook*; CRC Press: 2007.

37. Ball, M.; Mann, J. *Lipids and Heart Disease*, *A Guide for the Primary Care Team*; 2nd ed.; Oxford University Press: New York 1994.

38. Hanahan, D. J. *Guide to Phospholipid Chemistry*; Oxford University Press: New York 1997.

39. Vance, D. E.; Vance, J. E. *Biochemistry of lipids, lipoproteins and membranes*; 5th ed.; Elsevier: Amsterdam ; Boston, 2008.

40. Myant, N. B., *Cholesterol Metabolism, LDL, and the LDL Receptor*; Academic Press: San Diego 1990.

41. Betteridge, D. J. *Lipids and Vascular Disease*; Martin Dunitz: London 2000.

42. Hevonoja, T.; Pentikäinen, M. O.; Hyvönen, M. T.; Kovanen, P. T.; Ala-Korpela, M. *Biochim. Biophy. Acta*, **2000**, *1488*, 189-210.

43. Cromwell, W. C.; Otvos, J. D. *Curr. Atheroscler. Rep*. **2004**, *6*, 381-387.

44. Berliner, J. A.; Subbanagounder, G.; Leitinger, N.; Watson, A. D.; Vora, D. *Trends Cardiovas. Med*. **2001**, *11*, 142-147.

45. Leitinger, N. *Curr. Opin. Lipido*. **2003**, *14*, 421-430.

46. Berliner, J. A.; Watson, A. D. *New Engl. J. Med*. **2005**, *353*, 9-11.

47. Fruhwirth, G. O.; Loidl, A.; Hermetter, A. *Biochim. Biophys. Acta*, **2007**, *1772*, 718-736.

48. Ashraf, M. Z.; Kar, N. S.; Podrez, E. A. *Int. J. Biochem. Cell Biol*. **2009**, *41*, 1241-1244.

49. Podrez, E. A.; Poliakov, E.; Shen, Z.; Zhang, R.; Deng, Y.; Sun, M.; Finton, P. J.; Shan, L.; Gugiu, B.; Fox, P. L.; Hoff, H. F.; Salomon, R. G.; Hazen, S. L. *J. Biol. Chem*. **2002**, *277*, 38503-38561.

50. Tuzcu, E. M.; Kapadia, S. R.; Tutar, E.; Ziada, K. M.; Hobbs, R. E.; McCarthy, P. M.; Young, J. B.; Nissen, S. E. *Circulation*, **2001**, *103*, 2705−2710.

51. Stubiger, G.; Belgacem, O.; Rehulka, P.; Bicker, W.; Binder, B. R.; Bochkov, V. *Anal. Chem.* **2010,** *82*, 5502–5510.

52. Yang, J.; Yang, S.; Gao, X.; Yuan, Y.-J. **Mol. BioSyst. 2011**, **7**, 2428-2440.

53. Jónasdóttir, H. S.; Nicolardi, S.; Jonker, W.; Derks, R.; Palmblad, M.; Ioan-Facsinay, A.; Toes, R.; van der Burgt, Y. E. M.; Deelder, A. M.; Mayboroda, O. A.; Giera, M. *Anal. Chem*. **2013**, *85*, 6003−6010.

54. Mesaros, C.; Gugiu, B. G.; Zhou, R.; Lee, S. H.; Choi, J.; Laird, J.; Blair, I. A.; Salomon, R. G. *Chem. Res. Toxicol.* **2010,** *23*, 516–527.

55. Milic, I.; Hoffmann, R.; Fedorova, M. *Anal. Chem*. **2013**, *85*, 156−162.

56. Murphy, R. C.; Fiedler, J.; Hevko, J. *Chem. Rev.* **2001,** *101*, 479-526.

57. Hinterwirth, H.; Stübiger, G.; Lindner, W.; Lämmerhofer, M. *Anal. Chem*. **2013**, *85*, 8376−8384.

58. Mason, R. P.; Walter, M. F.; Mason, P. E. *Free Radic. Biol. Med*. **1997**, *23*, 419-425.

59. Stewart, C. R.; Tseng, A. A.; Mok, Y.-F.; Staples, M. K.; Schiesser, C. H.; Lawrence, L. J.; Varghese, J. N.; Moore, K. J.; Howlett, G. J. *Biochemistry* **2005,** *44*, 9108-9116.

60. Salomon, R. G.; Kaur, K.; Podrez, E.; Hoff, H. F.; Krushinsky, A. V.; Sayre, L. M. *Chem. Res. Toxicol.* **2000,** *13*, 557-564.

61. Beranova, L.; Cwiklik, L.; Jurkiewicz, P.; Hof, M.; Jungwirth, P. *Langmuir*, **2010**, *26*, 6140–6144.

62. Nishiyabu, R.; Anzenbacher, P. Jr. *Org. Lett.* **2006**, *8*, 359-362.

63. Danil de Namor, A. F.; Abbas, I.; Hammud, H. H. *J. Phys. Chem. B,* **2007**, *111*, 3098-3105.

64. Sessler, J. L.; Gross, D. E.; Cho, W.; Lynch, V. M; Schmidtchen, F. P.; Bates, G. W.; Light, M. E.; Gale, P. A. *J. Am. Chem. Soc.* **2006**, *128*, 12281-12288.

65. Musau, R. M.; Whiting, A. *J. Chem. Soc. Perkin Trans.* **1994**, 2881-2888.

66. Shorthill, B. J.; Glass, T. E. *Org. Lett.* **2001**, *3*, 577-579.

67. Shorthill, B. J.; Granucci, R. G.; Powell, D. R.; Glass, T. E. *J. Org. Chem.* **2002**, *67*, 904-909.

68. Esumi, K.; Syoji, K.; Miyazaki, M.; Torigoe, K.; Koide, Y. *Langmuir* **1999**, *15*, 6591-6593.

69. Liu, Y.; Liu, L.; Wang, Y.; Han, Y.; Wang, D.; Chen, Y. *Green Chem.* **2008**, *10*, 635-640.

70. Shimizu, S.; Shimada, N.; Sasaki, Y. *Green Chem*. **2006**, *8*, 608-614.

71. Harrowfield, J. M.; Mocerino, M.; Peachey, B. J.; Skelton, B. W.; White, A. H. *J. Chem. Soc., Dalton Trans.* **1996**, 1687-1699.

72. Shimizu, S.; Kito, K.; Sasaki, Y.; Hirai, C. *Chem Commun.* **1997**, 1629-1630.

73. Kim, J. S.; Quang, D. T. *Chem. Rev.* **2007**, *107*, 3780-3799

74. Homden, D. M.; Redshaw, C. *Chem. Rev.***2008**, *108*, 5086-5130.

75. Wang, J.; Gutsche, C. D. *J. Org. Chem.* **2000**, *65*, 6273-6275.

76. Makha, M.; Raston, C. L.; Sobolev, A. N.; Turner, P. *Cryst. Growth Des.* **2006**, *6*, 224-228.

77. Makha, M. McKinnon, I. R.; Raston, C. L. *J. Chem. Soc., Perkin Trans. 2*, **2002**, 1801-1806.

78. Ikeda, A.; Shinkai, S. *Chem. Rev.* **1997**, *97*, 1713-1734.

79. Atwood, J. L.; Orr, G. W.; Juneja, R. K.; Bott, S. G.; Hamada, F. *Pure & Appl. Chem.* **1993**, *65*, 1471-1476.

80. Wei, A. *Chem. Commun.* **2006**, 1581-1591.

81. Gurr, M. I.; Harwood, J. L.; Frayn, K. N. Lipid Biochemistry: An Introduction; 5th ed.; Oxford, UK 2002

82. Ryan, R. O.; van der Horst, D. J. *Annu. Rev. Entomol.* **2000**, *45*, 233.

83. Dykstra, M.; Cherukuri, A.; Sohn, H. W.; Tzeng, S.-J.; Pierce, S. K.; *Annu. Rev. Immunol.* **2003**, *21*, 457.

84. Kielian, M.; Chatterjee, P. K.; Gibbons, D. L.; Lu, Y. E. *Subcell. Biochem.* **2000**, *34*, 409.

85. Lauber, K.; Bohn, E.; Kröber, S. M.; Xiao, Y.-J.; Blumenthal, S. G.; Lindemann, R. K.; Marini, P.; Wiedig, C.; Zobywalski, A.; Baksh, S.; Xu, Y.; Autenrieth, I. B.; Schulze-Osthoff, K.; Belka, C.; Stuhler G.; Wesselborg, S. *Cell*, **2003**, *113*, 717.

86. Islam, S. A.; Thomas, S. Y.; Hess, C.; Medoff, B. D.; Means, T. K.; Brander, C.; Lilly, C. M.; Tager A. M.; Luster, A. D. *Blood*, **2006**, *107*, 444.

87. Virtanen, J. A.; Cheng K. H.; Somerharju, P. *Proc. Natl. Acad. Sci.* **1998**, *95*, 4964.

88. Tyurina, Y. Y.; Shvedova, A. A.; Kawai, K.; Tyurin, V. A.; Kommineni, C.; Quinn, P. J.; Schor, N. F.; Fabisiak, J. P.; Kagan, V. E. *Toxicology*, **2000**, *148*, 93.

89. Preta, G.; Fadeel, B. *PLoS One*, **2012**, *7*, 1.

90. Tung, T. T.; Nagaosa, K.; Fujita, Y.; Kita, A.; Mori, H.; Okada, R.; Nonaka, S.; Nakanishi, Y. *J. Biochem*. **2013**, *153*, 483.

91. Smith, B. A.; Gammon, S. T.; Xiao, S.; Wang, W.; Chapman, S.; McDermott, R.; Suckow, M. A.; Johnson, J. R.; Piwnica-Worms, D.; Gokel, G. W.; Smith, B. D.; Leevy, W. M. *Mol. Pharmaceutics*, **2011**, *8*, 583.

92. Smith, B. A.; Smith, B. D. *Bioconjugate Chem.*, **2012**, *23*, 1989.

93. Smith, B. A.; Xiao, S.; Wolter, W.; Wheeler, J.; Suckow, M. A.; Smith, B. D. *Apoptosis*, **2011**, *16*, 722.

94. Hanshaw, R. G.; Smith, B. D. *Bioorg. Med. Chem*. **2005**, *13*, 5035.

95. Bae, S. W.; Cho, M. S.; Jeong, A. R.; Choi, B.-R.; Kim, D.-E.; Yeo, W.-S.; Hong, J.-I. *Small*, **2010**, *6*, 1499.

96. Atkinson, P.; Murray, B. S.; Parker, D. *Org. Biomol. Chem*. **2006**, *4*, 3166.

97. Anai, T.; Nakata, E.; Koshi, Y.; Ojida, A.; Hamachi, I. *J. Am. Chem. Soc*. **2007**, *129*, 6232.

98. White, A. G.; Gray, B. D.; Pak, K. Y.; Smith, B. D. *Bioorg. Med. Chem. Lett*. **2012**, *22*, 2833.

99. Lakshmi, C.; Hanshaw, R. G.; Smith, B. D. *Tetrahedron*, **2004**, *60*, 11307.

100. Avetta, C. T.; Shorthill, B. J.; Ren, C.; Glass, T. E. *J. Org. Chem*. **2012**, *77*, 851.

101. Cooley, C. M.; Hettie, K. S.; Klockow, J. L.; Garrison, S.; Glass, T. E. *Org. Biomol. Chem.* **2013**, *11*, 7387.

102. Hettie, K. S.; Liu, X.; Gillis, K. D.; Glass, T. E. *ACS Chem. Neurosci*. **2013**, *4*, 918.

103. Secor, K. E.; Glass, T. E. *Org. Lett*. **2004**, *6*, 3727.

104. Feuster, E. K.; Glass, T. E. *J. Am. Chem. Soc.* **2003**, *125*, 16174.

105. Parker, C. A.; Rees, W. T. *Analyst*, **1960**, *85*, 587.

106. Shorthill, B. J.; Avetta, C. T.; Glass, T. E., *J. Am. Chem. Soc*. **2004**, *126*, 12732-12733.

107. Hileman, R. E.; Parkhurst, K. M.; Gupta, N. K.; Parkhurst, L. J. *Bioconjugate Chem.* **1994**, *5*, 436-444.

108. Crisalli, P.; Hernandez, A. R.; Kool, E. T. *Bioconjugate Chem.* **2012**, *23*, 1969-1980.

109. Zeng, Y.; Ramya, T. N. C.; Dirksen, A.; Dawson, P. E.; Paulson, J. C. *Nat. Methods*, **2009**, *6*, 207-209.

110. Key, J. A.; Li, C.; Cairo, C. W. *Bioconjugate Chem.* **2012**, *23*, 363-371.

VITA

Chad Cooley was born on December 12, 1984 in Jefferson City, Missouri. He fled to Iowa as quickly as his chubby baby legs could take him. Unfortunately, a series of poor choices led him back to Missouri in 2004. He earned a degree in chemistry with a minor in English from Truman State University in 2007. He joined Dr. Timothy E. Glass' lab at the University of Missouri-Columbia in 2008. In 2014 he completed his Ph. D. and accepted a faculty position at Indiana University in Bloomington, Indiana.